UNIVERSITEIT VAN PRETORIA
UNIVERSITY OF PRETORIA
YUNIBESITHI YA PRETORIA

# Suppressing Hydrogen Evolution by Aqueous Silicon Powder Dispersions

By

**Shepherd Masimba Tichapondwa**

Dissertation submitted in partial fulfilment of the requirements for the degree of

**Master of Engineering (Chemical Engineering)**

In the Faculty of Engineering, Built Environment and Information Technology
University of Pretoria

Pretoria

March 2012

© University of Pretoria

**DECLARATION**

**I**, **Shepherd Masimba Tichapondwa, student No. 29718092,** do hereby declare that this research is my original work and that to the best of my knowledge and belief, it has not been previously in its entirety or in part been submitted and is not currently being submitted either in whole or in part at any university for a degree or diploma, and that all references are acknowledged.

**SIGNED** on this ________________ day of ___________________________________ 2012.

________________________

**Shepherd M. Tichapondwa**

UNIVERSITEIT VAN PRETORIA
UNIVERSITY OF PRETORIA
YUNIBESITHI YA PRETORIA

# Suppressing Hydrogen Evolution by Aqueous Silicon Powder Dispersions

Student: Shepherd Masimba Tichapondwa

Supervisor: Prof. Walter W. Focke

Department: Chemical Engineering
University: University of Pretoria
Degree: Master of Engineering (Chemical Engineering)

## SYNOPSIS

Silicon dispersions in water are used to produce pyrotechnic time delay compositions employed in mine detonators. The delay elements are manufactured by pressing the pyrotechnic composition into aluminium tubes. The automated filling and pressing process requires powders with good free-flow behaviour. Spray drying of water-based slurries is an appropriate method for obtaining such free-flowing granules as it creates almost perfectly spherical particle agglomerates. In addition to the acceptable flow properties, this process provides well-mixed compositions at desired particle size distributions. However, a potential hazard situation arises when water reacts dissociatively with silicon to form $SiO_2$ and hydrogen gas according to $Si + 2H_2O \rightarrow SiO_2 + 2H_2\uparrow$. The propensity of the silicon to react with water and to release hazardous hydrogen gas must thus be suppressed. To this end, the following methods were investigated as a means of diminishing the rate of hydrogen evolution: (i) controlling the slurry pH; (ii) adding organic corrosion inhibitors; (iii) controlled silicon air oxidation before slurrying; and (iv) adding suitable metal ions to provide an additional cathodic reaction to that of water.

The effect of organic surface modifications and medium pH on the rate of corrosion of silicon was studied at ambient temperature. It was found that the rate of hydrogen evolution increased with increasing pH. Silanes proved to be more effective silicon corrosion inhibitors than alcohols, with vinyl tris(2-methoxyethoxy) silane producing the best results from the silanes investigated. Differential thermal analysis

(DTA) studies were performed using a near-stoichiometric amount of lead chromate as oxidant. Comparable combustion behaviour was observed when both the fuel and the oxidant powders were either uncoated or silane modified. Mixtures of neat oxidant with silane-coated silicon showed poor burn behaviour and this was attributed to poor particle–particle mixing due to the mismatch in surface energies.

The controlled silicon air oxidation results showed that the best hydrogen evolution inhibition was attained upon formation of a $SiO_2$ passivating layer at 350 °C. However, Fourier transform infrared (FTIR) data also suggest that some inhibition was imparted below 350 °C and this is due mainly to the removal of silicon surface hydroxyl groups rather than an increase in the $SiO_2$ thickness. DTA studies performed using a near-stoichiometric amount of lead chromate revealed that although heat treatment at higher temperatures provides better passivation; it reduces the reactivity of the silicon in pyrotechnic compositions. The ignition temperature increases while the energy output decreases.

Water oxidises silicon via an electrochemical reaction that produces hydrogen gas. The last approach considered in this study was the introduction of a competing cathodic reaction as a means of suppressing the liberation of hydrogen. It was found that the addition of metal ions with a higher reduction potential than hydrogen ions, e.g. copper (II) ions, reduced the amount of hydrogen liberated. In the presence of copper ions the reaction with water featured three distinct stages. During the initial stage, copper is deposited on the silicon and a rapid drop in solution pH is observed. Most of the hydrogen evolved during a second active stage, with the pH showing a slight upward drift. Finally, in the third stage, hydrogen evolution stopped as the silicon surface became passive. The reduction in the total hydrogen evolved was attributed to copper deposits reducing the active surface area available for the oxidation of silicon and to the presence of copper which facilitates accelerated passivation of the uncoated silicon surface. The nature of the anions present affected both the amount of copper deposited on the silicon and the amount of hydrogen released. DTA studies showed that exposure of silicon to copper metal salt solutions also decreases the reactivity of the silicon fuel in pyrotechnic compositions.

**Keywords:** Silicon; Oxidation; Hydrogen; Pyrotechnics; Silanes; Metal salts; Corrosion

## ACKNOWLEDGEMENTS

The author would like to thank:

- The Lord Almighty for His blessings and grace that He has abundantly bestowed on me.
- Prof. Walter W. Focke for his guidance and support, as well as the contributions and encouragement that he gave me throughout the course of this work.
- Ollie Del Fabbro for the long and engaging discussions that became a daily routine as we tried to understand and explain the numerous results obtained.
- AEL Mining Services as well as the personnel at AEL for granting me permission to use this material for the purposes of my degree, as well as for the financial and technical support.
- Dr Werner Jordaan (XPS), Thomas Malwela (FIB-SEM), Wiebke Grote (XRD) and Onius Sitando (ICP-OES).
- My fellow colleagues at the Institute of Applied Materials, Pedro Massinga Jr., Hermíno Muiambo, Nontete Nhlapo, Lumbi Moyo, Washington Mhike, Mthokozisi Sibanda, Shatish Ramjee and Hendrik Oosthuizen, for their unending support and companionship.
- My parents and brothers and sister for all the love, support and encouragement. I am what I am because of you.
- Last but not least I would like to thank my fellow engineer, researcher and soul mate, Mercy, for her patience, exchange of ideas and understanding during the course of these studies.

# TABLE OF CONTENTS

**SYNOPSIS** ..... **I**

**ACKNOWLEDGEMENTS** ..... **III**

**LIST OF FIGURES** ..... **VI**

**LIST OF TABLES** ..... **VIII**

**LIST OF SCHEMES** ..... **IX**

**ABBREVIATIONS** ..... **X**

**CHAPTER 1 : INTRODUCTION** ..... **1**

1.1 Introduction ..... 1
1.2 Aims and Objectives ..... 3
1.3 Outline of Dissertation ..... 4

**CHAPTER 2 : LITERATURE REVIEW** ..... **6**

2.1 Introduction ..... 6
2.1.1 Delay elements ..... 6
2.1.2 Delay compositions ..... 8
2.1.3 Delay element manufacture ..... 10
2.1.4 Silicon as a pyrotechnic fuel ..... 11
2.2 Oxidation of Metals ..... 12
2.2.1 Early metal corrosion theories ..... 14
2.2.1.1 Tammann–Pilling–Bedworth (TPB) parabolic law ..... 15
2.2.1.2 Wagner Parabolic Law ..... 17
2.2.1.3 Cabrera–Mott theory ..... 18
2.3 Silicon Air Oxidation ..... 19
2.3.1 Oxidation by ionic transport ..... 19
2.3.2 Silicon air oxidation kinetics ..... 20
2.3.2.1 Parabolic law ..... 20
2.3.2.2 Linear-parabolic law ..... 21
2.3.2.3 Power law ..... 23
2.3.2.4 Logarithmic law ..... 24
2.4 Silicon Water Oxidation ..... 24
2.4.1 Eh–pH diagram for silicon ..... 24
2.4.2 Silicon corrosion mechanism ..... 26
2.5 Corrosion Inhibition ..... 28
2.5.1 Organic barrier inhibition ..... 29
2.5.1.1 Alcohol inhibition ..... 30
2.5.1.2 Silane inhibition ..... 30
2.5.3 Environment modifying inhibitors ..... 33
2.5.3.1 Effect of pH modification ..... 35
2.5.3.2 Competing cathodic reactions ..... 36
2.5.3.3 Complexing agents ..... 38

**CHAPTER 3 : EXPERIMENTAL** ..... **39**

3.1 Organic Surface Modification and pH variation ..... 39
3.1.1 Materials ..... 39
3.1.2 Methods ..... 39

3.1.3 Characterisation ........ 41
3.2 Silicon Surface Oxidation ........ 43
3.2.1 Materials ........ 43
3.2.2 Method ........ 43
3.2.3 Characterisation ........ 44
3.3 Additional Cathodic Reaction ........ 45
3.3.1 Materials ........ 45
3.3.2 Methods ........ 46
3.3.3 Characterisation ........ 47

**CHAPTER 4 : RESULTS: ORGANIC COATING AND PH VARIATION ........ 49**

4.1 Initial Silicon Surface Structure ........ 49
4.2 Effect of pH on $H_2$ Evolution ........ 52
4.3 Effects of Treatment with Alcohols and Silanes on $H_2$ Evolution ........ 53
4.4 DTA Burning Behaviour ........ 55

**CHAPTER 5 : RESULTS: SILICON SURFACE OXIDATION ........ 57**

5.1 Effect of Surface Oxidation on $H_2$ Evolution ........ 57
5.2 Surface Characterisation ........ 58
5.3 Quantification of Silicon Oxidation ........ 60
5.4 FIB-SEM Images ........ 63
5.5 DTA Results ........ 66
5.6 Discussion ........ 68

**CHAPTER 6 : RESULTS: ADDITIONAL CATHODIC REACTIONS ........ 70**

6.1 Effect of Introducing Metal Salts on $H_2$ Evolution ........ 70
6.2 Optimisation of Cu $(NO_3)_2$ ........ 71
6.3 Copper Deposited ........ 72
6.3 Surface Characteristics of Silicon Treated with a Metal Solution ........ 75
6.4 Burn Behaviour of Pyrotechnic Composition ........ 76
6.4.1 Si–$BaSO_4$ open-flame test results ........ 76
6.4.2 Differential thermal analysis ........ 77
6.5 Discussion ........ 78

**CHAPTER 7 : CONCLUSIONS ........ 79**

**REFERENCES ........ 81**

**APPENDICES ........ 90**

Appendix A: Deal and Grove model for the oxidation of silicon ........ 90
Appendix B: XRD spectra ........ 93
Appendix C: FTIR spectra ........ 94
Appendix D: Calibration curves ........ 95
Appendix E: Copper ion concentration, solution pH and amount of hydrogen gas evolved as a function of time ........ 97
Appendix F: Calculation for the amount of hydrogen generated ........ 99
Appendix G: Publications resulting from this research ........ 101

## LIST OF FIGURES

Figure 2-1 Typical detonator construction (Ricco, 2005) ....7

Figure 2-2 Potential-pH equilibrium diagram for the system of silicon and water at 25 °C (constructed using some of the equilibrium equations presented by Pourbaix, 1966)....25

Figure 4-1 DRIFT spectra of neat silicon surface and silicon powders treated with cyclohexane solutions of silanes (10% A172 and 14% A1100 respectively) .. ....49

Figure 4-2 TG mass loss of neat and silane-coated silicon in a nitrogen atmosphere....52

Figure 4-3 Effect of pH on the hydrogen evolution rate from the neat silicon powder dispersions ....53

Figure 4-4 Amount of hydrogen gas produced after 1 h of exposure to distilled water for alcohol-treated or silane-coated silicon powders ....54

Figure 4-5 DTA characterisation of 20 wt % Si – 80 wt % $PbCrO_4$ pyrotechnic compositions in a nitrogen atmosphere and at a temperature scan rate of 50 °C/min....55

Figure 5-1 Amount of hydrogen gas produced in 1 h from silicon powders heated for 4 h at varying temperatures and submersed in distilled water with a solid:liquid ratio of 1:2.5 ....58

Figure 5-2 DRIFT spectra of silicon powder surfaces heat treated at various temperatures....59

Figure 5-3 Variation of maximum absorbance of the Si–O-Si band (1000–1300 $cm^{-1}$) with pretreatment temperature....60

Figure 5-4 TGA curves for neat silicon and silicon treated at 550 °C when heated in an oxygen atmosphere ....61

Figure 5-5 Amount of unreacted silicon present after thermal treatment at various temperatures based on TGA and ICP analysis ....62

Figure 5-6 FIB-SEM images showing the cross-section of milled neat silicon particles (a), as well as silicon particles heat treated at (b) 150 °C, (c) 250 °C, (d) 350 °C, (e) 450 °C and (f) 550 °C respectively....65

Figure 5-7 Particle size distribution of neat silicon....65

Figure 5-8 DTA characterisation of 20 wt% Si (preheated at different temperatures) – 80 wt% $PbCrO_4$ pyrotechnic compositions in a nitrogen atmosphere and at a temperature scan rate of 50 °C/min ....66

Figure 5-9 Variation of ignition temperature with silicon powder pretreatment temperature ....67

Figure 5-10 Comparison between the energy output from a 20 wt% Si (preheated at different temperatures) – 80 wt% $PbCrO_4$ pyrotechnic composition and the unreacted silicon available in the powder after preheating at various temperatures....68

Figure 6-1 Amount of $H_2$ gas released in 1 h by silicon powders submerged in 0.1 M metal ion solution ....71

Figure 6-2 The effect of $Cu(NO_3)_2$ concentration on the amount of hydrogen evolved in 1 h of exposure....72

Figure 6-3 Copper ion concentration, solution pH and amount of hydrogen gas evolved as a function of time for Si powder dispersed in 0.04 M $Cu(NO_3)_2$ and ultrasonically agitated....73

Figure 6-4 Rate of hydrogen evolution when silicon is dispersed in 0.04 M solutions of copper, as well as in distilled water....74

Figure 6-5 DRIFT spectra of silicon powders exposed to different copper metal solutions....76

Figure 6–6 DTA signals of 20 wt % Si (immersed in 0.1 M copper solutions) + 80 wt % $PbCrO_4$ pyrotechnic compositions in a nitrogen atmosphere and at a temperature scan rate of 50 °C/min....77

Figure A–1 Model of the oxidation of silicon....90

Figure E-1 Copper ion concentration, solution pH and amount of hydrogen gas evolved as a function of time for Si powder dispersed in 0.04M $CuCl_2$ and ultrasonically agitated....97

Figure E-2 Copper ion concentration, solution pH and amount of hydrogen gas evolved as a function of time for Si powder dispersed in 0.04M $CuSO_4$ and ultrasonically agitated....98

## LIST OF TABLES

Table 1-1 Lower explosion limit (LEL) and upper explosion limit (UEL) of selected fuels in air ..... 2

Table 1-2 Summary of some major explosives industry accidents that have occurred over the past 20 years ..... 3

Table 3-1 Commercial silanes used for the surface treatment of the silicon powder ..... 39

Table 3-2 Minimum surface coverage of the silanes used and the percentage silane required to coat 100 g of silicon with a surface area of 9.68 $m^2/g$ ..... 40

Table 3-3 List of metal salts used as inhibitors ..... 45

Table 4-1 XPS results for surface properties of raw silicon and silicon treated with a theoretical amount of silane for monolayer coverage ..... 50

Table 6-1 Amount of Cu deposition on Si after immersion in 0.1 M $Cu^{2+}$ salt solutions ..... 75

Table 6-2 Open-flame burn characteristics of 44% Si–$BaSO_4$ pyrotechnic composition prepared using silicon powders aged for different time lengths ..... 77

Table 6-3 DTA reactivity of the pyrotechnic compositions prepared with silicon powders treated with different metal salt solutions ..... 78

## LIST OF SCHEMES

Scheme I Overall silicon oxidation reaction with water ........ 1

Scheme II Overall silicon oxidation reactions corresponding to the dissolved oxygen and hydrogen cathodic reactions ........ 26

Scheme III Electrochemical model for the oxidation of silicon in neutral aqueous medium ........ 26

Scheme IV Schematic of bonding mechanism of silane to silicon surface before and after condensation (Zhu & Van Ooij, 2003) ........ 32

Scheme V Inhibition action of sulphites and hydrazine as scavenging inhibitors reducing the amount of dissolved oxygen ........ 35

Scheme VI Generalised reaction scheme for the reaction of silicon with metal ions ..... 36

Scheme VII Two-step local element reaction mechanism proposed by Jeske *et al*. (1995) and Kanungo *et al*. (2010) for silicon interacting with metal ions ........ 37

Scheme VIII Oxidation of silicon in oxygen atmosphere ........ 60

Scheme IX Reaction of HF with $SiO_2$ ........ 62

Scheme X Mechanism proposed by Bahruji *et al*. (2009) for the thermal passivation of silicon by dehydration of silanol groups at the surface ........ 69

## ABBREVIATIONS

| | |
|---|---|
| ATR | Attenuated total reflection |
| BET | Brunauer–Emmett–Teller |
| DRIFT | Diffuse reflectance infrared Fourier transform analysis |
| DTA | Differential thermal analysis |
| FCC | Face-centred cubic (structure) |
| FIB-SEM | Focus ion beam – scanning electron microscopy |
| FTIR | Fourier transform infrared (spectrometer/spectroscopy) |
| HF | Hydrofluoric acid |
| ICP-OES | Inductively coupled plasma optical emission spectrometer/spectroscopy |
| LEL | Lower explosion limit |
| PETN | Pentaerithritol tetranitrate |
| PSD | position sensitive detector |
| RDX | Cyclotrimethylene trinitramine |
| SHE | Standard hydrogen electrode |
| TEOS | Tetraethyl orthosilicate |
| TG/TGA | Thermogravimetric analysis |
| TNT | Trinitrotoluene |
| TPB | Tammann–Pilling–Bedworth |
| UEL | Upper explosion limit |
| UV-Vis | Ultraviolet – visible spectrometer |
| XPS | X-ray photoelectron spectroscopy |
| XRD | X-ray diffraction |

UNIVERSITEIT VAN PRETORIA
UNIVERSITY OF PRETORIA
YUNIBESITHI YA PRETORIA

# CHAPTER 1 : INTRODUCTION

## 1.1 Introduction

Silicon powder has found extensive use as fuel in pyrotechnic compositions (Koch & Clement, 2007). Of special interest is its use in mine detonator time delay compositions (Ricco *et al.*, 2004; Koch & Clement, 2007). Several oxidants have been shown to be compatible with silicon for compositions of this purpose (Ricco *et al.*, 2004). These delay elements are currently manufactured by pressing the pyrotechnic composition into aluminium tubes. The automated filling and pressing process requires powders with good free-flow behaviour. Spray drying of slurries is an appropriate method for obtaining such free-flowing granules as it creates almost perfectly spherical particle agglomerates (Chan *et al.*, 1996). In addition to the acceptable flow properties, this process also yields well-mixed compositions from dispersions containing different powders and provides control over the agglomerate particle size distribution. The spray-drying process requires that the silicon fuel and other constituents be slurried in water (Chan *et al.*, 1996; Morgan & Rimmington, 2010). This creates a potential hazard situation as water reacts dissociatively with silicon to form $SiO_2$ and hydrogen gas (Boonekamp *et al.,* 1994). The overall reaction is given in Scheme I:

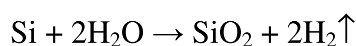

$$Si + 2H_2O \rightarrow SiO_2 + 2H_2\uparrow$$

**Scheme I Overall silicon oxidation reaction with water**

The evolved hydrogen presents an explosive hazard during the production process. $H_2$ + air gas mixtures can support deflagration in the concentration range 4–75% (volume hydrogen fuel basis) (Carcassi & Fineschi, 2005). Hydrogen has one of the broadest explosion limit ranges with air and comes second only to acetylene of all flammable gases. Table 1-1 shows a comparison of the lower and upper explosion limits for selected flammable fuels (Kirchsteiger *et al.*, 2007). Not only does hydrogen have a broad explosion limit range, but it is also easy to ignite, requiring 14 times less energy than natural gas (Lovins, 2003).

**Table 1-1** Lower explosion limit (LEL) and upper explosion limit (UEL) of selected fuels in air

| Substance | Lower Explosion Limit (%) | Upper Explosion Limit (%) |
|---|---|---|
| Hydrogen | 4.1 | 74.8 |
| Methane | 5.0 | 15.0 |
| Diesel fuel | 0.6 | 7.5 |
| Gasoline | 1.4 | 7.6 |
| Acetylene | 2.5 | 82.0 |

Statistics on hydrogen events/incidents are not readily accessible, although there is a significant amount of hydrogen hazard information available in the literature (Kirchsteiger *et al*., 2007). Some of the major causes of hydrogen-related incidents are:

- Undetected leaks
- $H_2$-$O_2$ off-gas explosions
- Piping and pressure vessel ruptures

Lovins (2003) reports that the hydrogen industry has an enviable safety record spanning over half a century. This is attributed to an assortment of design safety measures such as adequate ventilation and air extraction systems, as well as leak detectors and alarms. Some natural properties of hydrogen, such as low density and high diffusivity in air, cause hydrogen to disperse rapidly upwards and away from the source of the leak. This aids in preventing a build-up of hydrogen concentration to explosive limits.

The safety record in the explosives manufacturing industry is not so enviable. Table 1-2 gives a summary of some of major explosive accidents that have happened all over the world in the past two decades. The added risk presented by possible hydrogen incidents within an explosives plant might result in a higher frequency of already devastating explosives industry accidents.

**Table 1-2** Summary of some major explosives industry accidents that have occurred over the past 20 years

| Year | Place | Cause | Consequences | Reference |
|---|---|---|---|---|
| 1991 | Liaoning Province, China | Explosion at a TNT workshop of a chemicals factory | 17 deaths, 107 injured. All buildings within a 600 m radius destroyed | Guoshun (2000) |
| 1996 | Hunan Province, China | Explosion accident during mixed RDX high-explosive production | 134 deaths, 117 injured. 140 houses completely destroyed, 605 seriously damaged | Guoshun (2000) |
| 1998 | Nevada, US | Explosion of TNT and PETN high explosive during booster production | 4 workers killed, 6 injured. Plant completely destroyed, 21.3 tons of explosives consumed | CBS (2004) |
| 2000 | Enschede, Netherlands | A fire broke out in the plant igniting the stored fireworks | 22 people killed and over 900 injured. The plant and 600 homes completely destroyed | Adams *et al.* (2009) |
| 2005 | Kitwe, Zambia | Unknown causes in an explosives manufacturing factory | 37 killed, 3 injured. Entire factory damaged | Xinhuanet (2011) |

## 1.2 Aims and Objectives

The aim of the present study was to find ways to minimise the evolution of hydrogen by aqueous dispersions of a commercial silicon powder. Several approaches were used. The first approach was to investigate the effect of organic surface modifications and medium pH on the rate of corrosion of silicon. Organic surface modification was carried out using alcohols and silanes.

The second approach involved establishing the effect of heat treating the commercial silicon powder in air at varying temperatures on the rate of hydrogen evolution by aqueous dispersions. Characterisation of the Si powders was carried out, and the extent of induced surface oxidation was calculated. The effect of surface oxidation on the burn behaviour of a silicon-based pyrotechnic composition was also studied by differential thermal analysis (DTA).

The final approach focused on determining the effect of introducing an additional cathodic reaction to that of water reduction, by means of adding metal salts in solution, on the rate of hydrogen evolution. The minimum concentration for the best-performing metal salt was determined and the effect of these solutions on the reactivity of the silicon fuel in pyrotechnic compositions was also investigated.

### 1.3 Outline of Dissertation

The dissertation is structured in seven chapters. An outline of each of these chapters is given below.

*Chapter 1* gives an introduction to the problem, showing the practical application of the silicon powder being investigated and why the powder has to be dispersed in an aqueous medium resulting in formation of hazardous hydrogen. A general overview of hydrogen and explosives industry-related accidents and incidents is also given.

*Chapter 2* presents the literature review and is broken down into three main sections. The first section outlines the use of pyrotechnics as a means of imparting delays in detonator set-ups; it also gives an overview of the importance of silicon in pyrotechnics. An outline of some of the different methods used to produce the actual delay elements is given. The second section of the review focuses on the theory of corrosion in metals and how it links with corrosion in semi-conductor silicon material. The corrosion mechanisms and corrosion kinetic models for air and water oxidation of silicon are also reviewed. The last section of the chapter reviews the different methods used to inhibit corrosion in general and in silicon in particular. The main methods are barrier protection and manipulation of the environment in which the material is corroding.

*Chapter 3* outlines the materials, experimental procedures and methods, as well as the characterisation techniques and specifications used in each of the three main approaches.

*Chapter 4* presents the results and discusses the approach in which the use of organic coating of silicon was investigated, as well as the effect of varying pH on the rate of hydrogen evolved from silicon dispersions in an aqueous medium.

*Chapter 5* reports the results and discusses the effect of heating silicon in air at varying temperatures on the rate of hydrogen evolution when this silicon is dispersed in water.

*Chapter 6* presents the results and discusses the introduction of metal salt solutions as additional cathodic reactions to that of water reduction.

*Chapter 7* presents the overall conclusions and recommendations for the three different approaches and how they compare with each other.

# CHAPTER 2 : LITERATURE REVIEW

## 2.1 Introduction

Pyrotechnics is described as the science of using materials capable of undergoing self-contained and self-sustained exothermic chemical reactions in the absence of atmospheric oxygen, producing heat, light, gas, smoke, sound or pressure, depending on the choice of reactants (McLain, 1980). Pyrotechnic compositions have numerous uses in both military and civilian applications, such as flares, fireworks, tracers, smokes, gas generators and ignition sources, as well as time delays (McLain, 1980; Danali *et al*., 2010). The time delay compositions are used to impart delays in blasting caps, fuses and initiators of various types, such as squibs, detonators and primers. To generate such effects, most pyrotechnic compositions contain at a minimum one fuel (reducing agent) and one oxidiser which are capable of producing a highly exothermic, self-propagating oxidation–reduction reaction. Complementary ingredients such as binders, burn rate modifiers, colorants and processing aids may also be used (Berger, 2005). The pyrotechnic redox reactions take place in one of the following reaction states: solid–solid, solid–liquid or solid–gaseous, producing solid, liquid and gaseous reaction products (McLain, 1980; Berger, 2005).

### 2.1.1 Delay elements

In many explosive applications such as the blasting of an ore rock surface, or the demolition of an old high-rise building and other commercial applications of explosive charges, it is advantageous if the detonators are fired in a predetermined order rather than being fired simultaneously. This results in reduced vibrations and greater fragmentation, and thus leads to greater effectiveness of the blast (Ellern, 1968). This effect is achieved by using delay elements, which are essentially components that provide a specified delay between actuation and ignition (Answers, 2011).

There are two main classifications of delay elements: electronic and pyrotechnic delays. Electronic delays achieve the desired time delay through the use of wiring circuits or a programmed microchip with a timing circuit which is placed within the detonator. Electronic devices are generally more precise and more accurate than chemical pyrotechnic delays but they are considerably more expensive (Ricco, 2005). Pyrotechnic

delay elements, on the other hand, use a pyrotechnic composition to provide a time delay. These elements are generally simpler, more rugged, cheaper and do not require a power source. They also feature a higher degree of inherent safety compared with electronic elements (Danali *et al.*, 2010).

Delay detonators consist of a metallic shell which is closed at one end and contains the following sequence of material starting from the delivery end: a base charge of a detonating high explosive, such as pentaerithritol tetranitrate (PETN), followed by a primer charge of heat-sensitive detonable material, such as lead azide or lead styphnate, and then the burning pyrotechnic composition which provides the desired time delay (Davitt & Yuill, 1983; Beck & Flanagan, 1992). The delay composition in the detonator can be ignited by one of the following mechanisms; ignition using an electrically heated bridge wire or by the heat and flame of a low energy detonating cord or shock wave conductor (Davitt &Yuill, 1983; Beck & Flanagan, 1992). Figure 2-1 shows the typical detonator construction.

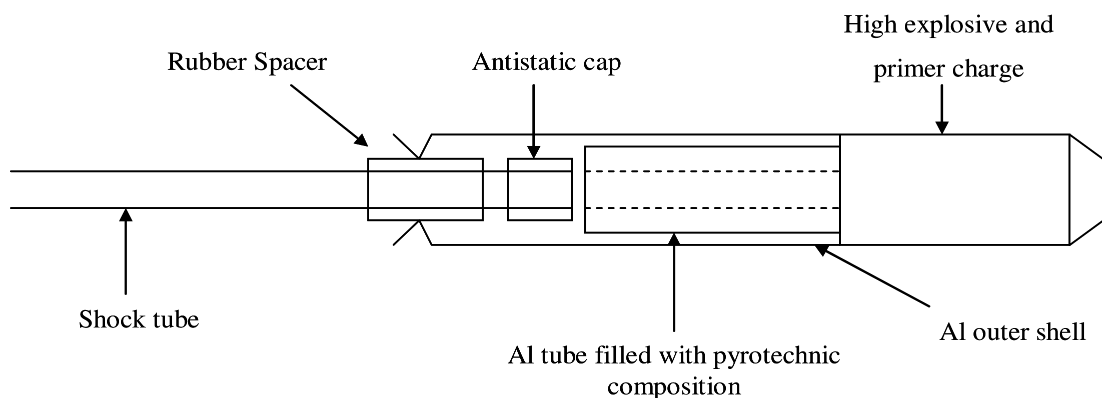


**Figure 2-1** Typical detonator construction (Ricco, 2005)

### 2.1.2 Delay compositions

The mixtures used for delay elements contain an easily oxidised element, often a finely divided metal, together with an oxy-salt or an easily reduced metal oxide (Fordham 1980). These react and form solid, liquid and in some cases gaseous products. In time delay applications gas production is deemed a problem and it is desirable to have gasless compositions which enhance reproducibility of burning rate in sealed assemblies (McLain, 1980; Kosanke *et al*., 2004).

According to McLain (1980), black powder was used as the first form of time delay as early as the 7th century and continued as the prime delay composition right up to the beginning of the Second World War. However, modern requirements for high levels of performance reliability and reproducibility under a wide range of environmental conditions resulted in the development of a multiplicity of gasless delay compositions (Kosanke *et al*., 2004). Bennett and Baltimore (1949) then developed the Ni–$KClO_4$ composition, followed by McLain & Ruble (1953) who developed a mixture of $Pb_3O_4$ with Mn and Si; this became the basis for the development of a large number of delay compositions over the past half-century. Gasless delay detonators are being manufactured to fire after pre-arranged delay times ranging from 20 ms to 10 s, depending on the composition and length of the delay column.

The combustion event in the column was found to be governed by a number of parameters. The thermal diffusivity of the mixture is one of the most important parameters since wave propagation is dependent on the repeated re-ignition of adjacent layers along the burning path (McLain & Mayer, 1943). Good mixing and adequate particle-particle contact between reactants is a prerequisite for stable and reproducible burning owing to the low values of diffusion coefficients. Khaikin and Merzhanov (1966) proposed the simplest theory relating burn rate to the physical properties of the mixture. The theory assumes composition and temperature-independent physical properties, a thin reaction zone and a gasless exothermic $n^{th}$ order solid-state reaction:

$$\frac{dx}{dt} = k(1-x)^n \tag{2-1}$$

The nth order solid-state reaction has an Arrhenius-type temperature dependence for the rate constant:

$$k = k_0 e^{E/RT} \tag{2-2}$$

The resulting relationship of the burn velocity to the physical properties of the system is shown in Equation 2-3.

$$v = \sqrt{\frac{\lambda k_0 R T_c^2}{\rho E \Delta_R g(n)} \exp^{E/RT_c}} \tag{2-3}$$

where
v = burn rate (m/s)

λ = thermal conductivity (W/m K)

R = gas constant (8.314 J/mol K)

$T_c$ = maximum temperature of the burning column (K)

E = Apparent Arrhenius activation energy (J/mol)

ρ = density ($kg/m^3$)

$\Delta_R$= heat of reaction (J/kg)

k = rate constant (1/s)

$k_o$ = pre-exponential factor (1/s)

g (n) = a weak function of the reaction order n which varies between 1 and 2

McLain & Mayer (1943) showed that cross-sectional area and packing density have an effect on the burn rate. This confirmed the planar layer-by-layer re-ignition mechanism of the reaction. The addition of material with low thermal conductivity was shown to reduce the rate of heat transfer and hence slow down the rate of reaction. Addition of thermally conductive fine powders, such as Cu and Al, was shown to increase the burn rate (Ricco *et al.,* 2004).

The stoichiometry, heat of reaction and burn rate in pyrotechnic delay compositions are interrelated (Berger, 2005). Pressure also has an influence on the burn rate of delay compositions. It is essential that detonators have accurate and predictable delay times to enable good blasting procedures. To minimise the effect of pressure on the burn rate, it is

important for the delays to seal well, since variation in effectiveness of the seal will affect the delay time.

Some of the other parameters that are important when designing a pyrotechnic delay are (McLain, 1980; Kosanke, 2004):

- Fuel/oxidiser ratio
- Mix homogeneity
- Particle sizes of the constituent powders
- Loading method and pressure
- Size and chemical nature of guest particles
- Adsorbed gases on particle surfaces
- Temperature and type of ignition
- Mix type – low gas or gassy
- Humidity during mixing and loading

### 2.1.3 Delay element manufacture

Delay compositions are not normally pressed directly into the delay element shells due to the irregular delay times that would result from the relatively low compression achieved. Two main methods are generally used in manufacturing delay elements (Fordham, 1980):

- Pressing delay compositions into preformed zinc, brass or aluminium tubes. These tubes are a sliding fit into the detonator shell and are thick enough to withstand the consolidating heavy pressure (rigid elements).
- Filling a lead tube with the pyrotechnic composition and drawing it down in diameter by conventional means. The required length of tube is then cut off. The process of drawing down the lead tube results in compaction of the composition.

There is a desire to phase out the use of the drawn-lead containment due to the poisonous nature of lead. The use of drawn elements of other metals, such as Al, is being promoted but more emphasis is being put on rigid elements (Beck & Flanagan, 1992). Regardless of the method used to produce the final element, the pyrotechnic composition has to be made in such a way that it is well mixed and is in free-flowing form. This allows easier filling of elements. The traditional method involves mixing the fine powders and then pelletising them. The formed pellets are subsequently broken down and sieved to

remove the fines, resulting in free-flowing granules. In cases where the mixture is difficult to pelletise, the mixture is granulated with a small amount of nitrocellulose solution in a suitable mixer (Fordham, 1980).

Chan *et al.* (1996) and Morgan & Rimmington (2010), however, show that a shift from the traditional sieving method to spray drying is taking place in some production processes. In this process, a solid fuel, a solid oxidiser and water are mixed together to form an aqueous slurry. The aqueous dispersion is passed through a spray nozzle, forming a stream of droplets which is contacted with hot air, thus removing the water. The process produces well-mixed, spherical, free-flowing pyrotechnic powder agglomerates. In addition, spray drying provides control over the agglomerate particle size distribution. It is important that the spray-dried particles have a high integrity so that they do not disintegrate easily; it is therefore standard practice to add binding agents into the aqueous dispersion before spraying (Berger, 2005). The binder type and content influence both the heat of reaction and rate of reaction of the pyrotechnic reaction (Berger, 2005; Morgan & Rimmington, 2010).

### 2.1.4 Silicon as a pyrotechnic fuel

Silicon is one of the most widely used fuels in pyrotechnic time delay compositions. Different grades and particle sizes may be used, with the burn rate being commonly controlled by the choice of oxidant. Ellern (1968), Rugunanan (1991) and Ricco *et al.* (2004) showed that oxidants such as barium sulphate ($BaSO_4$), red lead ($Pb_3O_4$), copper antimonite ($Cu(SbO_2)_2$, lead chromate ($PbCrO_4$), bismuth oxide ($Bi_2O_3$), etc. can all be used in conjunction with silicon. Ricco (2005) states that silicon is good for delay compositions as it is reasonably energetic and forms slags that have good heat-retaining properties.

Silicon is chemically abundant on the earths' surface and is found mainly as silica ($SiO_2$) in the form of quartz or sand. Pure silicon is obtained by the chemical reduction of silane or by the electrolytic decomposition of molten mixtures of $K_2SiF_6$–LiF–KF or $SiO_2$–$Na_3AlF_6$ (Rugunanan, 1991).

Clean silicon surfaces are hydrophobic and their wetting properties are dependent on the thickness of the native oxide film that forms spontaneously on exposure to air.

Williams & Goodman (1974) showed through contact angle measurements that an oxide thickness of ≥ 3 nm is required for complete wetting. They also showed that powders without a well-developed oxide surface will not disperse in water without the use of a surfactant.

Silicon hydrolysis in water causes processing difficulties as a result of the hydrogen gas evolved during the exothermic reaction (Williams & Ezis, 1983) shown in Scheme I:

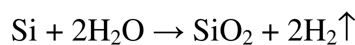

$$Si + 2H_2O \rightarrow SiO_2 + 2H_2\uparrow$$

**Scheme I** Silicon hydrolysis in water

The standard reduction potential E = -0.888V vs. SHE for silicon hydrolysis implies that silicon powder hydrolyses spontaneously when immersed in aqueous media. Hackley *et al.* (1997) reported the explosive evolution of hydrogen gas during wet milling of silicon. The evolved hydrogen presents an explosive hazard during the production process. $H_2$ + air gas mixtures can support deflagration in the concentration range 4–75% (volume hydrogen fuel basis) (Carcassi & Fineschi, 2005).

## 2.2 Oxidation of Metals

Metallic corrosion is described by West (1980) as the wastage that occurs when metals are exposed to reactive environments. According to Pourbaix (1966), virtually all metals are thermodynamically unstable in air or in aqueous solutions. Thus they corrode and transform into substances similar to the mineral ores from which they are originally extracted, e.g. oxides, sulphates or carbonates (Pourbaix, 1973).

Metals, however, find extensive applications because many of them form protective oxide films on the surface which retard and in some cases prevent oxidation altogether. Oxidation is not confined to metals but also occurs on surfaces of semiconductor materials (Fromhold, 1976). The general principles of metal oxidation are similar to those of semiconductor oxidation; however, some complexities arise due to the lower conductivity of semiconductors relative to metals (Fromhold 1976).

The mechanism by which oxidation and corrosion take place in metals is well established (Evans, 1971). The mechanism of metal oxidation at temperatures higher than 200 ℃ involves predominantly the reaction of metals and dry air. At these conditions corrosion is governed by the ionic conducting properties of the corrosion product. At temperatures where water is still a liquid and at room temperature, the corrosion mechanism is mainly an electrochemical process which results in anodic metal dissolution. This corrosion process is determined by the electrochemistry, heterogeneous electrode kinetics and influences of temperature, pH, concentration and properties of surface films, as well as the geometry of the corroding part (West, 1980).

The feasibility of an oxidation reaction taking place can be predicted by evaluating the Gibbs free energy of the system using the equation:

$$\Delta G = \Delta H - T\Delta S \tag{2-4}$$

where
$\Delta G$ = change in free energy
$\Delta H$ = change in enthalpy
$T$ = temperature
$\Delta S$ = entropy change

The criterion required for spontaneous oxidation reaction to occur is that the free energy of the system must decrease, i.e. $\Delta G < 0$.

The usefulness of chemical thermodynamics in corrosion taking place in an aqueous medium is meagre (Pourbaix, 1973). This is because the corrosion in the aqueous state is not only chemical but also electrochemical. In addition, corrosion is not an equilibrium process, the kinetics of the reaction is not accounted for and the anodic and cathodic reactions are completely different in nature (Lefrou *et al.*, 2010). In cases where corrosion is electrochemically determined and charged species are involved, the free energy expression is modified to include the electrical potential term to become:

$$\Delta E^{o} = \frac{\Delta G^{o}}{nzF} \qquad (2\text{-}5)$$

where

z = number of charges per ion

n = number of ions

F = Faraday's constant

Some electrochemical reactions are also dependent on the influence of pH on the system. The pH dependence arises naturally when the $\prod[\text{Products}]$ term in the Nernst equation (Equation 2-6) includes the concentration of $H^+$ ions. As such, thermodynamic information describing the onset of different metal transitions is used to develop the potential-pH diagrams. These diagrams are also referred to as the Pourbaix diagrams and indicate the various domains in which a metal is passive, immune or susceptible to corrosion (Evans, 1971).

$$\Delta E^{cell} = \Delta E^{O} + \frac{0.059}{n} \log \frac{\prod_i [\text{Products}]}{\prod_i [\text{Reactants}]} \qquad (2\text{-}6)$$

where

$\Delta E^{cell}$ = overall cell potential

$\Delta E^{o}$ = standard cell potential

$n$ = number of electrons transferred

$\prod[\text{Products}]$ = product of concentration of products

$\prod[\text{Reactants}]$ = product of concentration of reactants

### 2.2.1 Early metal corrosion theories

Various theories have been put forward in a bid to explain metal oxidation. They are all essentially governed by the nature of the oxide film that is formed on the surface of the metals (Leach, 1975). The oxide films may be present as physisorbed layers, chemisorbed layers and layers of recognisable 'oxide' which are one or two layers in thickness (Leach, 1975). The nature of the layer on the metal surface is dependent on the rate of oxidation (Benard *et al.*, 1959 quoted by Leach, 1975). In most practical situations oxides form

rapidly, usually under non-equilibrium conditions, resulting in films that tend to be thin and non-crystalline. At lower rates of oxide formation the resultant films are continuous and crystalline, and they form under near-equilibrium conditions. There are conflicting views on which particular type of oxide confers passivity to a metal. Cohen (1959) stated that thick multilayered oxides are required for passivity. Frankenth *et al*. (1967 quoted by Leach, 1975), on the other hand, argued that only one or two monolayers are required.

The parabolic rate law was one of the earliest metal oxidation models developed. Pilling and Bedworth developed what is now known as the Tammann–Pilling–Bedworth (TPB) parabolic law in the late 1920s (Gulbransen, 1949). This was developed on the basis of diffusion of oxygen through the oxide film. The parabolic law was then subjected to modifications by Wagner in 1938 and Mott in 1948 (Gulbransen, 1949). The basic principles of each of these three variations are presented in the next three subsections.

#### *2.2.1.1 Tammann–Pilling–Bedworth (TPB) parabolic law*

Pilling & Bedworth (1929, quoted by Gulbransen, 1949) postulated that the air oxidation of metals results in an increase in the oxide film thickness (L), which is proportional to the square root of time

$$L \propto t^{\frac{1}{2}} \tag{2-7}$$

They proposed that the atomic diffusion rate of atoms through an existing oxide film is inversely proportional to the thickness of the existing oxide and that it is this diffusion rate that controls the rate of oxide growth $dL/dt$:

$$\frac{dL}{dt} \propto \frac{1}{L} \tag{2-8}$$

The constant of proportionality (k) factors in the diffusion coefficient D and the concentration gradient in the metal–oxide–oxidant interfaces.

$$\frac{dL}{dt} = \frac{k}{L} \tag{2-9}$$

Equation 2-9 was integrated to yield the parabolic growth law for uncharged particles:

$$L(t)^2 - L(0)^2 = 2kt \tag{2-10}$$

The Tammann–Pilling–Bedworth law follows from Fick's laws of diffusion where the particle current (J) is linearly related to the spatial concentration gradient $\left(\frac{\partial C}{\partial x}\right)$:

$$J = -D\frac{\partial C}{\partial x} \tag{2-11}$$

Assuming steady-state conditions with no build-up of concentration with time, $\frac{\partial C}{\partial t} = 0$ and with Fick's second law being

$$\frac{\partial J}{\partial x} = -\frac{\partial C}{\partial t} = 0 \tag{2-12}$$

it shows that J is independent of position x in the film. Fick's first law reduces to

$$\frac{d\,C(x)}{dx} = -\frac{J}{D} = \text{constant} \tag{2-13}$$

Integration of Equation 2-13 gives

$$C(x) - C(0) = -(J/D)\,x \tag{2-14}$$

and for an interface where x = L

$$J = D[C(0) - C(L)]/L \tag{2-15}$$

Since the growth rate is given by

$$\frac{dL}{dt} = RJ \tag{2-16}$$

Substitution of Equation 2-15 into Equation 2-16, followed by the separation of variables and the application of fixed boundary concentrations upon integration yields the parabolic growth law (Equation 2-10).

#### *2.2.1.2 Wagner Parabolic Law*

Wagner (1938, quoted by Fromhold, 1976) presented the Wagner parabolic law which disagreed with the assumption in the TPB parabolic law that metal oxidation occurred as a result of diffusion of uncharged particles. Wagner developed an approach to allow for diffusion of charged particles (metal ions, non-metal ions and electrons). He showed that the particle current relationship could be expressed in the following form of a linear diffusion equation.

$$J = -D\frac{dC}{dx} + \mu EC \qquad (2\text{-}17)$$

This particular type of diffusion equation is commonly used to describe charge transport in ionic conductors and semiconductors. This relationship showed that the flux of each of the species through the oxide film is driven by concentration and electrical potential gradients. In Equation 2-17, E is the electric field, $\mu$ is the mobility and is related to the diffusion coefficient by the Einstein relationship:

$$ZeD = \mu k_B T \qquad (2\text{-}18)$$

where

Z = valence of diffusing species

e = electronic charge magnitude

$k_B$ = Boltzmann constant

T = temperature

C = concentration of diffusing charged defect

Wagner assumed that a charge-neutral oxide is formed during the growth process, and for this to happen he postulated that the number of equivalent positively charged cations moving through the oxide in unit time is equal to that of the negatively charged anions and electrons in that same time. The total charge transported through the film at each point in time is zero. In his theory, Wagner visualised a number of local chemical reactions taking place continuously in each element of volume of the oxide. The reactions in these elemental volumes were considered to be near equilibrium and thus equations of

equilibrium thermodynamics can be used. He acknowledged that there would be gradients in the film and therefore equilibrium relations were considered to be local relations. Upon factoring all his considerations, Wagner's theory eventually results in the parabolic growth law (Fromhold, 1976).

#### *2.2.1.3 Cabrera–Mott theory*

The Cabrera–Mott theory is the most widely used theory in explaining metal oxidation at low temperatures (Cabrera & Mott, 1948). This theory states that a thin oxide on its metal support grows at low temperatures since electronic equilibrium among the gas–oxide and metal–oxide interfaces establishes an electric field in the oxide. This drives oxygen anions through the oxide from the gas–oxide to the metal–oxide interface (Ocal, 1985). The electric field is operative for ion transport only if the potential drop in the unit cell is comparable to the activation barrier for ion diffusion. Oxides containing defects are said to have lower activation energy barriers than perfect oxides. Thus it was assumed by Cabrera and Mott that the injection of a defect into the oxide at the metal–oxide or at the gas–oxide interface is the rate-controlling step (Ocal, 1985). Cabrera & Mott (1948) state that any atom with electron affinity energy large enough to establish the electric field in the oxide should be a candidate for a field-assisted diffusion process.

Cabrera & Mott (1948) postulated that if an oxygen atom approaches the surface of a thin oxide lying on its metallic support, its electron affinity energy (E) moves below the Fermi energy of the metal due to the binding energy (W) of the oxygen at the oxide surface. If $\phi$ is the metal work function, X is the oxide thickness and eV is the energy of the affinity level of the O atom on the oxide surface, referred to as the Fermi level, it is clear that under the condition in which the inequality

$$(E + W) > \phi \tag{2-19}$$

holds, electrons will tunnel from the metal through the oxide film to raise the electron affinity level up to the metal Fermi energy. As a consequence, a plate capacitor is formed with a potential difference (V). This produces an electric field $E = V/X$ that acts as a driving force for anion diffusion through the oxide and that will be effective only if the potential drop in the unit cell is comparable to the activation energy for diffusion (Ocal,

1985). The Cabrera–Mott model is limited to thin films but can be extended to model thicker films by assuming electron transport via thermionic emission or via semiconducting oxides.

## 2.3 Silicon Air Oxidation

### 2.3.1 Oxidation by ionic transport

Wolters & Zeger-van Duynhoven (1989a) showed that the oxidation of silicon in ambient oxygen could be explained using the Wagner classic metal oxidation theory. This described the silicon oxidation mechanism by the transport of ionic and electronic species in an electrochemical cell, $Si|SiO_2|O_2$ (Wolters & Zegers-van Duynhoven, 1989a). Wagner derived an expression for the film oxide growth rate by assuming no net charge transport, i.e. the ionic and electronic currents are equal:

$$J_{ion} = J_{el} = (\sigma_{ion}^{-} + \sigma_{el}^{-1})^{-1} (\frac{1}{zq} \frac{d\mu_{o2}}{dX_{ox}}) \tag{2-20}$$

where

q = electronic charge

$\sigma_{ion}^{-}$ and $\sigma_{el}^{-1}$ = ionic and electronic conductivities respectively

$\mu_{o2}$ = thermodynamic potential of oxygen layer

z = number of charges per ion

During the oxidation of silicon, the cell is enabled by the thermal energy and driven by the concentration gradient of oxygen ions moving between $SiO_2$ towards Si. If there is no electron countercharge movement, the $O^{2-}$ ions charge the silicon negatively and build up an electric field which opposes their further transport, resulting in stoppage of growth of the $SiO_2$ film. However, when electrons escape over the energy barrier at the $Si–SiO_2$ interface, they move to the ambient and lower field (Wolters & Zegers-van Duynhoven, 1989b). In this case ionic transport takes place and oxide growth proceeds.

Mills & Kroger (1973) proved that the growth kinetics of silicon can be enhanced, retarded or even stopped by applying an electric field externally, depending on its magnitude and the direction of the field. They also concluded that the ions are negative

and have a double charge. A potential of -1.78V vs. SHE was found to be required to stop film growth. Modlin & Tiller (1985) argued the validity of the charged species being involved in the thermal oxidation of silicon after having carried out experiments that conflict with those of Jorgenson (1962). Upon rigorous treatment of Equation 2-20 when applied to silicon oxidation, the classic Wagner expression describing parabolic growth is obtained (Wolters & Zegers-van Duynhoven, 1989a):

$$\frac{dX_{ox}}{dt} = \sigma_{ion} X_{ox}^{-1} \Delta\mu_{o2} \qquad (2\text{-}21)$$

### 2.3.2 Silicon air oxidation kinetics

The oxidation kinetics of metals is reported to have two types of limiting oxidation mechanism (Cabrera & Mott, 1948):

- The oxide thickness is small in comparison with the extent of possible space-charge regions within the oxide, and the oxidation kinetics is strongly influenced by the space charge or by a voltage drop across the oxide film due to contact.
- The rate of diffusion of either the oxidising species or the metal across the oxide film determines the oxidation kinetics. The driving force for diffusion usually becomes smaller with an increase in thickness and this particular condition leads to a parabolic relationship.

The dry oxidation of silicon has an extremely slow oxidation rate. At 870 °C, oxidation of (100) Si covered with a 300 Å oxide film was found to be about 0.016 Å/s (Hopper *et al.,* 1975). This slow rate is reportedly caused by the low solubility of oxygen into the silica film. The silicon oxide growth rate in the presence of water at high temperatures is reported to be higher due to the higher solubility of water in silica (Wolters & Zegers-van Duynhoven, 1989b).

#### *2.3.2.1 Parabolic law*

Early results obtained from the oxidation of silicon showed that the rate of silicon oxidation in both oxygen and steam decreases with increasing time (Irene & Van der Meulen, 1976). As a result, most data on silicon oxidation kinetics have been evaluated using the parabolic rate law (Deal & Grove, 1965; Irene, 1978):

$$X_{ox}^2 \propto t \quad (2\text{-}22)$$

This law asserts that there is a decrease in the rate of increase of film thickness with time. The oxidation kinetics in this type of model is transport limited as deduced from the phenomenological diffusion equation, Fick's first law. The parabolic law was, however, found to be applicable only to thick oxide films (Irene, 1978). It has been argued that although the parabolic law and other purely mathematical functions may fit silicon oxidation data well, little understanding of the silicon oxidation phenomenon is gained through use of arbitrary data-fitting functions (Irene, 1978).

#### *2.3.2.2 Linear-parabolic law*

Deal & Grove (1965) established that both the parabolic and the power rate laws do not model precisely the oxidation of silicon. However, they reported that silicon oxidation by oxygen or water (steam) oxidant followed a linear-parabolic law which is generally expressed as

$$A X_{ox} + B X_{ox}^2 = t \quad (2\text{-}23)$$

where
$X_{ox}$ = thickness of the oxide film at a time (t)
A and B = reciprocals of the linear and parabolic rate constants respectively

An expanded form of the linear-parabolic model used when fitting silicon oxidation data is given by the form

$$t - t_0 = \frac{1}{k_{LIN}}(d - d_0) + \frac{1}{k_{PAR}}(d^2 - d_0^2) \quad (2\text{-}24)$$

where
t and d = time of oxidation and $SiO_2$ and film thickness respectively
$t_0$ and $d_0$ represent the upper bound of the initial oxidation regime that does not conform to the linear-parabolic kinetics
$k_{LIN}$ and $k_{PAR}$ = linear and parabolic rate constants respectively (Irene, 1978).

The rate constants of both the parabolic and linear regimes were found to be at least an order of magnitude larger when water (steam) acts as the oxidant as compared with oxygen (Deal & Grove, 1965). The linear-parabolic mode of oxidation is, however, preceded by a more rapid oxidation regime (Deal & Grove, 1965; Nakayama & Collins, 1966). The oxidation of silicon in the presence of oxygen and steam was found to be related to surface kinetics through the linear rate constant, $k_{LIN}$, and to diffusional kinetics through the parabolic constant, $k_{PAR}$ (Irene & Ghez, 1977). The oxidation mechanism at low temperatures is predominantly surface controlled while that of high temperatures is diffusion controlled (Kamins & MacKenna, 1971). The derivation of this law is shown in Appendix A.

The initial linear regime for silicon oxidation in dry oxygen displays a higher oxidation rate than the linear-parabolic mode, suggesting that the $SiO_2$ films produced by ultra-dry oxygen are less protective than films grown in water (steam) containing ambient oxygen.

Irene & Ghez (1977) reported that the effect of $H_2O$ (g) on the $SiO_2$ film oxidation kinetics is reversible, i.e. the oxidation kinetics of an oxide growing in $H_2O$ containing ambient oxygen reverts to dry oxidation kinetics soon after the wet ambient oxygen is switched to dry ambient oxygen. The greater protective effect of wet-grown thin oxides appears to be related to a stable form of OH in the $SiO_2$ (Irene, 1978 quoting Lee, 1964). This is, however, in contrast with the findings of Irene & Ghez (1977), who report that water has two effects on the kinetics of silicon oxidation: the water acts as an oxidant source converting Si to $SiO_2$; and the water also alters the $SiO_2$ by loosening the $SiO_2$ network, resulting in increased diffusion of other oxidant species. The loosening process is said to occur through formation of Si–OH groups and is reversible.

Although the Deal and Grove linear-parabolic model has become the standard silicon oxidation model, several shortcomings of this model have been pointed out by a number of authors, as follows:

- The linear-parabolic model fails to give a clear explanation for the initial part of the oxidation curve (Wolters & Zegers-van Duynhoven, 1989c).

- The model does not give details of the mechanism on nanoscale to submicron scale, with observed oxidation rates being considerably higher than the model predictions (Kim *et al.,* 1996).
- The rate constants have no physico-chemical interpretations (Wolters, 1980).
- The model assumes a first-order chemical reaction, i.e. $k_{PAR} / k_{LIN} \; \alpha \, P_{H2O}$, while experiments (Kim *et al*., 1996) show $k_{PAR} / k_{LIN} \; \alpha \sqrt{P_{H2O}}$ .
- The reaction-diffusion model cannot explain the 2-D effects in oxidation (Wolters & Zegers-van Duynhoven, 1989a).

#### *2.3.2.3 Power law*

Contrary to earlier postulations (Deal & Grove, 1965 quoting Fuller & Strieter, 1964) that the power law does not model silicon oxidation accurately, Wolters & Zegers-van Duynhoven (1989a quoting Reisman *et al*., 1987 and Blanc, 1987) found silicon oxidation kinetics to be more precisely described by the power law rather than the linear-parabolic expression. They argue that when the power law

$$t = k\, X_{ox}^{n} \tag{2-25}$$

where n and k are complex functions of temperature, pressure and oxide thickness (Deal and Grove, 1965 quoting Fuller and Strieter, 1964)

is expanded,

$$t = \tau + \frac{A}{B} X_{ox} + \frac{1}{B} X_{ox}^{2} + \ldots\ldots\ldots\ldots \tag{2-26}$$

The first three expressions in the series are similar to those in the linear-parabolic rate law and the linear-parabolic rate constants are substitutes for the coefficients of the series expansion. However, Wolters & Zegers-van Duynhoven (1989a) show that contrary to the linear-parabolic assumption that the processes of diffusional transport, interfacial reaction and fast initial growth are independent, a plot of the power law coefficients $\tau$ versus $A/B$ or $1/B$ shows interdependency between the processes, which is accounted for in the power law model.

#### *2.3.2.4 Logarithmic law*

Cabrera and Mott (1948) suggested that growth kinetics can be modelled with a logarithmic model which arises from the ability of electrons to tunnel through thin films of oxide where they associate with molecular oxygen and form oxygen ions. A field is formed across the oxide which allows ready diffusion of ions and the oxide grows according to the equation

$$X_{ox} = k \ln\left(\frac{t}{\tau} + 1\right) \tag{2-27}$$

where

$X_{ox}$ = oxide film thickness

t = time

k and $\tau$ = constants

As the oxide thickness grows, the field drops and the growth rate drops and this results in limited growth of the film. The corrosion rate is thus related to the rate of dissolution of the oxide film under the prevalent aqueous conditions of the silicon (Leach, 1975).

## 2.4 Silicon Water Oxidation

The corrosion of silicon, like that of metals, is usually electrochemical in nature when the silicon comes into contact with water or aqueous solutions. Pourbaix (1966) reported silicon as being one of the most powerful non-metal reducing agents.

### 2.4.1 Eh–pH diagram for silicon

Pourbaix (1966) evaluated the stability of silicon in water and aqueous solutions in the absence of complex formation at 25 °C and reported that the stability is affected by a variety of equilibrium conditions; these are reported in his work. These equilibrium conditions were used to draw the potential-pH equilibrium diagram in Figure 2-2.

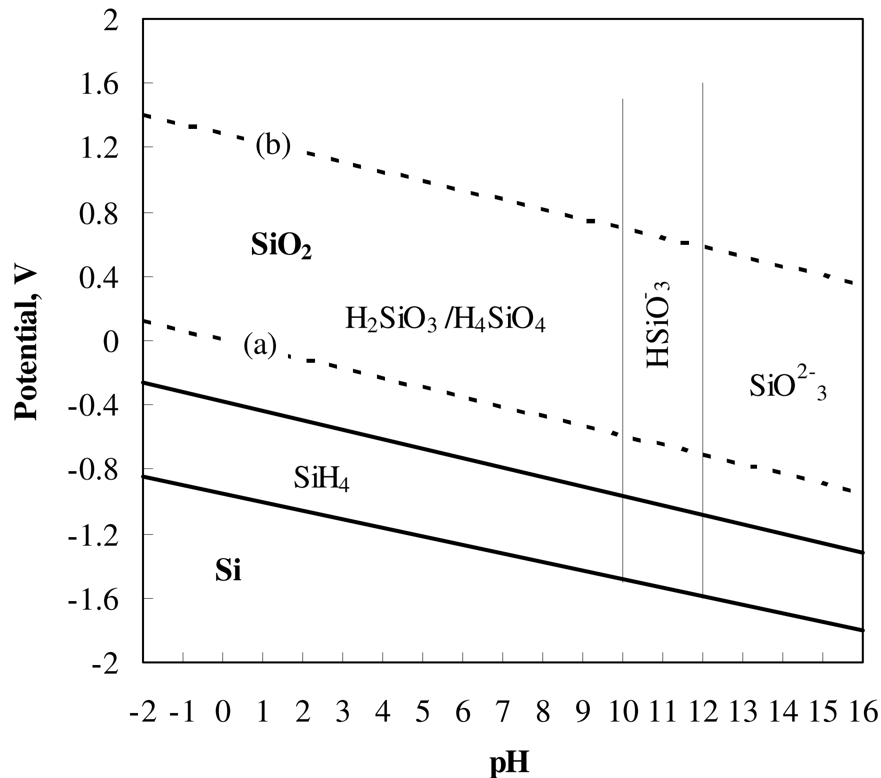


**Figure 2-2** Potential-pH equilibrium diagram for the system of silicon and water at 25 °C (constructed using some of the equilibrium equations presented by Pourbaix, 1966). (a) Represents the line for $2H^+ + 2e^- = H_2$, while (b) represents the reaction $O_2 + 4H^+ + 4e^- = 2H_2O$

Silicon is shown to be stable in a region below the stability of water line (a). Water is unstable below the water line (a) and tends to be reduced with the evolution of hydrogen, with the resulting bulk solution becoming alkaline (Zhang, 2001). Silicon is oxidised with the formation of silica and silicates, and this is accompanied by the evolution of hydrogen and gaseous silicon hydride (Zhang, 2001). The silicon hydride ($SiH_4$) is unstable in the presence of water and decomposes into hydrogen and silica or silicates. Meyers (1999) reports that it is unlikely that $SiO_2$ forms directly in an aqueous environment. Instead, hydrated silica species, such as $H_2SiO_3$ or $H_2SiO_4$, both of which have limited solubility, form first. Upon drying, these silicic acids are then converted to dehydrated $SiO_2$. Simple silicic acids have not been isolated and polysilicic acids are more likely to form and cause passivation on the silicon surface (Unger, 1979).

The thermodynamically favourable reactions for the oxidation of silicon to silicic acid can be deduced from the anodic half-cell reaction:

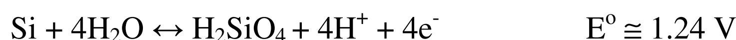

$$Si + 4H_2O \leftrightarrow H_2SiO_4 + 4H^+ + 4e^- \qquad E^o \cong 1.24\ V$$

Both dissolved oxygen and hydrogen ions (water) are viable oxidants and the overall reactions are given in Scheme II.

$$Si + 2H_2O + O_2 \rightarrow H_4SiO_4 \qquad \Delta E^o \cong 2.47\ V$$

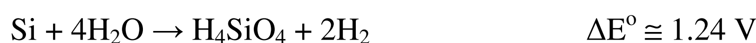

$$Si + 4H_2O \rightarrow H_4SiO_4 + 2H_2 \qquad \Delta E^o \cong 1.24\ V$$

**Scheme II** Overall silicon oxidation reactions corresponding to the dissolved oxygen and hydrogen cathodic reactions

The reactivity of silicon is not apparent at room temperature due to the formation of a thin passive oxide film on the surface (Zhang, 2001) and also due to the irreversibility of the oxidation-reduction reaction of silicon, resulting in it displaying great chemical stability (Zhang, 2001). Pourbaix (1966, quoting Weiss & Engelhardt, 1966) reported that silicon reacts very slowly with water at room temperature and also that it is not affected by acids but is attacked by caustic alkalis. In the case of hot alkalis it forms silicates and silicon hydride.

### 2.4.2 Silicon corrosion mechanism

Shea *et al.* (2004) reported that silicon corrosion in aerated neutral to slightly basic aqueous media with direct formation of $SiO_2$ can also be described in electrochemical terms. The possible half-reactions are shown in Scheme III.

Anode: $Si + 2\ OH^- + 2\ h^+ \rightarrow SiO_2 + H_2\uparrow$

Cathode: $2H^+ + 2\ e^- \rightarrow H_2$

Overall: $Si + 2H_2O \rightarrow SiO_2 + 2H_2\uparrow$

**Scheme III** Electrochemical model for the oxidation of silicon in neutral aqueous medium

Nakayama & Collins (1966) state that although it is standard to explain electrochemical oxidation in terms of the oxidation potential of the cell ( $E^o$ ), the effect of the oxide film has to be taken into account. Therefore, the effective potential difference across the film $\Delta V$ is given by:

$$\Delta V = -E^o + \Delta\phi \qquad (2\text{-}28)$$

where

$E^o$ = potential of the electrochemical cell representing the oxidation process

$\Delta\phi$ = Fermi potential difference across the film, i.e.

$$\Delta\phi = \frac{4q\rho}{M}\frac{k_2}{N_o\sigma_e} \qquad (2\text{-}29)$$

where

M/4 = equivalent weight of $SiO_2$

$\rho$ = density of $SiO_2$

$\sigma_e$ = electronic or hole conductivity of the oxide

$N_o$ = Avogadro's number

$k_2$ =parabolic rate constant

The half-reactions in Scheme III are not necessarily primitive reactions. Gräf *et al.* (1989) postulated that silicon corrosion is initiated by the formation of Si–H functional groups. They and Boonekamp *et al.* (1994) also posited that the subsequent nucleophilic reaction with hydroxyl ions and conversion to Si–OH, accompanied by the release of hydrogen, represents the rate-limiting reaction. Their proposed mechanism also provides a plausible explanation for the corrosion of neat silicon in water. Once the formation of Si–OH has taken place on the silicon surface, preferential attack of water on the Si–OH is said to take place, resulting in the induction of polarity on the surface due to the strong electronegativity of the OH groups. The strong electronegativity of the OH group results in the silicon bonded to it having a net positive charge (δ+). This charge induces a net negative charge in a neighbouring silicon atom ($\delta^-$) which, in turn, induces a net positive

charge (δ+) to its neighbour. According to Gräf *et al.* (1989), this induced polarisation enables an $H_2O$ molecule to attack the polarised Si–Si bond:

$$Si^{\delta+}–Si^{\delta-} + H_2O \rightarrow Si–H + Si–OH \qquad (2\text{-}30)$$

Ultimately, Si–O–Si bridges are formed by the condensation of neighbouring Si-OH groups:

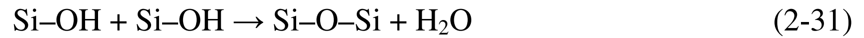

$$Si–OH + Si–OH \rightarrow Si–O–Si + H_2O \qquad (2\text{-}31)$$

Gräf *et al*. (1989) assume slow conversion of Si–H to Si–OH. This revised anodic reaction involves the nucleophilic attack of $OH^-$ ions on Si–H bonds and releases hydrogen which is evolved as a gas:

$$2\ Si–H + 2\ OH^- + 2\ h^+ \rightarrow 2\ Si–OH + H_2\uparrow \qquad (2\text{-}32)$$

The partial dissociation of Si–OH into $SiO^-$ + $H^+$ leads to a charging of the interface and generates a surface potential. Gräf *et al*. (1989) took this into account and showed that, with the additional assumption that the Si–H concentration remains approximately constant

$$\frac{d[\text{Si-OH}]}{dt} \propto e^{-c[\text{Si-OH}]/RT} \qquad (2\text{-}33)$$

where $c$ is a constant describing the dissociative behaviour of Si-OH.

According to Gräf *et al.* (1989), this primitive anodic reaction is rate limiting and it therefore determines the overall kinetics of hydrogen evolution. Integration of Equation 2-24 yields a logarithmic growth law.

## 2.5 Corrosion Inhibition

Numerous methods of corrosion inhibition in metals have been proposed. However, these can all be classified under two main methods, i.e. barrier protection resulting in isolation

of metals from corroding environments, and manipulating the nature of the corroding environment (West, 1980).

The use of corrosion inhibitors has been extensively investigated (Klechka, 2001; Sherif, 2006; Knag, 2006). They are described as substances that, when added to an environment, decrease or slow down the rate of material wastage (Sastri, 1998; Afolabi & Borode, 2010). They function by adsorbing ions or molecules onto a substrate surface and reduce corrosion by one of the following means (Raja & Sethuraman, 2008):

- Decreasing the diffusion rate of reactants to the substrate surface
- Increasing or decreasing the anodic or cathodic reaction
- Decreasing the electrical resistance of the substrate surface

### 2.5.1 Organic barrier inhibition

The addition of certain organic compounds to corroding materials greatly diminishes the velocity of attack without stopping it altogether (Klechka, 2001; Lindsay & Lyon, 2010). The decrease in corrosion rate is attributed to adsorption of the organic compounds on the material surface. The organic molecules can attach to the surface by either chemical adsorption or physical adsorption, with chemical adsorption providing more resistance to corrosion. The degree of surface coverage is an important factor affecting the organic inhibition performance (Lindsay & Lyon, 2010).

Organic material enforces inhibition through one of the following mechanisms:

- Participation in electrode reactions, thereby interfering with the usual reaction pathway
- Formation of a diffusion barrier, thus restricting mass transfer between the material surface and the environment or vice versa
- Blocking of the reaction site, which in turn prevents bound metal atoms from taking part in corrosion reactions

Licciardello *et al*. (1986) reported that silicon surfaces contaminated with organic compounds show significantly reduced rates of oxidation in humid environments. They attribute this effect to the hydrophobisation of silicon surfaces which prevents the

absorption of water. This observation suggests that organic surface modification of the silicon powder may inhibit hydrogen evolution in aqueous dispersion.

#### *2.5.1.1 Alcohol inhibition*

Stroscio *et al*. (1985) followed the chemical transformation of methanol on the Si (111) surface. They and Crowell *et al*. (1990) found that methanol undergoes a dissociative adsorption which proceeds readily at ambient temperatures and forms a strongly bound methoxy species ($CH_3O$) and SiH on the silicon surface. Methanol reacts with silicon by breakage of the OH bond (Glass, 1995). Salonen *et al*. (1997) studied the reaction of porous silicon with water, methanol and ethanol. They found that the alcohols reacted at rates that are more than two orders of magnitude faster than the reaction with water. Fourier transform infrared spectroscopy (FTIR) revealed silicon surface passivation by the formation of $Si–OCH_3$ or $Si–OC_2H_5$ groups. Williams & Ezis (1983) also reported that although silicon hydrolyses rapidly in water during wet milling, non-aqueous solvents such as isopropanol are effective in preventing such hydrolysis.

#### *2.5.1.2 Silane inhibition*

Organofunctional silanes are extensively used as coupling agents for fillers and fibre reinforcements in polymer composites. They have been proposed as corrosion inhibitors for metals (Van Ooij *et al.*, 2005) and silicon wafers (Wang & Jin, 2004). Silanes provide inhibition by forming a barrier on the surface of the coated material, as well as rendering the coated surface hydrophobic. Silane coupling agents have the general structure:

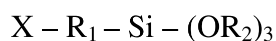

$$X – R_1 – Si – (OR_2)_3$$

where
$OR_2$ = a hydrolysable group capable of reacting with inorganic materials
$R_1$ = an alkyl chain that (optionally) is terminated by an organoreactive group X
(Yuan & Van Ooij, 1997; Demjen *et al.*, 1997)

The degree of hydrophobicity imparted by a particular silane to a coated surface naturally depends on the nature of the alkyl substituents (Wang & Jin, 2004).

The hydrolysable part of the silane molecule is able to react chemically with surface hydroxyl groups on inorganic surfaces to form a [surface]–O–Si–$R_1$–X hydrophobic barrier that prevents the transport of water through the coated surface (Zhu & Van Ooij, 2003). The barrier formation can be represented by the following stages.

**Hydrolysis**

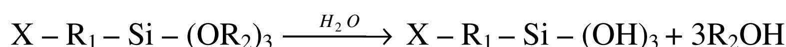

$$X - R_1 - Si - (OR_2)_3 \xrightarrow{H_2O} X - R_1 - Si - (OH)_3 + 3R_2OH$$

The hydrolysable group reacts with ambient moisture or purposefully added water to form a silanol, accompanied by the release of alcohol. The rate of reaction is dependent on the pH, as well as on the steric bulk and polarity of the alcohol residue (Momentive, 2010). The pH also affects the stability of silanes in aqueous solutions (Van Ooij *et al*., 2005). The natural alkalinity or acidity of most inorganic surfaces is reported to be adequate to catalyse silane hydrolysis (Momentive, 2010).

**Silanol condensation on a surface**

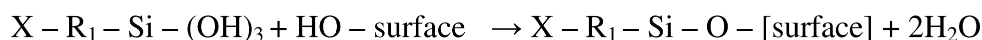

$$X - R_1 - Si - (OH)_3 + HO - \text{surface} \rightarrow X - R_1 - Si - O - [\text{surface}] + 2H_2O$$

Upon drying, the silanol undergoes a condensation reaction with the hydroxyl groups on the surface of the inorganic material. Since only one of the three hydrolysed sites reacts with the material surface, the unreacted silanols condense with each other and form a Si–O–Si network on the substrate surface (Van Ooij *et al*., 2006). The structure of the final network is influenced by factors such as concentration of the solution, pH of the aqueous slurry, ageing of the silane, specific surface area of the coated material and its chemical functionality, as well as the alkoxyl and organofunctionality of the silane (Demjen, 1997).

Karmaker (2007) showed that silane film thickness is proportional to the concentration of the silane solution, regardless of the type of silane used, and is independent of contact time. Silane coupling agents are said not to adsorb in a single layer

on filler surfaces but instead form an interphase composed of both chemisorbed and physisorbed layers (Demjen *et al*., 1997).

The passivity inferred by the silane film is not permanent, especially in cases where the film is continuously immersed in water. This is because, despite the film's hydrophobicity, silanes eventually hydrolyse and water can penetrate to the interface (Van Ooij, 2005). The siloxane hydrolysis is a reversible process (see below) and the siloxane groups are reformed if the partly hydrolysed film is able to dry out again.

$$Si - O - Si + H_2O \leftrightarrow Si - OH + Si - OH$$

**Silane treatment of silicon surfaces**

The use of silanes as a means of treating silicon surfaces is reported by Wang & Jin (2004) who used silanes to modify the silicon wafer surface, rendering it more hydrophobic. The surface chemistry of the silicon greatly influences the effectiveness of silane coupling to silicon. The surface of silicon is normally covered with a hydroxyl layer in cases where the silicon is exposed to moisture. When the silicon surface has been exposed to an acidic medium, a surface coating of hydride occurs. The hydroxyl surface promotes adsorption of silane onto the silicon surface by forming hydrogen bonds with the silanol groups of the silane. This is then followed by the condensation reaction when drying takes place. The process is shown in Scheme IV.

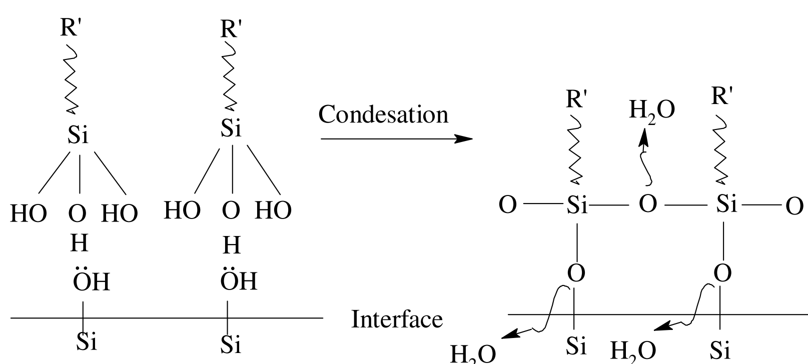


**Scheme IV** Schematic of bonding mechanism of silane to silicon surface before and after condensation (Zhu & Van Ooij, 2003)

### 2.5.2 Oxide barrier inhibition

Corrosion inhibition by means of protective coatings, which separate susceptible surfaces from the factors that cause corrosion in the surrounding environment, is well documented (Twite & Bierwagen, 1998). Gruvin *et al*. (1985) and Mack *et al.* (2010) reported that silicon, just like metals such as aluminium and titanium, forms an adherent oxide cover that protects the underlying substrate from further corrosion. Methods for creating a silicon oxide layer on a silicon substrate have been extensively explored (Debrage *et al*., 1998; Simoen *et al.,* 2011). They include thermal oxidation, chemical vapour deposition, ozonation, $H_2O_2$ and nitric acid oxidation, etc. Thermally produced $SiO_2$ is said to have the best passivating effect (Dingemans *et al*., 2011) and has been shown to reduce the amount of hydrogen evolved when coated silicon powders are placed in water (Bahruji *et al.,* 2009).

Silicon undergoes oxidation at room temperature in the presence of oxygen, water or both. The rate of oxidation of silicon increases with increase in temperature (Irene & Van der Meulen, 1976). Continued oxidation leads to thickening of the oxide layer (Na *et al*., 2009). Silicon thermal oxidation is initially a surface reaction which changes over to a diffusion-controlled reaction at the silicon–silicon dioxide interface. Oxygen or water must diffuse through the $SiO_2$ layer to reach the Si below for reaction to take place. The diffusion coefficient of oxidant through the $SiO_2$ layer is relatively low at room temperature, but increases with higher temperatures (Irene, 1988). A number of silicon oxidation models have been developed, but the Deal and Grove linear-parabolic model is the one most widely used (Irene, 1988).

### 2.5.3 Environment modifying inhibitors

Instead of inhibiting corrosion by modifying the surface of the corroding material, another alternative is to modify the environment in which the material is corroding. Inhibition by environmental modification is generally divided into two main categories (Lindsay & Lyon, 2010):

- Corrosive agent removal, involving the modification of an environment to reduce its chemical and electrochemical activity towards a substrate material by removing specific corrosive reagents

- Protective barrier inducement, involving deliberate addition of a chemical species that interacts with the corroding substrate so as to form a protective barrier that reduces the corrosion rate to acceptable levels and promotes passivity

Some of the strategies for reducing the kinetics of the corrosion process involve interference with at least one of the electrochemical processes taking place during corrosion. This can be achieved by:

- Removal of the cathodic reactant such as oxygen so that the cathodic reaction is stifled. It is common practice to use oxygen scavengers for this purpose (West, 1980).
- Removal of the electrolyte solution such as water so that the anodic reaction becomes stifled since the metal ions would have limited ability to be solvated (Lindsay & Lyon, 2010).
- Reduction of the electrolytic conductivity so that a large resistance is developed between the anode and the cathode, and hence the electrochemical corrosion is stifled with a decrease in electron and ion transfer (Lindsay & Lyon, 2010).

In aqueous environments in which water is the main component, control of the amount of dissolved oxygen is the most viable control mechanism. Lindsay & Lyon (2010) state that the dissolved oxygen can be reduced by physical as well as chemical means.

Physical methods include:

- Heating the water since solubility of oxygen decreases with an increase in temperature
- Lowering the gas pressure above the water, resulting in a reduction in dissolved gas content
- Bubbling gases such as nitrogen or steam in the water, thus replacing dissolved oxygen

Chemical methods involve the use of reducing agents such as sulphites and hydrazine which react directly with oxygen to form another, more innocuous species

(Lindsay and Lyon, 2010; West, 1980). Some examples of such reactions are shown in Scheme V.

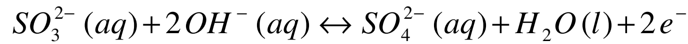

$$SO_3^{2-}(aq) + 2OH^-(aq) \leftrightarrow SO_4^{2-}(aq) + H_2O(l) + 2e^-$$

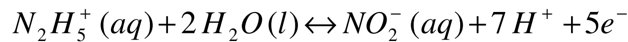

$$N_2H_5^+(aq) + 2H_2O(l) \leftrightarrow NO_2^-(aq) + 7H^+ + 5e^-$$

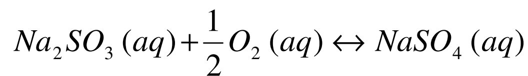

$$Na_2SO_3(aq) + \frac{1}{2}O_2(aq) \leftrightarrow NaSO_4(aq)$$

**Scheme V** Inhibition action of sulphites and hydrazine as scavenging inhibitors reducing the amount of dissolved oxygen

Protective barrier inducement involves in situ substrate–fluid interface modifications to impede one or more steps in the corrosion process (Lindsay & Lyon, 2010). This is achieved through addition of chemical reagents which effects synthesis of a protective substrate adhered layer. A common route is the precipitation of a low-solubility, low-porosity compound that adheres to the material surface (Evans, 1971), thereby isolating the material surface from the corroding environment.

#### *2.5.3.1 Effect of pH modification*

Corrosion can be suppressed or eliminated by controlling the pH of the corroding environment in such a way that the material is maintained within a domain in which the solid phase has significant thermodynamic or kinetic stability, i.e. in a region of passivity. The effect of pH on the corrosion of silicon is shown by Pourbaix (1966) (Figure 2-2). Generally, silicon is stable in acidic to neutral pH but readily corrodes to form soluble silicates in alkaline pH. It has been reported in a number of publications that silicon treated with hydrofluoric acid forms a stable Si–H surface bond which results in the surface being hydrophobic and passive in low-pH environments (Buriak, 2002; Lui *et al*., 2010).

Dillinger *et al*. (quoted by Hackley *et al.,* 1997) measured the volumetric production of hydrogen with time as a function of suspension pH and found that alkaline solutions show an exponential rise in the gas formation, whereas in acid solutions gas formation ceased after a period of time.

### *2.5.3.2 Competing cathodic reactions*

The oxidation of silicon by water is an electrochemical reaction that consists of the anodic oxidation of silicon reaction and an accompanying cathodic reaction (Harraz *et al*., 2002). The release of hydrogen gas when silicon is immersed in water is a result of the cathodic breakdown of the water. Most corrosion literature focuses on the elimination of the anodic material-wasting reaction (Szklarska-Smialowska, 1999; Knag, 2006; Antonijevic and Petrovic, 2008). In the present study the anodic reaction of silicon to form silicon oxide, although not desired, is tolerable. It is, however, desired to eliminate the accompanying cathodic reaction which results in hydrogen gas evolution.

Silicon is a strong reducing agent and is capable of reducing many substances, including water and metal ions in solution. This property has been used extensively to disperse noble metals reductively onto the internal surface of porous silicon from appropriate solutions (Coulthard *et al*., 1993). Sham *et al.* (1994) and Kanungo *et al.* (2010) reported that, depending on the slurry conditions, reduction of noble metal ions by silicon can either be accompanied by simultaneous hydrogen evolution or be altogether independent of it. In the case where simultaneous reduction of the metal ion and water takes place, the increased number of cathodic reactions results in an increased rate of the anodic reaction, leading to passivation of the silicon surface. When no hydrogen evolution is observed, it is likely that there is preferential metal deposition due to the combination of the silicon and metal half-cells, which have a more positive overall electrochemical potential than that of silicon and water, assuming similar kinetics.

Since silicon is a semi-conductor, its surface electrochemistry differs from that of a good electronic conductor in that only limited spatial separation of the anodic and cathodic half-cells is possible. This promotes the deposition of corrosion products on the reaction sites, thus stifling any further reactions. The reduction of metal ions in solution to metal by silicon can be generalised to the reaction Scheme VI (Sham *et al.*, 1994). Based on these reactions, it a pH decrease would be expected to accompany metal deposition.

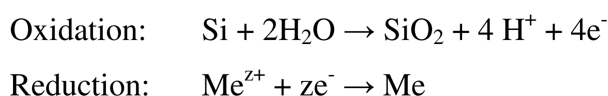

Oxidation: $Si + 2H_2O \rightarrow SiO_2 + 4\,H^+ + 4e^-$

Reduction: $Me^{z+} + ze^- \rightarrow Me$

**Scheme VI** Generalised reaction scheme for the reaction of silicon with metal ions

Sham *et al.* (1994) and Kanungo *et al*. (2010) also found that during the chemical reduction process, $h^+$ holes are released by silicon, subsequently oxidising its surface to $SiO_2$. This surface oxide passivates any surface defects present. The generalised reaction is shown in Scheme VI.

Jeske *et al*. (1995) and Kanungo *et al*. (2010) proposed the two-step local element mechanism shown in Scheme VII. In the first step, silicon oxidation occurs by hole injection from the metal ions into the valence band of the silicon. The second step involves the injection of electrons from the hydroxide into the conduction band of silicon.

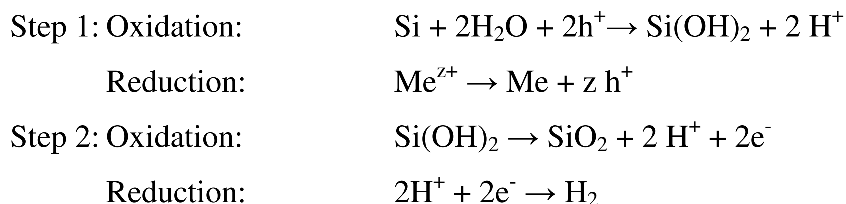

Step 1: Oxidation: $Si + 2H_2O + 2h^+ \rightarrow Si(OH)_2 + 2\,H^+$

Reduction: $Me^{z+} \rightarrow Me + z\,h^+$

Step 2: Oxidation: $Si(OH)_2 \rightarrow SiO_2 + 2\,H^+ + 2e^-$

Reduction: $2H^+ + 2e^- \rightarrow H_2$

**Scheme VII** Two-step local element reaction mechanism proposed by Jeske *et al.* (1995) and Kanungo *et al*. (2010) for silicon interacting with metal ions

This mechanism, however, suggests that the pH of the overall system should remain constant since the $H^+$ produced is immediately released as hydrogen.

#### *2.5.3.3 Complexing agents*

Kuznetsov (1996) reported that complexing agents can induce inhibition in metals through one of the following ways:

- Hydrophobic ligands in which the complexes formed are easily soluble in the corroding medium
- Ligands that are hydrophobic, but provide complexes that are sparingly soluble or almost completely soluble
- Corrosion behaviour of the metal being controlled by the interaction with complexes of this or another metal where such complexes are soluble in the medium and are relatively stable

Although, generally, complex formation results in enlargement of the corrosion domains in the Pourbaix diagram, leading to easier metal wastage as stated in the first point, it is possible that the steady-state potential of the metal ($E_{st}$) may be outside the region of equilibrium potentials ($E_{eq}$) in which the ionisation of a metal with formation of a soluble complex is thermodynamically feasible (Kuznetsov, 1996). When $E_{st} < E_{eq}$, adsorption of the corresponding ligand will not lead to complex formation, but instead the ligand can partially block the corroding surface and change the potential of the electrode system, thereby slowing down the kinetics of the electrode processes (West, 1980).

# CHAPTER 3 : EXPERIMENTAL

## 3.1 Organic Surface Modification and pH variation

### 3.1.1 Materials

Ball-milled type 4 silicon was supplied by Millrox. Middle chrome L-GXD grade ($PbCrO_4$) pigment was supplied by Rolfes Pigments. The commercial silanes evaluated are listed in Table 3-1. They were selected from the Silquest range produced by Momentive Performance Materials. Merck Chemicals supplied the following: tetraethyl orthosilicate (TEOS), ethanol absolute 99.6%, butanol and hexanol, acetone and the pH buffer solutions (pH 2, 4, 5, 7, 9, and 10). The distilled water (pH ≈ 6) was obtained from a laboratory still.

**Table 3-1** Commercial silanes used for the surface treatment of the silicon powder

| Silane | ( Silquest code) | Surface area[a] ($m^2/g$) |
|---|---|---|
| γ-aminopropyl triethoxysilane | (A1100) | 353 |
| γ-glycidoxypropyl triethoxysilane | (A187) | 330 |
| Octyl triethoxysilane | (A137) | 283 |
| Methyl trimethoxylsilane | (A1630) | 575 |
| Vinyl trimethoxysilane | (A171) | 527 |
| Vinyl tris(2-methoxyethoxy)silane | (A172) | 279 |

[a]Surface area coverage data supplied by manufacturer

### 3.1.2 Methods

**Hydrogen evolution**

Hydrogen evolution studies were performed by placing 80 g of silicon into a 500 mL flask that was immersed in a 30 °C ± 1 °C water bath. The flask was connected to an inverted graduated burette filled with water. An aliquot 150 ml of distilled water or pH buffer solution was added to the silicon. The mixture was continuously agitated using a magnetic stirrer. The volume of gas in the inverted cylinder was recorded at the following time intervals: 2, 5, 10, 15, 20, 30, 45 and 60 min. Each experiment was repeated at least five times for statistical purposes. The moles of hydrogen produced per kg of Si were calculated assuming that the ideal gas law applies.

**Silane coating**

The amount of silane required for monolayer coverage was calculated on the basis of information provided by the supplier. In all cases 25% excess silane was added. Equation 3-1 shows the formula that was used to calculate the quantity of silane required.

$$\text{Silane required (g)} \equiv \frac{\text{mass of silicon (g) x silicon surface area (m}^2\text{/g)}}{\text{silane minimum surface coverage (m}^2\text{/g)}} \qquad (3\text{-}1)$$

The amounts of silane calculated and those applied per 100 g of Si are shown in Table 3-2.

**Table 3-2** Minimum surface coverage of the silanes used and the percentage silane required to coat 100 g of silicon with a surface area of 9.68 $m^2/g$

| Silane | Molecular weight [g/mol] | Minimum surface coverage [$m^2/g$] | Theoretical mass of silane required [g/100 g Si] | Mass of silane required [g/100g Si (25 % excess)] |
|---|---|---|---|---|
| A 137 | 276.4 | 283 | 3.42 | 4.28 |
| A187 | 236.1 | 330 | 2.93 | 3.66 |
| A1100 | 221.4 | 353 | 2.74 | 3.43 |
| A171 | 148.2 | 527 | 1.84 | 2.30 |
| A172 | 280.4 | 279 | 3.47 | 4.34 |
| A 1630 | 136.0 | 575 | 1.68 | 2.10 |
| TEOS | 208.3 | 242 | 4.00 | 5.00 |

The silane-ethanol treatment solutions were prepared by adding the mass of silane required to coat 100 g of silicon powder (with 25% excess) to an equivalent mass of distilled water, and then ethanol was added to this mixture until the total mass was 100 g (Wang & Jin, 2004; Van Ooij *et al.*, 2005). To this was added 100 g of silicon powder. The slurry was stirred for 8 h with a magnetic stirrer. The solids were recovered by centrifugation, washed with acetone and left to dry in open air for one day. The amount

of hydrogen evolved from the treated silicon was measured using the experimental procedure described for the hydrogen evolution experiment. However, instead of measuring the evolved gas at different time intervals, a reading was taken after 60 min. Distilled water was used as the dispersing medium.

The amount of silane absorbed by the silicon was determined using a modification of the procedure described by Demjen *et al*. (1997). Silane-cyclohexane solutions with different concentrations were prepared and their FTIR spectra recorded using an attenuated total reflection (ATR) crystal attachment. A calibration curve was established based on Beer's law. Next, 20 g of silicon powder was dispersed in 50 g of cyclohexane solutions containing different silane concentrations. The dispersions were stirred for 8 h and then left to stand for a day. The liquid was decanted from the solids and the residual concentration of the silane in the cyclohexane supernatant was determined by FTIR.

The silicon powder was also pretreated by stirring in ethanol, butanol and hexanol. The alcohol-silicon slurries were recovered and left to dry. The resultant powder was then tested for hydrogen evolution under the same conditions as in the previous experiments using distilled water.

$PbCrO_4$ coated with silane A187 was prepared using the same procedure described for silicon. A 25% excess silane based on the available surface area was used, i.e. 7.11 g A187/100 g $PbCrO_4$.

**Composition preparation**

An Si-$PbCrO_4$ pyrotechnic composition was prepared using 20 mass % Si. One gram of mixture was wet mixed using a mortar and pestle with cyclohexane as a wetting agent. Differential thermal analysis (DTA) runs were then carried out on the air-dried mixture.

### 3.1.3 Characterisation

The particle sizes and specific surface areas of the Si and $PbCrO_4$ powders were determined on a Mastersizer Hydrosizer 2000 and a Quantachrome Nova 1000e BET instrument (using $N_2$ at 77K), respectively.

X-ray diffraction (XRD) analysis on a PANalytical X-pert Pro powder diffractometer was used for phase identification. The instrument featured variable divergence and receiving slits and an X'celerator detector using Fe-filtered Co Kα radiation (0.17901 nm). X'Pert High Score Plus software was used for data manipulation.

Fourier transform infrared (FTIR) spectra of the liquids were recorded on a PerkinElmer spectrum RX 1 FTIR spectrometer with an ATR attachment. The surfaces of the treated and untreated silicon powders were analysed by diffuse reflectance infrared Fourier transform analysis (DRIFT) on a PerkinElmer Spectrum 2000GX FTIR spectrometer. The ratio of sample mass to KBr mass was set at 1:20. All FTIR spectra were recorded at a resolution of 2 $cm^{-1}$ for 30 scans from 4000 to 400 $cm^{-1}$ and represent the average of 30 scans.

X-ray photoelectron spectroscopy (XPS) spectra were obtained on a Quantum 2000 Physical Electronics spectrometer equipped with a Mg/Al dual-mode source and a small-area analyser with a position sensitive detector (PSD). An achromatic Al Kα X-ray (1486 eV) source was operated at 20 W. The vacuum pressure was $10^{-8}$ torr during spectra acquisition. Survey spectra were obtained at take-off angles of 15º, 45º and 80º. Before analysis, samples were dried over $P_2O_5$ in a vacuum desiccator. In order to obtain the atomic concentrations, each raw XPS signal was corrected by dividing its intensity (number of electrons detected) by standard sensitivity factors and normalized to 100%.

DTA was carried out using a Shimadzu DTA-50 instrument. Approximately 5 mg of the sample and standard ($\alpha$-$Al_2O_3$) were weighed into alumina sample pans. Copper discs 500 µm thick were placed at the bottom of the sample pans. These acted as heat sinks to protect the DTA temperature detector from high-temperature excursions (Ilunga *et al.,* 2011). The DTA runs were carried out in a nitrogen atmosphere and the temperature was scanned from ambient temperature to 1 000 °C at a scan rate of 50 °C $min^{-1}$ with air flowing at a rate of 50 mL $min^{-1}$.

Thermogravimetric analysis (TGA) of silane-treated and untreated silicon was performed using the dynamic method on a Mettler Toledo A851 TGA/SDTA instrument.

About 15 mg of powder was placed in open 70 µL alumina pans. The temperature was scanned from 25 to 1 000 °C at a rate of 10 °C $min^{-1}$ with nitrogen flowing at a rate of 50 mL $min^{-1}$.

## 3.2 Silicon Surface Oxidation

### 3.2.1 Materials

Ball-milled type 4 silicon supplied by Millrox with a $d_{50}$ particle size of 2.06 µm (determined with the Mastersizer Hydrosizer 2000) and a specific surface area of 9.68 $m^2/g$ (Quantachrome Nova 1000e BET, $N_2$ at 77 K) was used. Lead chromate ($PbCrO_4$) middle chrome L-GXD grade supplied by Rolfes Pigments with a $d_{50}$ particle size of 2.14 µm (determined with the Mastersizer Hydrosizer 2000) and a Brunauer-Emmett-Teller (BET) specific surface area of 16.7 $m^2/g$ was used. The distilled water was obtained from a laboratory still.

### 3.2.2 Method

**Hydrogen evolution**

Hydrogen evolution studies were performed by placing 40 g of neat or heat-treated silicon powder in a 250 mL flask and immersing it in an ultrasonic water bath with the temperature maintained at 30 °C ± 1 °C. The flask was connected to an inverted graduated burette filled with water to an initial level. An aliquot 100 mL of distilled water was added to the silicon. The mixture was continuously agitated in an MRC ultrasonic cleaner D150H bath. The operating frequency was 43 kHz and the power dissipation was 150 W. The volume of water displaced by the gas in the inverted burette was recorded after 60 min. Each experiment was repeated at least five times for statistical purposes. The moles of hydrogen produced per kg Si were calculated assuming that the ideal gas law applies.

**Powder heating**

Samples (400 g) of neat silicon powder were measured out into alumina crucibles and heated in air at 75, 150, 250, 300, 350, 450 and 550 °C for 4 h. The amount of surface oxide formed on the silicon powder was determined as follows. Approximately 0.5 g (500 mg) of silicon powder was contacted with 10 mL of 10 wt % hydrofluoric acid (HF)

to selectively remove the $SiO_2$ (Nakamura *et al*., 1999) by etching. The mixture was agitated for 10 min and then centrifuged. The resultant solution was analysed for the Si concentration using inductively coupled plasma optical emission spectroscopy (ICP-OES).

**Preparation of pyrotechnic composition**

The Si + $PbCrO_4$ pyrotechnic composition was prepared using 20 wt % Si. One gram of mixture was dry mixed by passing it through a 75 µm sieve several times.

### 3.2.3 Characterisation

Thermogravimetric analysis (TGA) of the silicon powders was performed in an oxygen atmosphere using a combined dynamic and isothermal heating method on a Mettler Toledo A851 TGA/SDTA instrument. About 20 mg of powder was placed in open 70 µL alumina crucibles. The temperature was scanned from 25 to 800 °C at a rate of 50 °C $min^{-1}$, followed by a temperature scan from 800–1 200 °C at a rate of 5 °C $min^{-1}$ and finally isothermal heating at 1 200 °C for 15 h. The $O_2$ flow rate was maintained at 50 mL $min^{-1}$.

A SPECTRO ARCOS ICP-OES was used to establish the quantity of $SiO_2$ etched out when contacted with HF. Calibration with a multi-element standard (ICP grade) was carried out before the leached samples were run. Each sample was measured three times and the average ICP value was recorded.

A Zeiss AURIGA CrossBeam Workstation focus ion beam – scanning electron microscopy (FIB-SEM) was used to mill and view the cross-section of silicon particles treated at various temperatures. The powder samples were platinum coated using methyl cyclopentadienyl (trimethyl) platinum ($C_9H_{16}Pt$) before milling. A Ga source was used for the ion beam.

The surfaces of the heat-treated and neat silicon powders were analysed by diffuse reflectance infrared Fourier transform analysis (DRIFT) on a PerkinElmer Spectrum 2000GX FTIR spectrometer. The ratio of sample mass to KBr mass was set at 1:20. All

FTIR spectra were recorded at a resolution of 2 $cm^{-1}$ for 30 scans from 4000 to 450 $cm^{-1}$ and represent the average of 30 scans.

DTA was carried out using a Shimadzu DTA-50 instrument. Approximately 5 mg of the sample and standard ($\alpha$-$Al_2O_3$) were weighed into alumina sample pans. Copper discs 500 µm thick were placed at the bottom of the sample pans. These acted as heat sinks to protect the DTA temperature detector from high-temperature excursions. The DTA runs were carried out in a nitrogen atmosphere and the temperature was scanned from ambient temperature to 1 000 °C at a scan rate of 50 °C $min^{-1}$ with nitrogen flowing at a rate of 50 mL $min^{-1}$.

## 3.3 Additional Cathodic Reaction

### 3.3.1 Materials

Silicon and lead chromate from the same source and with the same physical properties reported in the previous materials sections was also used in this stage of experiments. Barium sulphate ($BaSO_4$) with a $d_{50}$ of 5.55 µm was supplied by AEL Mining Services. The distilled water was obtained from a laboratory still. The metal salts (Table 3-3), 25% ammonia solution and the de-ionised water were obtained from Merck Chemicals.

**Table 3-3** List of metal salts used as inhibitors

| Metal salt | Chemical formula |
|---|---|
| Copper sulphate | $CuSO_4.5\ H_2O$ |
| Copper chloride | $CuCl_2.2H_2O$ |
| Copper nitrate | $Cu\ (NO_3)_2.3H_2O$ |
| Cobalt nitrate | $Co(NO_3)_2.\ 6\ H_2O$ |
| Iron (III) nitrate | $Fe(NO_3)_3.9H_2O$ |
| Nickel nitrate | $Ni(NO_3)_2.6\ H_2O$ |
| Zinc nitrate | $Zn(NO_3)_2.6H_2O$ |
| Zinc sulphate | $ZnSO_4.7H_2O$ |
| Manganese nitrate | $Mn(NO_3)_2.4H_2O$ |
| Manganese sulphate | $MnSO_4.H_2O$ |
| Potassium permanganate | $KMnO_4$ |

### 3.3.2 Methods

**Silicon hydrolysis rate measurement**

Silicon hydrolysis measurements were carried out using the same procedure and set-up as those described in *Section 3.2.2*. However, instead of adding distilled water to the silicon powder, 0.1 M solutions of the metal salts listed in Table 3-3 were prepared and used. The volume of water displaced by the gas in the inverted burette was recorded as a function of time. Each experiment was repeated at least five times for statistical purposes. The moles of hydrogen produced per kg of Si were calculated assuming that the ideal gas law applies. The effect of dissolved oxygen on the amount of hydrogen released was also investigated. This was done by de-oxygenating 500 mL of distilled water. The water was first heated to 80°C and maintained at this temperature for 30 min, followed by nitrogen purging for 15 min at a flow rate of 50 mL/s (Butler *et al*., 1994). This water was then tested with silicon powder under the conditions stated above.

After it had been established that the 0.1 M $Cu(NO_3)_2$ solution was one of the best inhibiting metal solutions, varying concentrations of copper nitrate solution were prepared (0.001, 0.005, 0.01, 0.02, 0.04, 0.1, 0.3 and 0.5 M). Their effectiveness as inhibitors was investigated by measuring the gas evolved in 1 h and the minimum concentration at which the least gas is evolved was established.

With the minimum concentration (0.04 M) having been established, the rate of hydrogen evolution using solutions of the three copper salts was measured. This was done by following the volume of displaced water in the burette at the following time intervals: 0, 1, 2, 5, 10, 15, 20, 25, 30, 40, 50 and 60 min. pH measurements of the bulk slurry were also taken at the same time intervals.

**Ageing of Si in powder in slurries of distilled water and $Cu(NO_3)_2$**

The effect of ageing silicon powder in aqueous suspensions on the burn properties of a pyrotechnic composition produced from the resultant silicon was investigated. Slurries with 40 wt % silicon were prepared using distilled water and 0.04 M $Cu(NO_3)_2$ solution as the aqueous medium. The two slurries were continuously stirred for 6 weeks. Small

samples of the slurry were collected at different time intervals. These were air dried and then used to prepare pyrotechnic compositions.

**Determination of the amount copper consumed during inhibition**

An initial standard solution of approximately 11.5 g/L of $[Cu(NH_3)_4]^{2+}$ complex was prepared by adding the required amount of copper salt into a 100 mL volumetric flask and topping it up to the mark with de-ionised water. An aliquot 50 mL of this copper solution was then transferred into another 100 mL volumetric flask where 8 g of 25% ammonia solution was added to form the complex and then topped up to the mark with de-ionised water. Half of the initial complex solution was then transferred into another 100 mL flask and topped up to the mark. Step dilutions taking 50 mL of each previous solution and topping it up to 100 mL were carried out until six standards had been obtained. The ultraviolet-visible (UV-Vis) spectra of the standard solutions were then recorded. A calibration curve was established based on Beer's law. Next, 200 g of silicon powder was dispersed in 500 mL of 0.04 M Cu solution. The slurry was continuously stirred and 20 mL samples of the slurry were taken at the following time intervals: 1, 2, 5, 10, 15, 20, 30, 40, 50, and 60 min. These slurry samples were immediately filtered and the copper concentration in the resultant filtrate was analysed using UV-Vis after the addition of ammonium solution.

**Preparation of pyrotechnic composition**

Pyrotechnic compositions of Si + $PbCrO_4$ were prepared using 20 wt % Si slurried in the three 0.1 M copper salt solutions. Compositions of Si + $BaSO_4$ were prepared using 44 wt % Si collected at different time intervals during the ageing tests. One gram of each composition was weighed out and dry mixed by passing it through a 75 µm sieve several times. The burn properties of the Si + $PbCrO_4$ pyrotechnic compositions were then tested using DTA and open-flame tests were carried out on the Si + $BaSO_4$ compositions.

### 3.3.3 Characterisation

A SPECTRO ARCOS ICP-OES was used to quantify the amount of Cu deposited when silicon powder was immersed in the three different copper solutions. The samples were prepared by contacting the dried silicon powder with 0.5 M $HNO_3$ and hence dissolving

the precipitated copper (Harraz *et al.*, 2002). Calibration with a multi-element standard (ICP grade) was carried out before the samples were run.

The UV-Vis spectrophotometric determinations were carried out using a PerkinElmer LAMBDA™ 750 UV/VIS spectrometer in the wavelength range of 300 to 1 100 nm. Experimental spectra were expressed as absorbance (A) against wavelength (nm). Each investigated solution was measured against a blank of suitable composition. The data was analysed using Excel to determine the maximum peak heights.

The surfaces of the neat silicon powders and those treated with copper solution were analysed by DRIFT on a PerkinElmer Spectrum 2000GX FTIR spectrometer. The ratio of sample mass to KBr mass was set at 1:20. All FTIR spectra were recorded at a resolution of 2 $cm^{-1}$ for 30 scans from 4000 to 450 $cm^{-1}$ and represent the average of 30 scans.

DTA on the Si + $PbCrO_4$ pyrotechnic compositions was carried out using the same equipment and conditions described in Section 3.2.3.

# CHAPTER 4 : RESULTS: ORGANIC COATING AND PH VARIATION

## 4.1 Initial Silicon Surface Structure

The silicon Type 4 powder was found to have a $d_{50}$ particle size of 2.06 µm and a specific surface area of 9.7 $m^2/g$. The lead chromate ($PbCrO_4$) $d_{50}$ particle size was 2.14 µm and the BET surface area was 16.7 $m^2/g$. XRD analysis confirmed that the silicon was crystallographically pure (spectra shown in Appendix B).

Figure 4-1 shows DRIFT spectra for neat silicon and silicon powders exposed to hexane solutions containing 10% A172 and 14% A1100 respectively. Consider first the spectrum obtained for the neat silicon. The band observed at 3400 $cm^{-1}$ is attributed to the O–H stretching vibrations of the Si–OH groups. The band observed at 1000–1300 $cm^{-1}$ represents the asymmetric stretch vibration of the Si–O–Si bonds. The presence of this band confirms the existence of $SiO_2$ at the surface of the silicon powder. The peak at 1600 $cm^{-1}$ confirms the presence of water or O–H bonds at the surface (Boonekamp *et al.,* 1994).

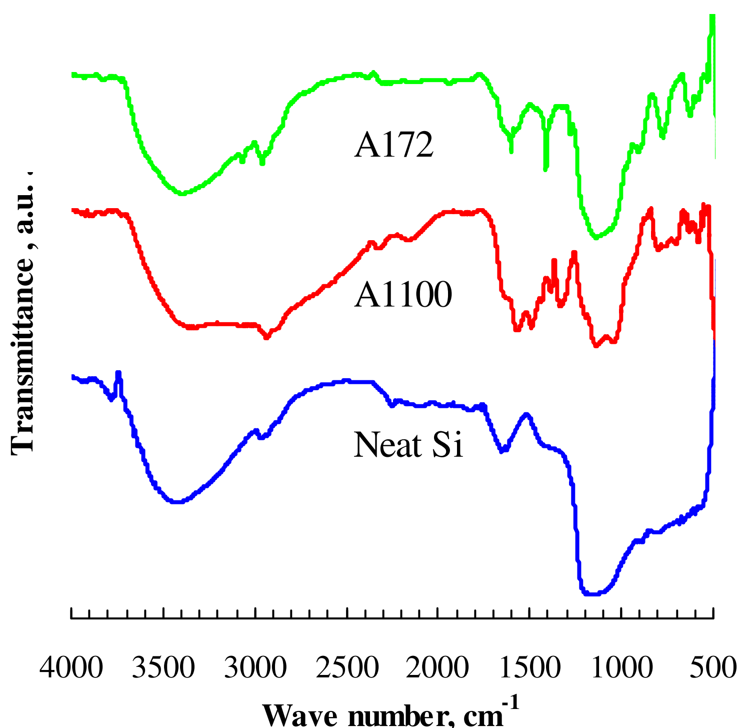


**Figure 4-1** DRIFT spectra of neat silicon surface and silicon powders treated with cyclohexane solutions of silanes (10% A172 and 14% A1100 respectively)

The bands observed at 3000–2700 $cm^{-1}$ reveal the existence of organic alkyl groups. Their presence in the spectrum of the neat powders implies contamination of the neat silicon surface. However, there are clear differences between these bands in the spectra for the neat silicon and those for the silane-coated samples. This suggests that the nature of the organic component present at the silicon surface has changed. The spectra reported for the two treated samples in Figure 4-1 also differ. This is expected because the two silanes featured different functional groups. Unfortunately, the C=C stretching band and the band for N-H bending of the silane molecules overlap with the range for the O–H band observed for the silicon powder. This made it difficult to allocate the peaks accurately.

XPS has been used as a characterisation technique in various surface modification studies (Olander & Albertsson, 2002). The technique samples the composition of the matter at a surface depth of a few nanometres. The XPS-determined elemental surface concentrations for the neat silicon and silane-coated silicon are compared in Table 4-1. The results for the neat silicon indicate 18.2% carbon, and this confirms the presence of the organic contamination first revealed by DRIFT. The silane-coated materials showed higher carbon contents, indicating surface alterations due to organic coating. The presence of the organic coating was additionally confirmed for silane A1100. In this case the unique nitrogen component was detected on the silicon surface by XPS.

**Table 4-1** XPS results for surface properties of raw silicon and silicon treated with a theoretical amount of silane for monolayer coverage

| **Element** | **Atomic concentration (wt %)** | | |
|---|---|---|---|
| **Silicon** | **Neat** | **A172** | **A1100** |
| C | 18.2 | 28.0 | 23.0 |
| O | 43.3 | 40.2 | 41.9 |
| Si | 38.5 | 31.7 | 32.5 |
| N | - | - | 2.6 |

The dissolution experiments showed that the actual amount of silane adsorbed on the silicon surface was independent of the initial silane content of the hexane solutions to which the silicon powders were exposed. The average amount of silane adsorbed for the

six different silane concentrations considered was found to be 3.5 g of A172 silane/100 g of silicon and 8.4 g A1100 of silane/100 g of silicon. The results obtained for A172 were in agreement with the theoretical quantity based on monolayer surface coverage and on the measured surface area of the silicon. However, the amount of experimentally determined for A1100 significantly exceeded the theoretically expected coverage. This discrepancy may have been caused by multilayer silane deposition on the silicon powder surface.

TGA analysis was also used to estimate the amount of silane actually bound to the silicon (Figure 4-2). The neat silicon showed no significant mass loss in the range 25-600 °C. Instead, at 600 °C it showed a mass increase associated with the formation of silicon nitride. The A172 silane-coated silicon showed a maximum mass loss of 1.62% between 25 and 800 °C. This mass loss exceeded that expected from the dissolution experiments. Corrections were made to the dissolution data to take into account that only the organic component of the silane will vaporise upon heating. The expected mass loss, based on the vaporisation of the organic component of the silane, was 4.35% for A1100-coated silicon. This compares favourably with the maximum TG-mass loss of 4.55% observed above 150 °C. Note that this powder also showed a mass loss of 2.63% between ambient temperature and 125 °C due to the loss of moisture and possibly to unbound excess silane.

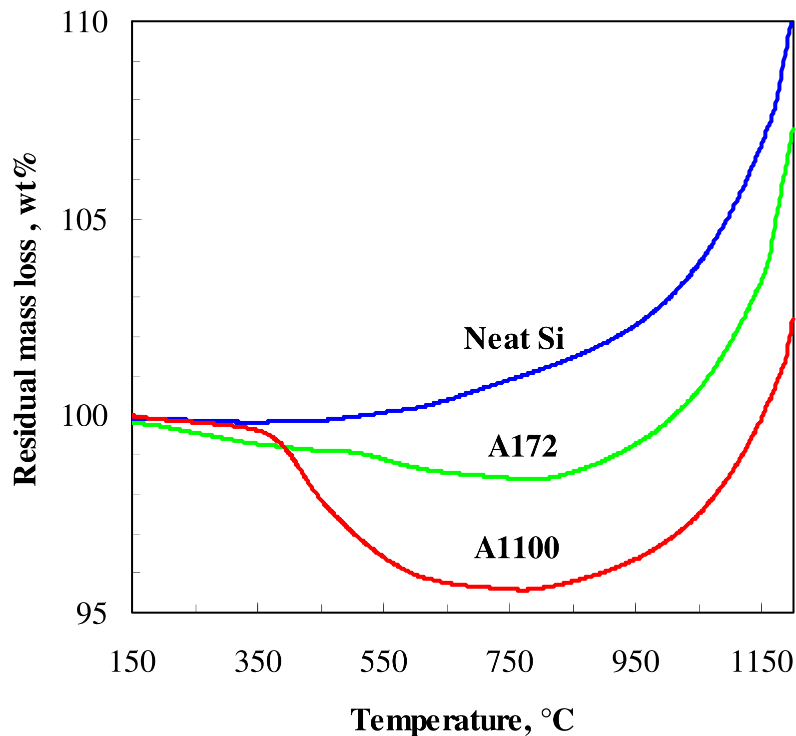


**Figure 4-2** TG mass loss of neat and silane-coated silicon in a nitrogen atmosphere

## 4.2 Effect of pH on $H_2$ Evolution

The hydrogen-release measurements showed considerable scatter. Figure 4-3 shows representative curves that correspond to an average of at least five different runs. In the series pH = 2 buffer, distilled water (pH ≈ 6), and a pH = 10 buffer solution, the rate of $H_2$ evolution increases with pH. In each case the apparent rate also decreases over time. Metal oxidation rates are usually expressed in terms of either the mass gain or the increase in the thickness of the oxide layer. The Deal-Grove linear-parabolic oxide growth law applies when this growth is diffusion limited (Deal & Grove, 1965). If the oxidation reaction involves only water, the amount of hydrogen evolved is proportional to the amount of oxide formed. In this case the parabolic law can be expressed as follows:

$$N_{H_2} = a\sqrt{(t+b)} - a\sqrt{b} \tag{4-1}$$

where

$N_{H_2}$ = moles of $H_2$ released per unit mass of silicon

$a$ and $b$ = empirical constants

Gräf *et al.* (1989) found that the oxidation of HF-etched silicon in water follows the so-called "logarithmic law". Expressed in terms of the amount of hydrogen gas evolved, it reads:

$$N_{H_2} = a\ell n(t+b) - a\ell nb \tag{4-2}$$

This equation provided a better fit to the present data and this is indicated by the solid and dotted lines in Figure 4-5. However, an unequivocal conclusion in this regard is not possible due to the considerable scatter in the data.

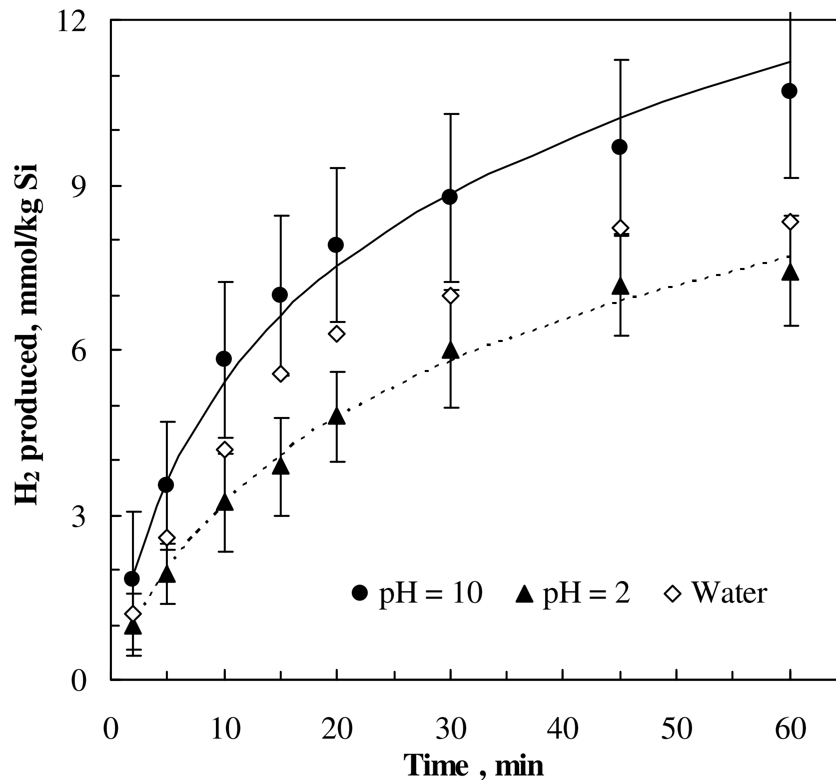


**Figure 4-3** Effect of pH on the hydrogen evolution rate from the neat silicon powder dispersions.

The solid lines represent logarithmic rate law fits according to Equation 4-2

## 4.3 Effects of Treatment with Alcohols and Silanes on $H_2$ Evolution

Figure 4-4 shows the amount of hydrogen evolved after the surface treated silicon powder had been immersed in distilled water for 1 h. The neat, i.e. uncoated, silicon powder produced 8.3 ± 1.2 mmol $H_2$/kg Si. Both the alcohols and the silane-treated silicon powders reduced the amount of $H_2$ gas produced. TEOS was not very useful because its

performance was in the range found for the alcohols. However, the silanes were significantly more effective. The best performance was 0.25 ± 0.50 mmol $H_2$/kg Si obtained with Silquest A172, i.e. vinyl tris(2-methoxyethoxy)silane. The worst result was 1.47 ± 0.06 mmol $H_2$/kg Si provided by Silquest 187 (γ-glycidoxypropyl triethoxysilane). This still represents a reduction of 83% in the amount of $H_2$ released over a period of 1 h. The performance of the other silanes tested here was comparable. Surprisingly, this group included octyl triethoxysilane (Silquest 137), which features the longest alkyl chain and, in addition, there is no substituent present at the end of this tail. It was therefore actually expected to provide the best effect with respect to imparting hydrophobicity to the silicon surface. Silquest A172 and A171 share the same vinyl substituent but differ with respect to their alkoxy groups. In the former the hydrolysable group consist of the 2-methoxyethoxy functionality rather than the more commonly employed methoxy functionality present in Silquest A171.

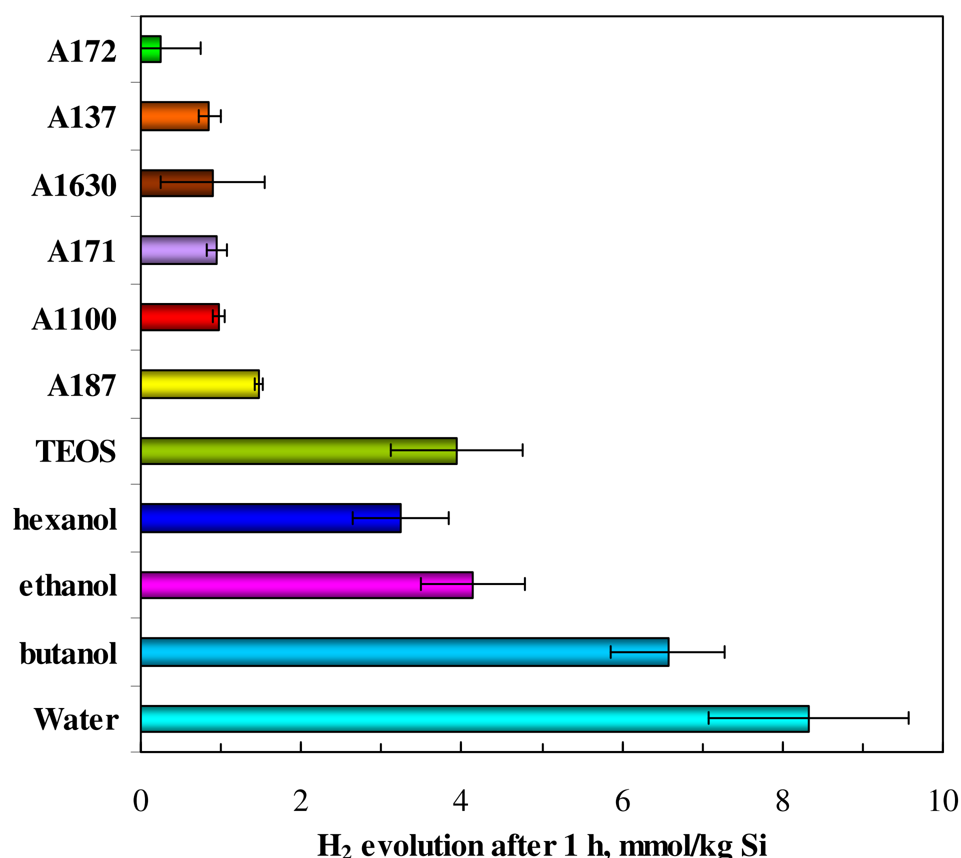


**Figure 4-4** Amount of hydrogen gas produced after 1 h of exposure to distilled water for alcohol-treated or silane-coated silicon powders

The theoretical amount of hydrogen gas evolved was calculated considering the face-centred cubic unit cell structure of silicon crystals (Hanfland *et al.*, 1999). It was assumed that the Si was initially not oxidised and that exactly one layer of Si reacts to form $SiO_2$. The amount of hydrogen produced with these assumptions was estimated as 664 mmol $H_2$/kg Si. The Si exposed to water for 1 h produced an average of 8.3 mmol $H_2$/kg Si This implies that the approximate amount of surface Si available for reaction in the experiments was only about 1.25% that of pure silicon surface.

## 4.4 DTA Burning Behaviour

A pyrotechnic composition of silicon and lead chromate ($PbCrO_4$) was used to establish the effect of silane coating on the DTA response of the composition. The DTA response is shown in Figure 4-5. The untreated silicon gives a sharp exothermic peak with an ignition temperature of about 660 ℃. The two silane-coated silicon compositions show weaker exotherms with an ignition temperature of around 690 ℃. The presence of silane coatings apparently decreased the reactivity of the silicon as characterised by DTA measurements. Berger (2005) stated that the particle size, the active surface area of the oxidiser or fuel, and the degree of mixing are parameters influencing pyrotechnic reaction rates.

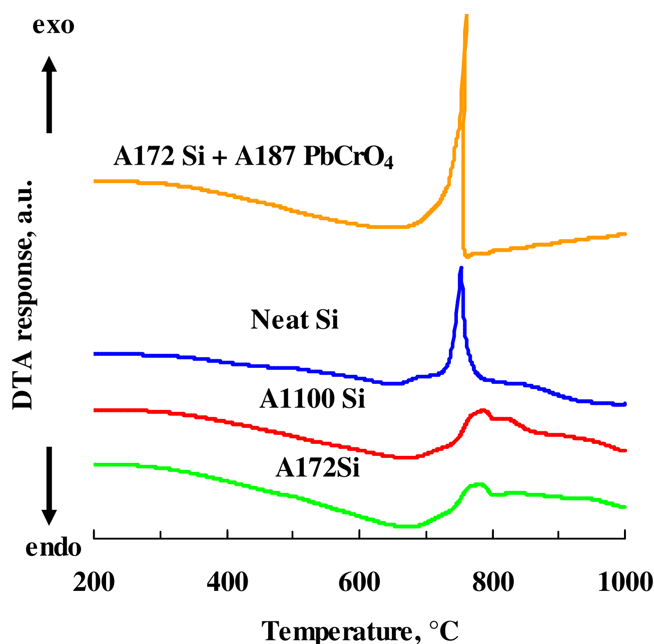


**Figure 4-5** DTA characterisation of 20 wt % Si – 80 wt % $PbCrO_4$ pyrotechnic compositions in a nitrogen atmosphere and at a temperature scan rate of 50 °C/min

It is unlikely that the first two factors were changed by silane treatment. The most likely explanation is that a poorly mixed composition was obtained when the hydrophobic silane-coated sample was processed with the neat, hydrophilic oxidiser. Support for this contention is provided by the results obtained for the composition containing A172-coated silicon and A187-coated $PbCrO_4$. It produced the sharpest exotherm, sharper than the composition consisting of the untreated compounds. This means that the presence of the silane coating *per se* was not responsible for the impairment of the burning behaviour when uncoated oxidiser was used.

# CHAPTER 5 : RESULTS: SILICON SURFACE OXIDATION

## 5.1 Effect of Surface Oxidation on $H_2$ Evolution

Figure 5-1 compares the volume of hydrogen produced from the neat silicon with that produced from silicon powders heated in air at various temperatures before reaction. The results show that the neat silicon produces 13.7 ± 1.0 mmol $H_2$/kg Si when ultrasonically agitated. This represents a 65% increase in hydrogen gas output as compared with the result previously reported using magnetic stirring (Tichapondwa *et al*., 2011) for the same powder. Thermally treating the silicon had varying effects on its reactivity towards water, depending on the pretreatment temperature. Figure 5-1 shows a two-step inhibition process with an initial step decrease to 9.3 ± 0.4 mmol $H_2$/kg Si for silicon heated at 75 °C. This was followed by a gradual decrease in gas evolved from silicon heated from 75 to 300 °C. The gas evolved from silicon heated at 300 °C is 5.6 ± 0.4 mmol $H_2$/kg Si. The second step decrease in the $H_2$ release rate occurred between 300 and 350 °C, with the gas evolved decreasing further to 2.1 ± 0.2 mmol $H_2$/kg Si. This represents an 85% decrease in hydrogen gas evolved as compared with the control. Further increases in heat treatment temperature had no significant effect on the amount of $H_2$ gas evolved thereafter.

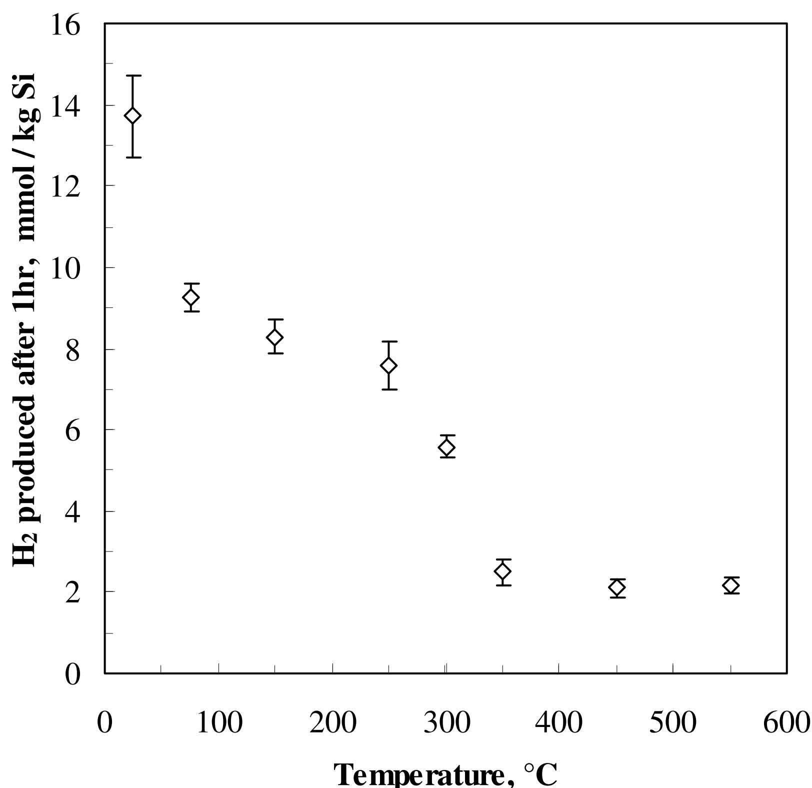


**Figure 5-1** Amount of hydrogen gas produced in 1 h from silicon powders heated for 4 h at varying temperatures and submersed in distilled water with a solid:liquid ratio of 1:2.5

## 5.2 Surface Characterisation

DRIFT spectra were recorded in order to assess the extent and the nature of the change brought about by the thermal treatments. Figure 5-2 shows DRIFT spectra for the neat silicon and silicon powders heated at different temperatures in air. Consider first the spectrum obtained for the neat silicon. The band observed at 3400 $cm^{-1}$ represents the O-H stretch vibration of the Si–OH surface bond. The absorption intensity of this band decreased with increasing heat treatment temperature from the neat silicon to silicon heated at 250 °C. The band location showed a slight shift to lower wave numbers, while the intensity decreased sharply for silicon powders heated at 300 °C and above. This indicates progressive removal of the surface silanol groups. A broad band from 1000–1300 $cm^{-1}$ (asymmetric Si–O–Si stretch vibration) was observed in all the silicon powders characterised. This confirms the presence of $SiO_2$ on the surface of the silicon (Boonekamp *et al.*, 1994). Figure 5-3 shows the variation of the absorbance of the Si-O-Si band at 1000–1300 $cm^{-1}$ with an increase in heat treatment temperature. The

observed absorbances for the neat silicon and samples heat treated at 300 °C or below were similar. This suggests that, in this temperature range, the silica scale layer did not increase much in thickness. Above 300 °C a distinct increase in absorbance of this band is evident. This increase parallels a similar intensity increase of the Si–O–Si bending band (650-820 $cm^{-1}$) from 350 to 550 °C. These observations indicate that the degree of surface oxidation increased from 350 °C and beyond.

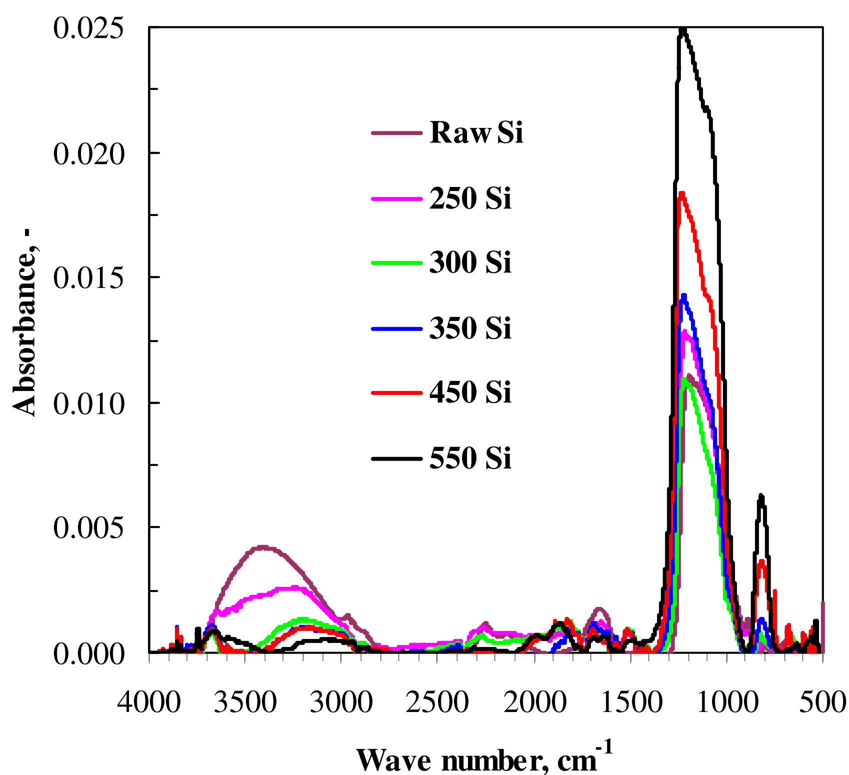


**Figure 5-2** DRIFT spectra of silicon powder surfaces heat treated at various temperatures

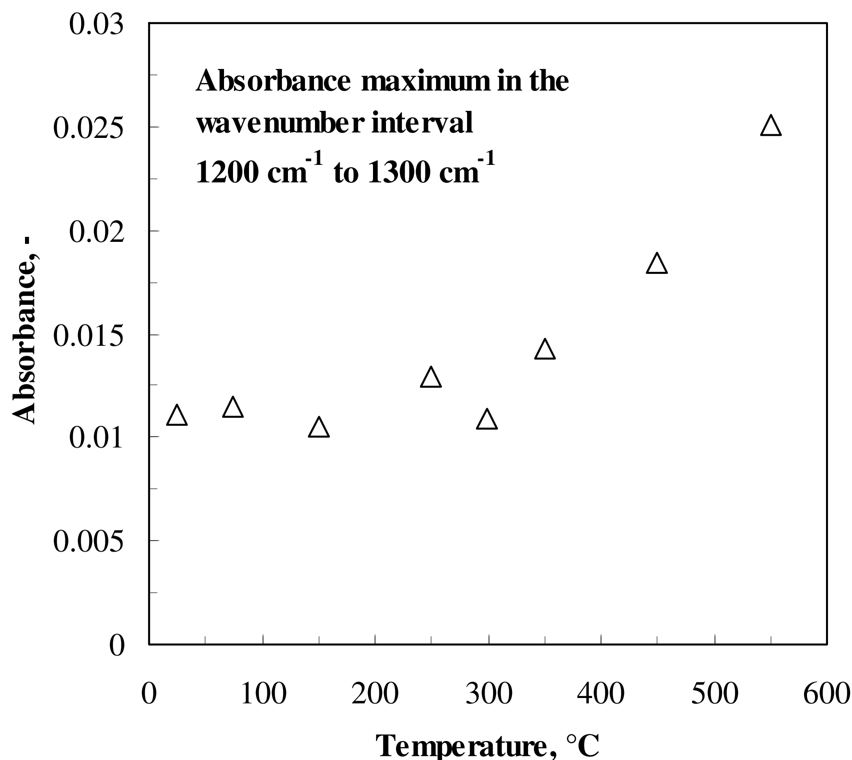


**Figure 5-3** Variation of maximum absorbance of the Si–O-Si band (1000–1300 $cm^{-1}$) with pretreatment temperature

## 5.3 Quantification of Silicon Oxidation

TG analysis was used to estimate the extent of oxidation of the silicon powder. This was done by measuring the total oxygen uptake from the mass increase observed in the TG runs and relating that to the amount of silicon reacted according to Scheme VIII.

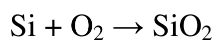

$$Si + O_2 \rightarrow SiO_2$$

**Scheme VIIVIII** Oxidation of silicon in oxygen atmosphere

Figure 5-4 shows the TG results obtained after oxidisation of the neat silicon and the powder obtained by a 4-h heat treatment at 550 °C. Little oxidation occurred during the initial, fast dynamic heating step. The mass increase for the neat silicon was only 2.6% during this stage. However, significant silicon oxidation occurred during the second, slower dynamic heating step. This resulted in a total 49.1% mass increase for the neat silicon. Over time, the isothermal stage also resulted in significant silicon oxidation,

ultimately reaching 87.0% for the neat silicon. Figure 5-4 shows that the TG curves of the neat Si and the silicon heat treated at 550 °C were similar in shape but showed a different overall mass gain. This indicates that the mass of Si available for reaction with oxygen was different. Figure 5-5 reports the silicon content values calculated on the assumption that complete conversion was achieved by the end of the TG runs. The slight difference between the two curves during the dynamic scans indicates that the preformed oxide layer had an effect on the rate of oxidation of the underlying Si.

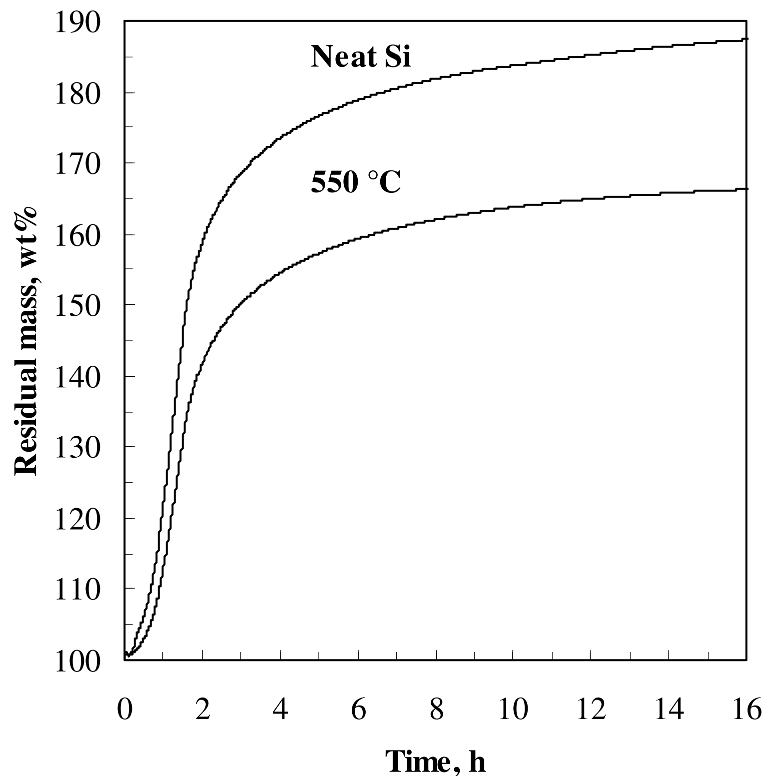


**Figure 5-4** TGA curves for neat silicon and silicon treated at 550 °C when heated in an oxygen atmosphere

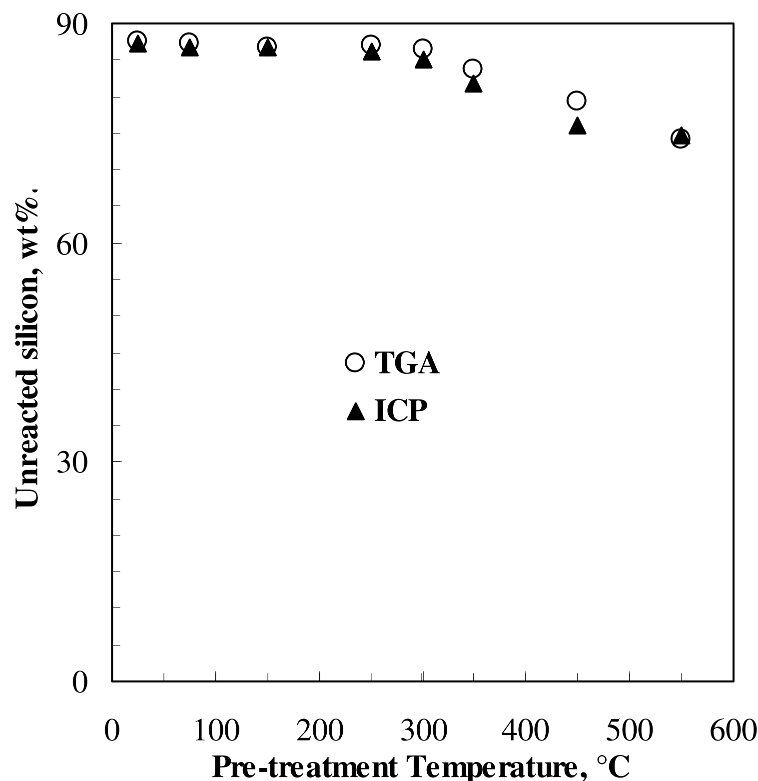


**Figure 5-5** Amount of unreacted silicon present after thermal treatment at various temperatures based on TGA and ICP analysis

ICP-OES was also used to quantify the extent of surface oxidation resulting from the heating processes. The silica layer on the silicon powders was etched away with 10% hydrofluoric acid (HF) solution according to Scheme IX. Although HF reacts with $SiO_2$, it does not attack Si, instead leaving it with a passive layer of surface hydrides (Nakamura *et al.*, 1999).

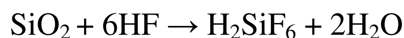

$$SiO_2 + 6HF \rightarrow H_2SiF_6 + 2H_2O$$

**Scheme IIX** Reaction of HF with $SiO_2$

The concentration of Si in the etch solution was determined using ICP-OES. These results were then used to estimate the concentration of the Si associated with $H_2SiF_6$. The ICP-measured concentration was then used to estimate the $SiO_2$ content of the original silicon powder. The assumption was that the HF removed all of the silica. The results are presented in Figure 5-5. The unreacted silicon content values determined via these two methods were in close agreement. It was found that the neat silicon powder

is already significantly oxidised. About 13% of the neat silicon had already been converted to $SiO_2$ before any thermal treatment. The quantities of unreacted silicon obtained between with the neat silicon and the silicon heated to 300 °C are almost identical, with averages of 87.0 ± 0.4% for TG and 86.4 ± 0.8% for ICP respectively. This implies that no noticeable oxidation occurred at this heat treatment temperature or below. These results are consistent with the DRIFT data. A significant decrease in unreacted silicon is observed when the silicon is heat treated at 350 °C. The change, compared with the neat silicon, amounted to 3.32 and 4.59% according to the TG and ICP results respectively. A further increase in the preheating temperature resulted in even greater extents of silicon oxidation. The silicon content of the sample heat treated at 450 °C decreased by 7.6 and 10.5% according to the TG and ICP results respectively. The corresponding values for heat treatment at 550 °C were 12.8 and 11.7%. These observations are consistent with the trend indicated by DRIFT.

## 5.4 FIB-SEM Images

Figure 5-6 shows the cross-sectional focus ion beam – scanning electron microscopy (FIB-SEM) images obtained after selected silicon powder particles heat treated at different temperatures had been milled. The cross-sections for the neat silicon and the silicon treated at 150 and 250 ℃ presented in Figures 5-6 (a), (b) and (c) did not show any detectable oxide layer formation. This suggests that no significant oxidation occurred at these temperatures. This observation is consistent with the results obtained from DRIFT, TG and ICP characterisation. However, it was expected that a detectable oxide film would be present on the neat silicon since approximately 13% of the silicon had already been converted into oxide. The apparent absence of a perceptible oxide layer on the large particles may be due to the relatively wide particle size distribution of the silicon powder (Figure 5-7). The smaller particles with higher specific surface areas and greater surface activity were probably more susceptible to oxidation and had a greater specific surface area available for oxidation than the large particles that were selected for milling with the ion beam (Na *et al.*, 2009). However, a thin film of the deposited platinum is observed. A thin oxide layer was observed on the silicon heated at 350 ℃ (Figure 5-6 (d)). Thicker oxide layers were also detected on the silicon powders heated at 450 and 550 ℃. This indicates increased surface oxidation. These observations confirm earlier

characterisations and give a clear indication that increased $SiO_2$ thickness results in decreased hydrogen evolution.

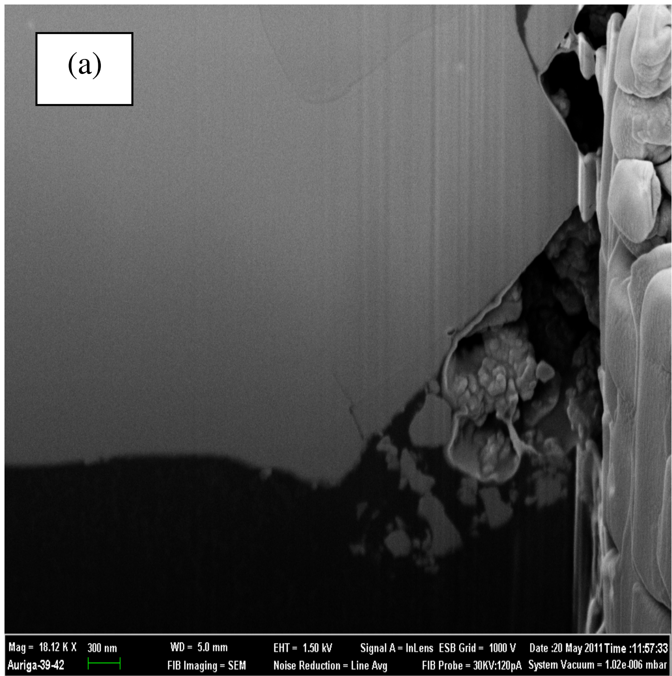


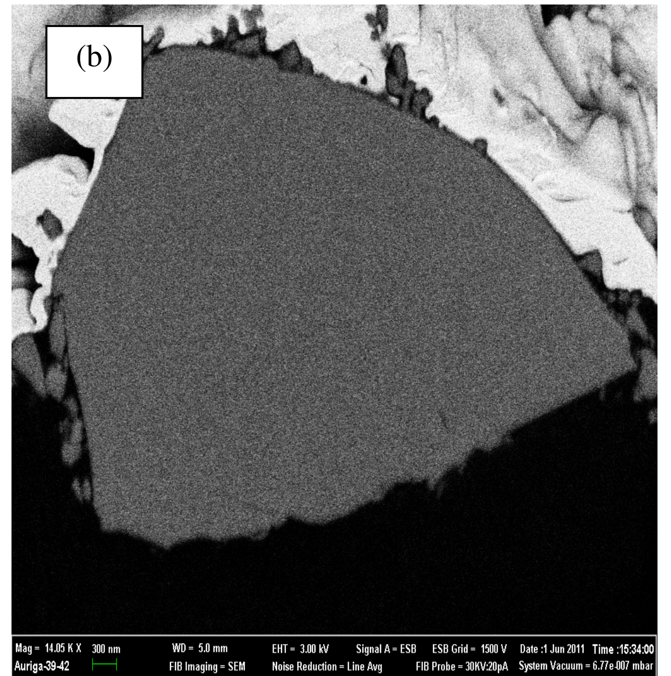


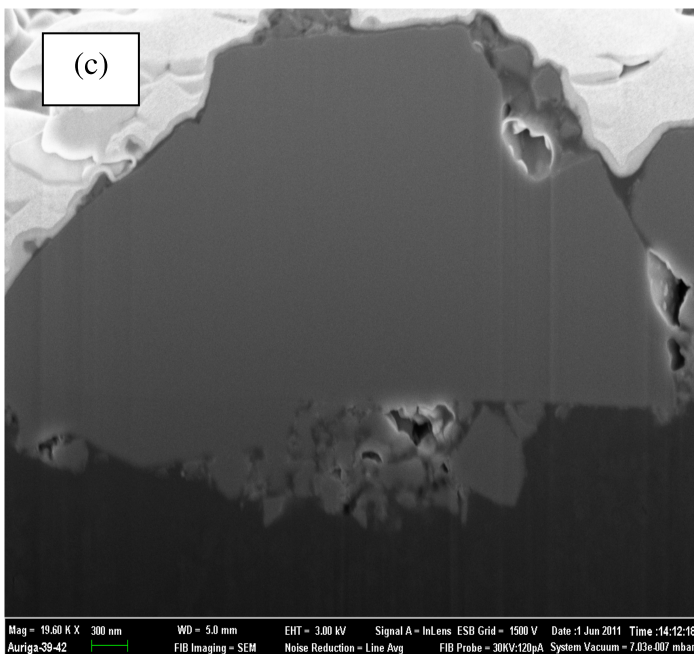


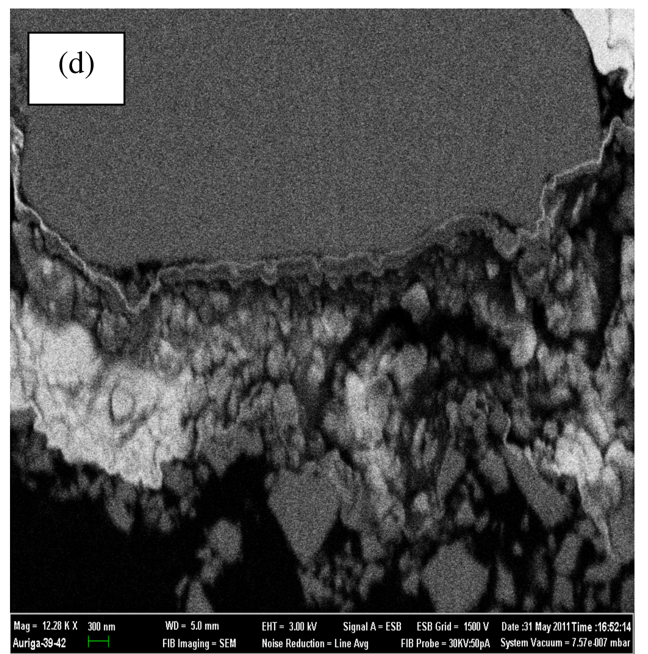

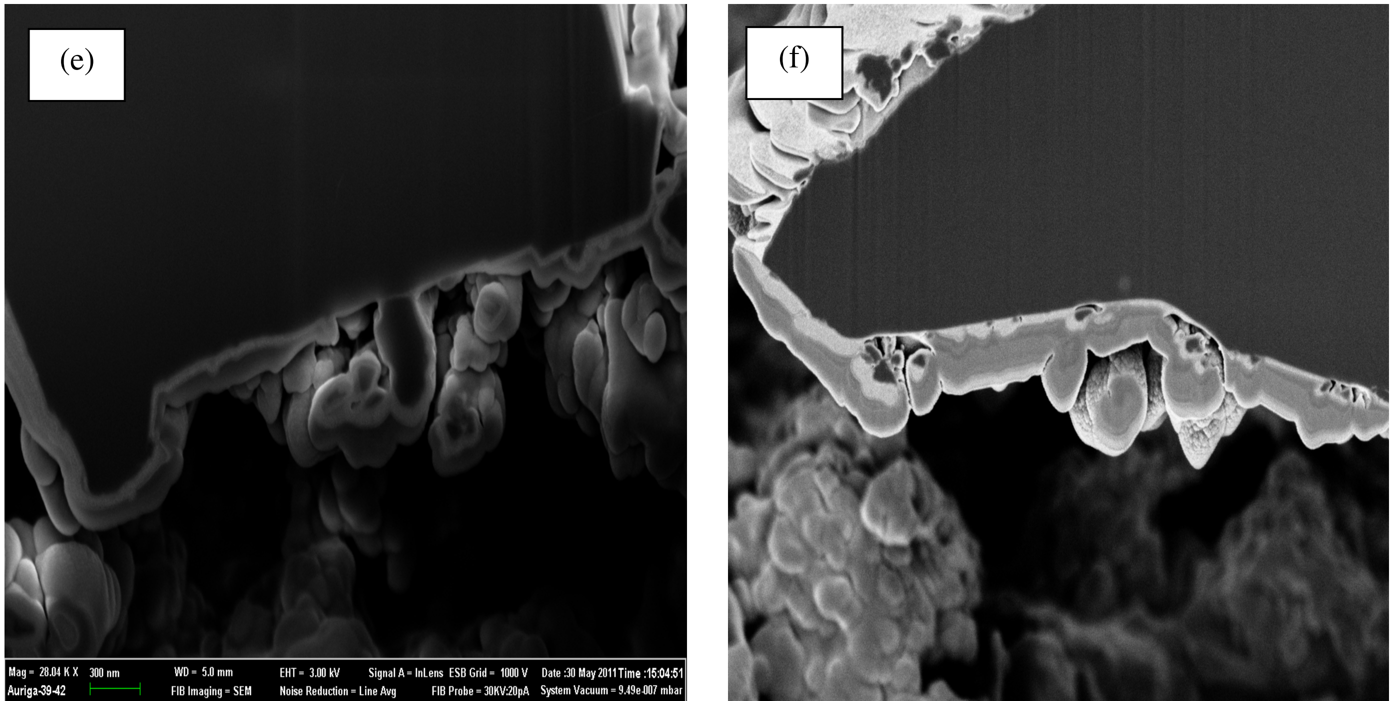


**Figure 5-6** FIB-SEM images showing the cross-section of milled neat silicon particles (a), as well as silicon particles heat treated at (b) 150°C, (c) 250°C, (d) 350°C, (e) 450°C and (f) 550°C respectively

(Note the development of a lighter coloured oxide layer at the bottom edge of particles d to f)

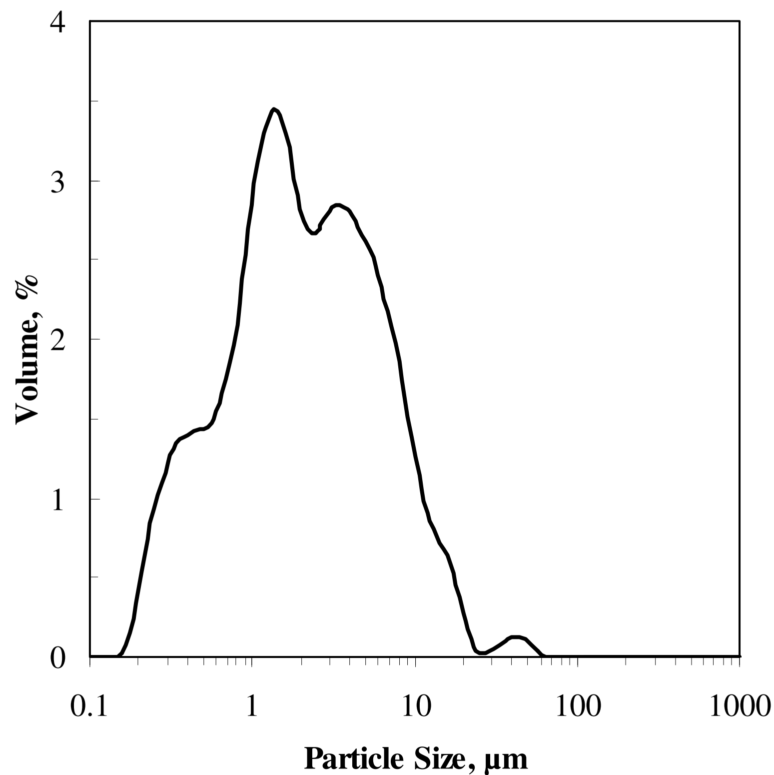


**Figure 5-7** Particle size distribution of neat silicon

## 5.5 Differential Thermal Analysis Results

A pyrotechnic composition of silicon and lead chromate ($PbCrO_4$) was used to establish the effect of preheating silicon powders in air on the DTA response of the composition. Typical DTA responses are shown in Figure 5-8.

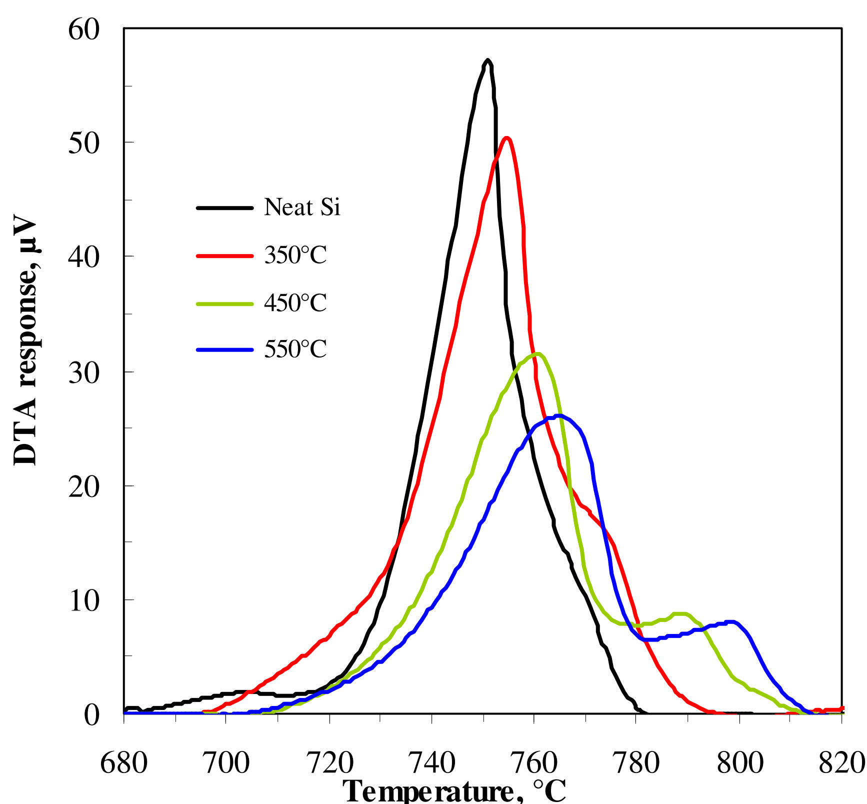


**Figure 5-8** DTA characterisation of 20 wt% Si (preheated at different temperatures) – 80 wt% $PbCrO_4$ pyrotechnic compositions in a nitrogen atmosphere and at a temperature scan rate of 50 °C/min

The silicon powders heat treated at 75 and 300 °C show very similar DTA traces, except that the onset temperature is more than 20 °C higher. The shape of the DTA traces takes on a distinctly bimodal form for silicon heat treated at 350 °C and above. The reason for this is not understood at present. The variation of the reaction onset temperature with silicon preheating temperature is shown in Figure 5-9.

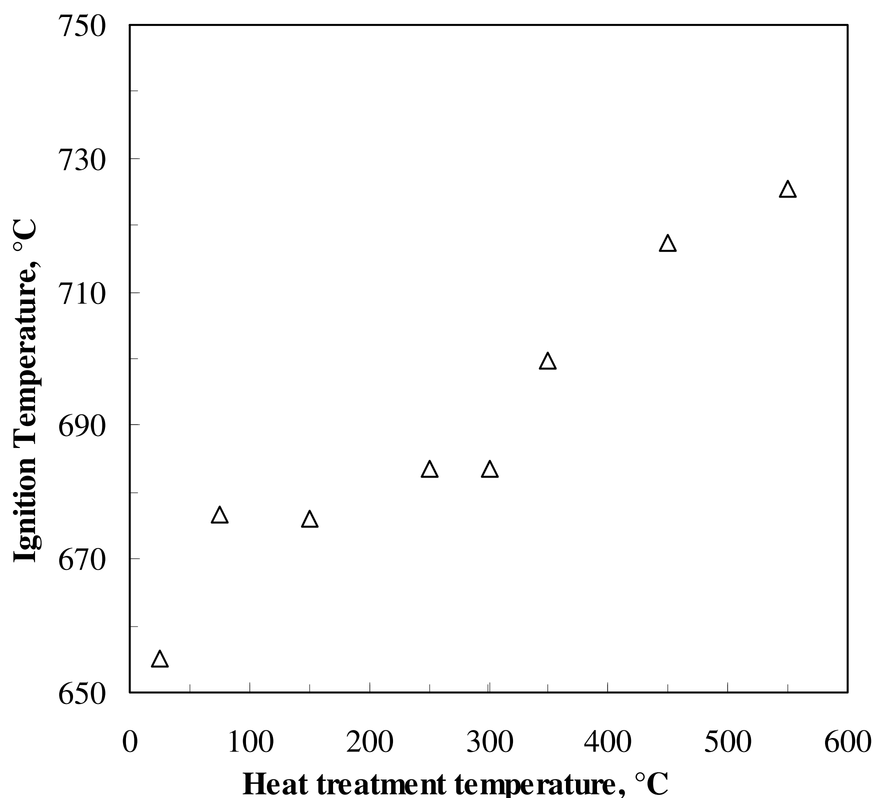


**Figure 5-9** Variation of ignition temperature with silicon powder pretreatment temperature

Neat silicon as fuel gives an exothermic peak with an ignition temperature of about 655 ℃. The onset temperature increases approximately linearly with a heat treatment temperature of 250 °C and higher. The apparent heat of the reaction (Figure 5-10) was estimated from the area under the DTA curves (Laye & Charsley, 1987). The heat of reaction for the compositions with neat silicon and with silicon heat treated up to 300 ℃ were similar. This trend is in agreement with the TG results which showed a minimal decrease in silicon content in this heat treatment temperature range. Samples heat treated at temperatures from 350 to 550℃ showed progressively lower energy outputs. This trend coincides with the decrease in silicon content observed in the TG results in the same range. The DTA results support the notion that the growth of a $SiO_2$ film decreases the reactivity and activity of the silicon. Berger (2005) stated that the particle size, the active surface area of the oxidiser or fuel, the degree of mixing and the ratio of fuel to oxidiser are the main parameters influencing pyrotechnic reaction rates. It is possible that by increasing the thickness of the surface oxide layer, the active surface of the silicon is altered, ultimately affecting the DTA response. Another possible

explanation is that the amount of silicon available per unit mass in the oxidised silicon powder (at 350 ℃ and above) is less than that in the neat silicon powder and hence less energy output should be expected (Ellern, 1968).

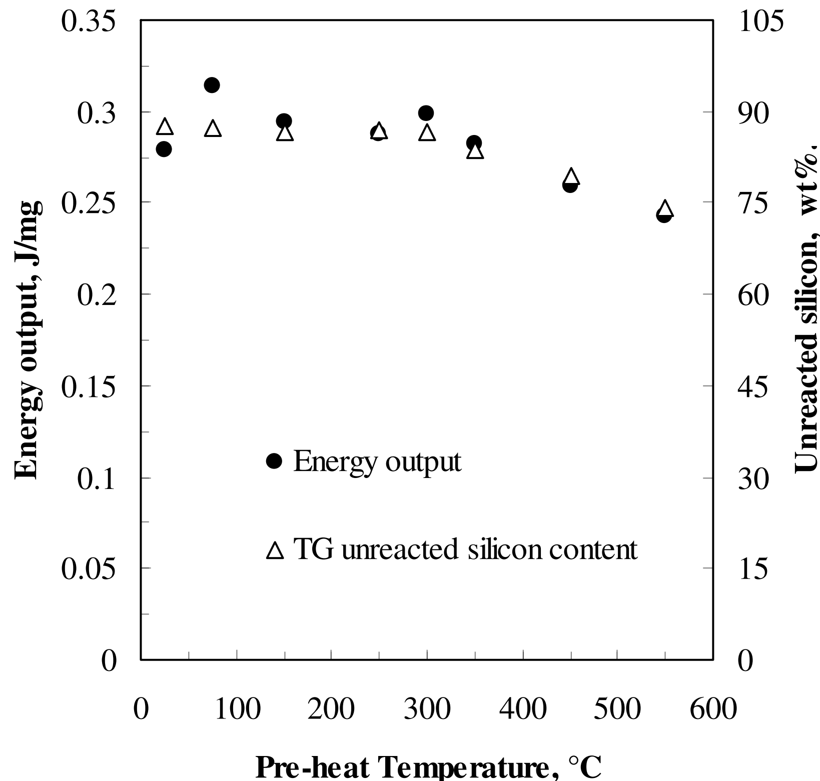


**Figure 5-10** Comparison between the energy output from a 20 wt% Si (preheated at different temperatures) – 80 wt% $PbCrO_4$ pyrotechnic composition and the unreacted silicon available in the powder after preheating at various temperatures

## 5.6 Discussion

It is postulated that the initial step-decrease in hydrogen evolution observed in Figure 5-1 results from the removal of small surface defects in the passivating oxide layer (Bahruji *et al.*, 2009). These defects can be associated with grain boundary sites, as well as silanol terminations (Si–OH). The Si–OH surface bonds were shown by Gräf *et al.* (1989) to be electronegative in nature. This induces polarisation of the nearby Si–Si bonds, making them susceptible to nucleophilic attack by water, which in turn releases hydrogen gas (Gräf *et al.,* 1989). Bahruji *et al.* (2009) state that the silanol terminations are known to be metastable in relation to the oxidised surface and therefore mild heating could lead to a dehydration reaction, removing the defects and replacing them with a passivated $SiO_2$

layer with uniform charge distribution. Bahruji *et al.* (2009) proposed Scheme X to explain the effect of mild heating on the nature of the surface of the silicon powder.

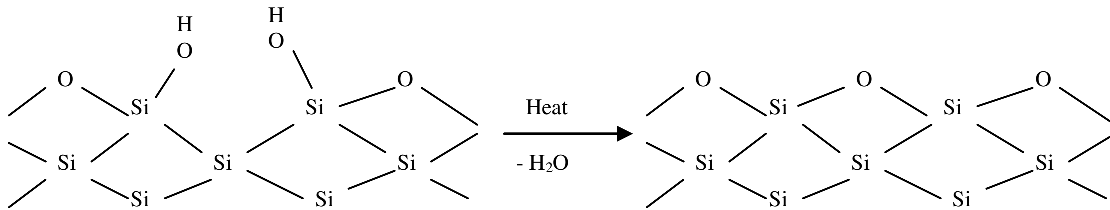


**Scheme X** Mechanism proposed by Bahruji *et al.* (2009) for the thermal passivation of silicon by dehydration of silanol groups at the surface

The second step-decrease in $H_2$ evolution takes place between 300 and 350 °C. This is attributed to thickening of the $SiO_2$ layer due to increased oxidation rather than to mere removal of surface defects. The increased oxide layer thickness represents a greater mass transfer resistance as it limits the rate of oxidant diffusion through it and hence reduces the hydrogen gas evolved. It is, however, surprising to note that increasing the extent of oxidation beyond 350 °C had little effect on the amount of hydrogen evolved.

# CHAPTER 6 : RESULTS: ADDITIONAL CATHODIC REACTIONS

## 6.1 Effect of Introducing Metal Salts on $H_2$ Evolution

Figure 6-1 shows the effect of different metal salts (0.1 M solutions) on hydrogen evolution. The neat silicon powder immersed in distilled water produced 13.7 ± 1.0 mmol $H_2$/kg Si. The nitrogen-purged water produced a comparable amount of hydrogen, i.e. 12.3 ± 0.4 mmol $H_2$/kg Si. These results revealed that under the test conditions studied dissolved oxygen has little influence on the hydrogen evolved. Nearly all the metal salts used reduced the amount of $H_2$ gas produced. The best performance was observed from the copper ($Cu^{2+}$) ion solutions. Copper chloride solution evolved the least hydrogen, i.e. 2.7 ± 0.4 mmol $H_2$/kg Si. This represents an 80.2% reduction in the amount of $H_2$ released over a period of 1 h. The $[Cu\ (NH_3)_4]^{2+}$ complex solution, however, was not as effective as the other copper solutions and resulted in a moderate decrease of 29%. Addition of $KMnO_4$ gave the highest gas volume, but this was most likely due to the release of oxygen via the reduction of $MnO_4^-$ rather than to the release of hydrogen. The performance of the other metal salts tested here was comparable. They all followed the prediction that the more positive the reduction potential, the less hydrogen gas was evolved. Surprisingly, the $Cu^{2+}$ solutions outperformed the $Fe^{3+}$ solutions, even though $Fe^{3+}$ has a higher cell potential. The reason for this may be the high stability of $Fe^{3+}$ (Jeffery *et al.*, 1989). While reduction to $Fe^{2+}$ or Fe may be thermodynamically feasible, it may not be kinetically favourable.

The nature of the anions associated with the metal cations was found to have an effect. In all the metal salt solutions tested, the nitrates consistently outperformed the sulphates for that particular metal. In the case of copper, the volume of hydrogen evolved increased in the following order: $Cl^- < NO_3^- < SO_4^{2-}$. Surprisingly, the $CuCl_2$ solution was the best inhibitor, even though chloride ions tend to increase the rate of corrosion in most metals. These observations can be attributed to the oxidising nature of nitrates which may result in an increased rate of silicon surface oxidation, thus forming a passive silicon dioxide layer which would slow down the rate of transfer of the oxidant to the interface of the reaction. Another plausible explanation may emanate from the differences in interaction of the different ions in solution. Chloride ions are more electronegative than nitrate ions, which in turn are more electronegative than sulphate ions. The more

electronegative the anion, the more likely it is to have been attracted to cations in solution. This results in the preferential formation of an acidic solution rather than the combination of the $H^+$ ions in solution to form $H_2$.

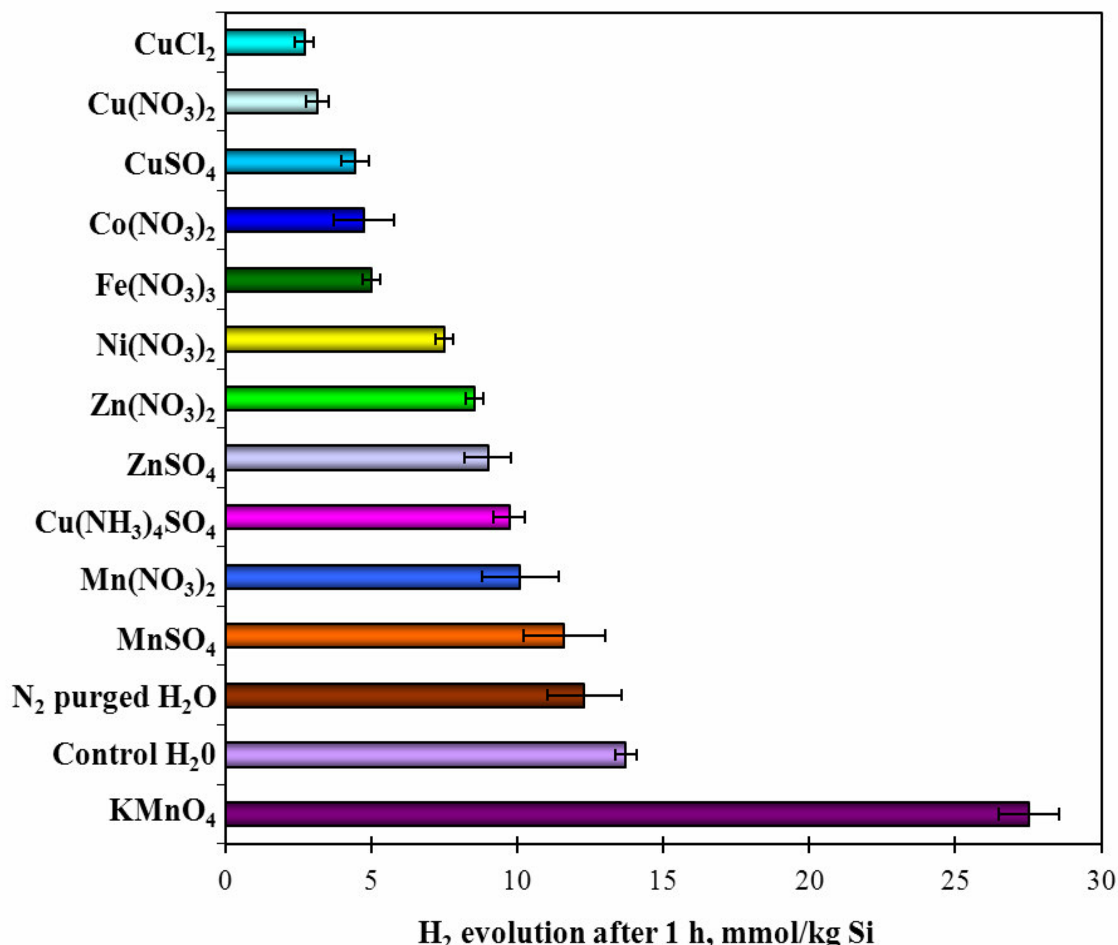


**Figure 6-1** Amount of $H_2$ gas released in 1 h by silicon powders submerged in 0.1 M metal ion solution

(The solid:liquid mass ratio was 1:2.5. The gas evolved by $KMnO_4$ is probably oxygen rather than hydrogen.)

## 6.2 Optimisation of Cu $(NO_3)_2$

Figure 6-2 shows the amount of hydrogen evolved as a function of copper nitrate concentration. The results indicate a rapid decrease in the amount of gas evolved with increasing concentration, but a plateau value is reached above a critical concentration. Any further increase in metal ion concentration did not affect the amount of gas evolved. The critical solution concentration is about 0.04 M $Cu(NO_3)_2$. The Nernst equation for the

reaction of silicon with copper ions shows that the value of the cell potential ($E^{cell}$) is a function of both metal ion concentration and pH (Pourbaix, 1996). The relationship for the silicon and copper cell is given by:

$$E^{cell} = 1.23 - 0.118pH - 0.059 \log [Cu^{2+}] \tag{6-1}$$

According to Equation (6-1), the overall cell potential increases with the copper ion concentration. This could, in part, explain the greater inhibition effect at higher copper salt concentrations. Also, solutions with lower copper concentrations featured higher pH values which enhance hydrogen evolution (Hackley *et al.,* 1997).

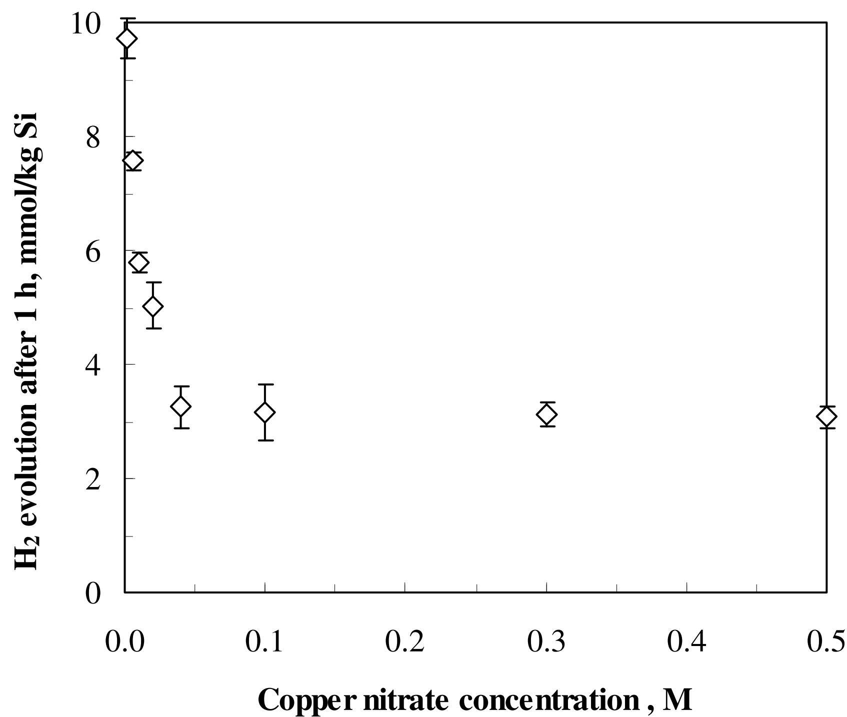


**Figure 6-2** The effect of $Cu(NO_3)_2$ concentration on the amount of hydrogen evolved in 1 h of exposure

## 6.3 Copper Deposited

Figure 6-3 shows a representative data set obtained with a 0.04 M $Cu(NO_3)_2$ solution as dispersing medium. It shows the solution pH and copper concentration, as well as the amount of hydrogen evolved as a function of time. Careful inspection of this and other data sets reveals that the interaction of silicon powder with the electrolyte shows three distinct stages. The first stage is very short, lasting less than 2 min, and it is characterised

by a sudden drop in both the solution pH (from pH = 4.35 to pH = 4.06) and the copper concentration (from about 2.74 g/L to 2.26 ± 0.16 g/L in the data set shown in Figure 6-3. The drop in the copper concentration amounts to about 1.06 mg Cu/g Si. Little or no gas evolution occurred during this stage, during which the copper deposited. The theoretical amount of copper required to cover the surface of silicon, assuming monolayer coverage, was calculated taking into consideration the face-centred cubic unit cell structure of copper. The amount of copper required with these assumptions was estimated to be 14 mg Cu/g Si. This implies that the approximate amount of surface silicon available for reaction with copper ions in the experiments was 7.5% of pure silicon surface.

The second step lasted for about 23 min. The copper concentration in the solution apparently remains unchanged, although the pH shows a slight upward drift. Virtually all the hydrogen gas evolves during this stage. At the end of the second stage, hydrogen evolution stops as the silicon surface becomes passivated.

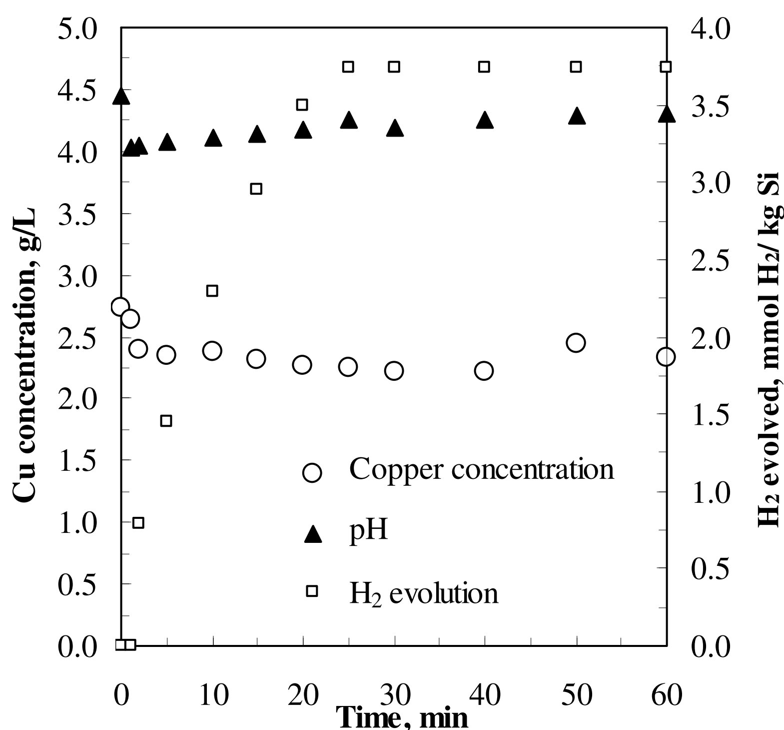


**Figure 6-3** Copper ion concentration, solution pH and amount of hydrogen gas evolved as a function of time for Si powder dispersed in 0.04 M $Cu(NO_3)_2$ and ultrasonically agitated

Figure 6-4 compares hydrogen evolution with silicon dispersed in distilled water or in 0.04 M solutions of the three copper metal solutions. Compared with distilled water, all the copper salts show a significant inhibiting effect on hydrogen evolution. During the test period of 1 h, all the copper solutions stopped releasing hydrogen after 30 min, while the silicon dispersed in distilled water was still releasing hydrogen at 60 min, although the rate of hydrogen release appears to decrease. The anion effect on the rate of hydrogen release is also clearly demonstrated in these results.

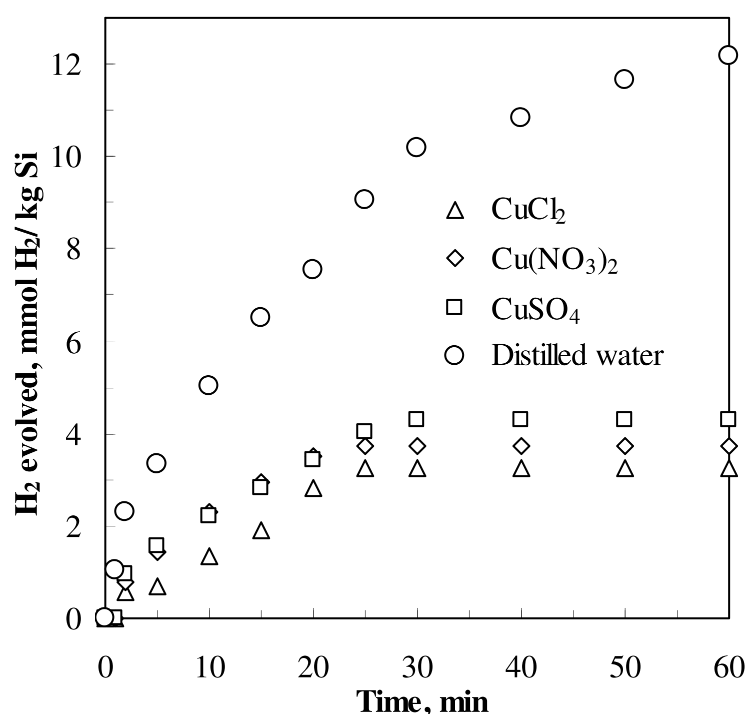


**Figure 6-4** Rate of hydrogen evolution when silicon is dispersed in 0.04 M solutions of copper, as well as in distilled water

Table 6-1 gives the quantities of copper deposited in relation to the silicon added in three different 0.1 M solutions of copper. The amount of copper deposited varied with the type of anion present. Surprisingly, the amount of copper deposited did not follow a trend consistent with that observed for hydrogen evolution. Harraz *et al.* (2002) previously reported on the effect of anions on copper deposition. They found that an increase in chloride ion concentration decreased copper deposition. They postulated that the chloride ions deactivate silicon's ability to reduce copper ions by attaching to the

active sites on the silicon surface. Silicon immersed in $CuCl_2$ solution showed the least amount of copper deposited, which is in agreement with their observations.

**Table 6-1** Amount of Cu deposition on Si after immersion in 0.1 M $Cu^{2+}$ salt solutions

| Metal salt | Cu deposited (mg Cu/g Si) |
|---|---|
| Copper chloride ($CuCl_2$) | 0.61 |
| Copper nitrate ($Cu(NO_3)_2$) | 0.85 |
| Copper sulphate ($CuSO_4$) | 2.28 |

## 6.3 Surface Characteristics of Silicon Treated with a Metal Solution

Copper deposition during the initial stage of the reaction represents a competing cathodic reaction. Consequently, it is not surprising that hydrogen evolution is effectively inhibited during this stage. Nevertheless, copper deposition also drives the oxidation of silicon as the anodic reaction (Jeske *et al*., 1995; Harraz *et al*., 2002). DRIFT spectra of the neat silicon, as well as those of silicon aged by lengthy immersion in copper salt solutions, are shown in Figure 6-5. The adsorption band located between 1000 and 1300 $cm^{-1}$ is assigned to the asymmetric stretch vibration of the Si–O–Si bond. The intensity of this band provides a measure of the extent of silicon oxidation. Figure 6-5 also indicates just a slight increase in the maximum absorbance corresponding to this band for silicon dispersed in the three different copper solutions. Once the silicon surface was adequately oxidised, and for practical purposes effectively passivated, virtually no further oxidation occurred. This explains the slight increase in the magnitude of the Si–O–Si asymmetric stretch band. A slight increase in the magnitude of the band at 3400 $cm^{-1}$, which represents the stretch vibration of the O–H in the Si–OH surface bond, is noted in the spectra. It is attributed to incomplete drying of the powder following the recovery of the silicon powder after immersion in metal salt solution.

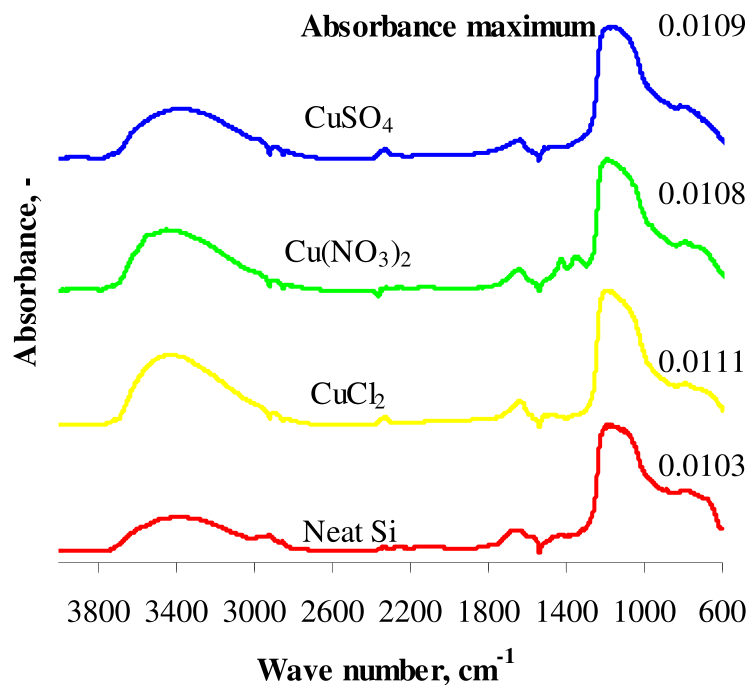


**Figure 6-5** DRIFT spectra of silicon powders exposed to different copper metal solutions

(The measured absorbance maximum in the wave number interval 1000 $cm^{-1}$ to 1300 $cm^{-1}$ is indicated.)

## 6.4 Burn Behaviour of Pyrotechnic Composition

### 6.4.1 Si–$BaSO_4$ open-flame test results

The reactivity of silicon aged for different time periods in distilled water and 0.04 M $Cu(NO_3)_2$ solution was analysed by testing the open-flame reactivity of a 44 wt % Si–56 wt % $BaSO_4$ pyrotechnic composition prepared using these silicon powders. The results obtained (see Table 6-2) indicate that although copper nitrate solution is effective as a hydrogen inhibitor, it negatively affects the reactivity of silicon in the composition tested faster than water. It took 35 days before the pyrotechnic composition, prepared with silicon slurried in distilled water, failed to ignite. It took only 4 days to deactivate the silicon slurried in the copper nitrate solution. This is likely to be a result of the presence of unreactive copper metal, as well as of increased silicon oxidation caused by the metal solution.

**Table 6-2** Open-flame burn characteristics of 44% Si–$BaSO_4$ pyrotechnic composition prepared using silicon powders aged for different time lengths

| Exposure time (days) | 0 | 2 | 4 | 10 | 14 | 21 | 28 | 35 |
|---|---|---|---|---|---|---|---|---|
| **Distilled water** | I | I | I | I | I | I | I | D |
| **0.04 M $Cu(NO_3)_2$ solution** | I | I | X | D | D | D | D | D |

** I = Ignites and propagates; D = Difficult to ignite and does not propagate; X = Difficult to ignite but does propagate

### 6.4.2 Differential thermal analysis

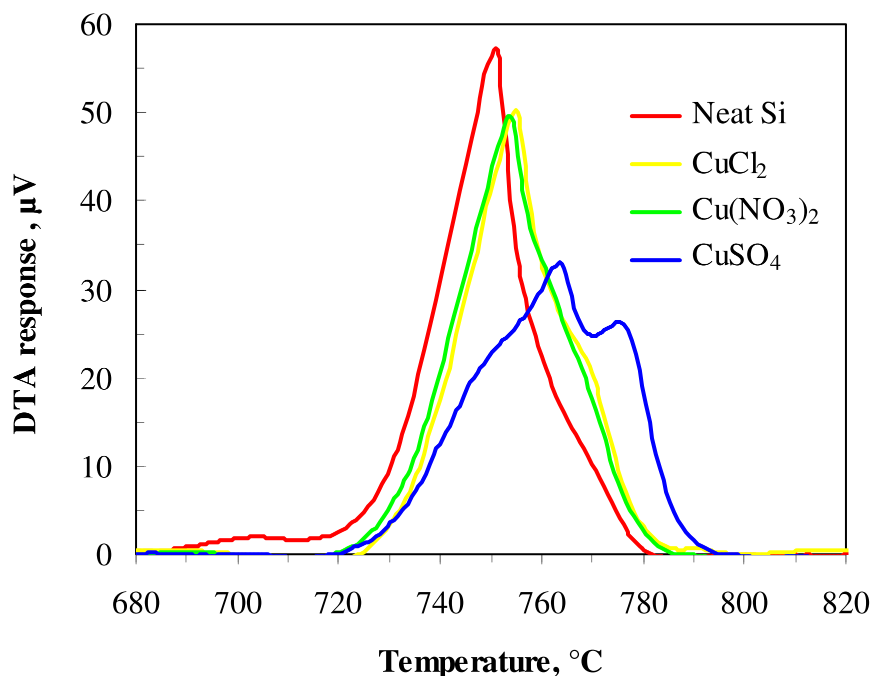


**Figure 6–6** DTA signals of 20 wt % Si (immersed in 0.1 M copper solutions) + 80 wt % $PbCrO_4$ pyrotechnic compositions in a nitrogen atmosphere and at a temperature scan rate of 50 °C/min

The reactivity of the silicon exposed to metal ion solutions was studied using the DTA response of the pyrotechnic composition containing 80 wt % lead chromate ($PbCrO_4$) (see Figure 6-6). The silicon powders dispersed in $CuCl_2$ and $Cu(NO_3)_2$ solutions showed DTA traces similar to that of the neat silicon, although there is a shift in the onset temperature by more than 35 °C for the silicon dispersed in the metal solutions. The shape of the DTA trace of silicon dispersed in $CuSO_4$, however, took on a distinctly bimodal form. Table 6-2 reports the DTA reactivity data for the compositions prepared

using different silicon powders. The energy output from the compositions prepared using neat silicon and $Cu(NO_3)_2$-treated silicon are similar, while there is a progressive decrease in heat output for $CuCl_2$ and $CuSO_4$ respectively. The decrease in energy output is attributed to both the thicker oxide layer on the silicon particles (confirmed by FTIR) and the presence of unreactive copper metal.

**Table 6-3** DTA reactivity of the pyrotechnic compositions prepared with silicon powders treated with different metal salt solutions

| Metal salt | Onset temperature (°C) | Energy output (kJ/kg) |
|---|---|---|
| Neat Si | 690 | 284 |
| Copper nitrate ($Cu(NO_3)_2$) | 729 | 284 |
| Copper chloride ($CuCl_2$) | 731 | 278 |
| Copper sulphate ($CuSO_4$) | 729 | 266 |

### 6.5 Discussion

Figure 6-3 showed three distinct stages of hydrogen evolution. The first stage showed a small quantity of gas being evolved in the first 2 min of the reaction. This was attributed to a partial blocking of the silicon surface by copper deposits. This reduces the active surface area available for the oxidation. The copper deposition is accompanied by silicon oxidation which also contributes to the passivity of the silicon surface. The second stage showed a near-linear increase in $H_2$ evolution after the initial passivation. This is possibly as a result of the surface oxide layer not having attained the minimum thickness required to hinder the diffusion of water to the underlying silicon. Previous work showed that for minimal hydrogen to be evolved it is essential that a certain oxide thickness be achieved. Since the mechanism of silicon oxidation involves the diffusion of the oxidant to the silicon surface through the oxide layer (Deal & Grove, 1965), it is unlikely that copper ions will preferentially diffuse through the oxide layer compared to water molecules since water molecules have a higher diffusion coefficient (Heiser & Mesli, 1993; Tomozawa, 2011). As a result no further decrease in copper concentration is recorded. The last stage, in which no more gas is evolved after 30 min, is a result of complete passivation of the underlying silicon.

# CHAPTER 7 : CONCLUSIONS

The oxidation of silicon powder in water was studied and the effects of medium pH and organic surface modifications on the oxidation rate were investigated. The hydrogen evolution kinetics of unmodified silicon submerged in buffer solutions appeared to follow the logarithmic rate law. It was found that silane coupling agents are effective short-term inhibitors of silicon corrosion in water and that approximately a monolayer attaches to the silicon, despite the presence of an organic contaminant. Vinyl tris(2-methoxyethoxy) silane was identified as the most effective inhibitor. The present data also hint at the possibility that the nature of the hydrolysable group may affect the corrosion inhibition performance of the silane with respect to silicon exposed to water. The DTA evaluations indicate that employment of a silane coating on the silicon fuel necessitates a corresponding surface treatment of the oxidiser powder to ensure that intimate mixing of the reagents is achieved.

The oxidation of silicon powder in water was studied and the effect of air oxidation of silicon at different temperatures on the rate was investigated. It was found that the extent of surface oxidation varied with the heat treatment temperature, with 350 °C being the onset temperature for silicon oxidation of the powder examined. The rate of silicon oxidation in water decreased with increases in surface oxidation; this shows that a passivated $SiO_2$ barrier layer has an effect on the underlying silicon. The FTIR data also suggest that some inhibition is imparted below 350 °C and that this is due mainly to the removal of silicon surface hydroxyl groups rather than to an increase in the $SiO_2$ thickness. The DTA evaluations indicate that the development of a silicon surface oxide affects the DTA response of the pyrotechnic composition tested.

The effect of introducing an additional cathodic reaction to that of water reduction on the amount of gas evolved was tested. The effect of this silicon treatment on the reactivity of pyrotechnic compositions was also studied. The use of metal salt solutions was found to be effective in decreasing the amount of hydrogen gas released. The inhibition effect generally followed the thermodynamic feasibility trend predicted using the standard cell potentials, with the metal solutions with the more positive overall cell potential having the greater hydrogen-inhibition effect. The preferential deposition of copper in place of hydrogen evolution was shown to take place only in the initial stages of

the reaction. Therefore passivation is achieved as a result of accelerated oxidation of silicon due to additional cathodic reactions rather than competing cathodic reactions.

The effect of the metal salt treatments on the reactivity of silicon in different pyrotechnic compositions was determined. The chemical reactivity and activity of a 20 wt % silicon + 80 wt % lead chromate pyrotechnic composition were determined as the DTA onset temperature and the reaction heat released. The DTA onset temperature for neat silicon was about 690 °C. The onset temperature, however, increased after exposure to copper metal salts by more than 30 °C. The heat release also decreases with metal salt treatment. Open-flame tests on a 44 wt % silicon + 56 wt % $BaSO_4$ composition showed that 4-day exposure of silicon to $Cu(NO_3)_2$ retards silicon reactivity as compared with 35-day exposure in distilled water.

An overall comparison of the three different approaches showed that organic coating using silane A172 was the most effective, with a 97% reduction in hydrogen evolved. This was followed by air oxidation of silicon at 350 °C, which resulted in an 85% reduction. The use of copper chloride solution as the aqueous dispersion medium for silicon resulted in an 80.2% decrease in gas evolved. A comparison of the DTA responses when the treated silicon powder was used in producing Si–$PbCrO_4$ pyrotechnic compositions showed that although silicon air oxidation and dispersion in copper solutions negatively affected the DTA response of the composition, silane coating actually enhanced the response, but only after the lead chromate had been coated with a silane and the mixing had been improved.

**REFERENCES**

Adams, D., Danielsson, F., Lalaut, S., Lundorf Wessman, B. and Schwarz, S. (2009). Safety practices related to the storage of fireworks in the context of land use planning. Issue paper presented at OECD WGCA Steering Group on Development of Safety Practises Related to the Storage of Fireworks in Context of Land Use Planning. Accessed in September 2011 at: http://www.vinnueftirlit.is/vinnueftirlit/upload/files/efna-storslysavarnir/oecdissuepapersafetyfirework-090909.pdf

Answers (2011). Accessed in July 2011 at: http://www.answers.com/topic/delay-element#ixzz1EPQkiMsW

Antonijevic, M.M. and Petrovic, M.B. (2008). Copper corrosion inhibitors. A review. *Int. J. Electrochem. Sci.*, **3**: 1-28.

Atolabi, A.S. and Borode, J.O. (2010). Effect of ammonia molybdate inhibition on corrosion behaviour of mild steel in chloride and sulphide media. *Int. J. Ind. Chem.*, **1**: 11-16.

Bahruji, H., Bowker, M. and Davies, P.R. (2009). Photoactivated reaction of water with silicon nanoparticles. *Int. J. Hydrogen Energ.*, **34**: 8504-8510.

Beck, M.W. and Flanagan, J. (1992). Delay composition and device. *US Patent 5 147 476.*

Bennett, O.G. and Baltimore, J.D. (1949). Delay fuse compositions. *US Patent 2 457 860.*

Berger, B. (2005). Parameters influencing the pyrotechnic reaction. *Prop. Explos. Pyrotech.*, **30**: 27-35.

Boonekamp, E.P., Kelly, J.J., Van de Ven, J. and Sondag, A.H.M. (1994). The chemical oxidation of hydrogen – Terminated silicon (111) surfaces in water studied in situ with Fourier transform infrared spectroscopy. *J. Appl. Phys.*, **75:** 8121-8127.

Buriak, J.M. (2002). Organometallic chemistry on silicon and germanium surfaces. *Chem. Rev.*, **102**: 1271-1308.

Butler, I.B., Schoonen, M.A.A. and Rickard, D.T. (1994). Removal of dissolved oxygen from water: A comparison of four common techniques. *Talanta*, **41**: 211-215.

Cabrera, N. and Mott, N.F. (1948-1949). Theory of the oxidation of metals. *Rep. Prog. Phys.*, **12**: 163.

Carcassi, M.N. and Fineschi, F. (2005). Deflagrations of $H_2$–air and $CH_4$–air lean mixtures in a vented multi-compartment environment. *Energy*, **30**: 1439–1451.

CBS (2004). Sierra Chemical Co. High Explosives Accident. U.S. Chemical Safety and Hazard Investigation Board. Accessed in September 2011 at: www.csb.gov/assets/document/CSB_Sierra.pdf

Chan, S.K., Hsu, N.Y.W. and Oliver, R. (1996). Process for the preparation of gas-generating compositions. *European Patent Application 0735013 A1*, 10 – 02.

Cohen, M. (1959). The formation and properties of passive films on iron. *Can. J. Chem.*, **37**: 286-29.

Coulthard, I., Jiang, D.T., Lorimer, J.W. and Sham, T.K. (1993). Reductive deposition of Pd on porous silicon from aqueous solutions of $PdCl_2$: An X-ray adsorption fine structure study. *Langmuir*, **9**: 3441-3445.

Crowell, J.E., Tedder, L.L., Cho, H–C., Cascarano, F.M. and Logan, M.A. (1990). The chemical vapour deposition of $SiO_2$ from TEOS. *J. Electron. Spectrosc. Relat. Phenom.*, **54-55**: 1097-1104.

Danali, S.M., Palaiah, R.S. and Raha, K.C. (2010). Developments in pyrotechnics. *Defence Sci. J.*, **60**: 152-158.

Davitt, A.L. and Yuill, K.A. (1983). Delay composition for detonators. *US Patent 4 374 686*.

Deal, B.E. and Grove, A.S. (1965). General relationship for the thermal oxidation of silicon. *J. Appl. Phys.*, **36**: 3770-3778.

Debarge, L., Stoquert, J.P., Slaoui, A., Stalmans, L. and Poortmans, J. (1998). Rapid thermal oxidation of porous silicon for surface passivation. *Mat. Sci. Semicon. Proc.,* **1**: 281-285.

Demjen, Z., Pukanszky, B., Foldes, E. and Nagy, J. (1997). Interaction of silane coupling agents with $CaCO_3$. *J. Colloid Interface Sci.,* **190**: 427-436.

Dingemans, G., Van der Sanden, M.C.M. and Kessels, W.M.M. (2011). Excellent Si surface passivation by low temperature $SiO_2$ using an ultrathin $Al_2O_3$ capping film. *Physica Status Solidi RRL 5*, **1**: 22-24.

Ellern, H. (1968). *Military and Civilian Pyrotechnics*. Chemical Publishing Co, New York, US.

Evans, U.R. (1971). *The Corrosion and Oxidation of Metals*. Edward Arnold, London, UK.

Fordham, S. (1980). *High Explosives and Propellants*, second revised edition. Pergamon Press, Oxford, UK.

Fromhold, A.T. (1976). *Theory of Metal Oxidation*. North Holland Publishing Co, Amsterdam, Netherlands.

Glass, J.A, Wovchko, E.A. and Yates, J.T. (1995). Reaction of methanol with porous silicon. *Surf. Sci.*, **338:** 125-137.

Gräf, D., Grunder, M. and Schulz, R. (1989). Reaction of water with hydrofluoric acid treated silicon (111) and (100) surfaces. *J. Vac. Sci. Technol. A.*, **7:** 808-813.

Gruvin, B.E., Johansson, T. and Hatcher, M.E. (1985). Low temperature oxidation of silicon powders. *Mater. Sci. Eng.*, **71**: 363-367.

Gulbransen, E.A. (1949). Kinetic and structural factors involved in oxidation of metals. *Ind. Eng. Chem. Res.*, **47**: 1385-1391.

Guoshun, Z. (2000). Causes and lessons of five explosion accidents. *J. Loss Prevent. Proc.*, **13**: 439-442.

Hackley, V.A., Paik, U., Kim, B. and Malghan, S.G. (1997). Aqueous processing of sintered reaction-bonded silicon nitride. I. Dispersion properties of silicon powder. *J. Am. Ceram. Soc.*, **80**: 1781-88.

Harraz, F.A., Sakka, T. and Ogata, Y.H. (2002). Effect of chloride ions on immersion plating of copper onto porous silicon from methanol solution. *Electrochim. Acta*, **47**: 1249-1257.

Heiser, T. and Mesli, A. (1993). Determination of the copper diffusion in silicon from transient ion drift. *Appl. Phys. A.*, **57**: 325-328.

Hopper, M.A., Clarke, R.A. and Young, L. (1975). Thermal oxidation of silicon. *J. Electrochem. Soc.*, **122**: 1216-1222.

Ilunga, K. Del Fabbro, O., Yapi, L. and Focke, W.W. (2011). The effect of Si-$Bi_2O_3$ on the ignition of the Al-CuO thermite. *Powder Technol.*, **205**

Irene, E.A. (1978). Silicon oxidation studies: Some aspects of the initial oxidation regime. *J. Electrochem. Soc.*, **125**: 1708-1714.

Irene, E.A. (1988). Models for the oxidation of silicon. *Crit. Rev. Solid State.*, **14**: 175-223.

Irene, E.A. and Ghez, R. (1977). Silicon oxidation studies: The role of $H_2O$. *J. Electrochem. Soc.*, **124**: 1757-1761.

Irene, E.A. and Van der Meulen, Y.J. (1976). Silicon oxidation studies: Analysis of $SiO_2$ film growth rate. *J. Electrochem. Soc.*, **123**: 1380-1384.

Jeffery, G.H., Bassett, J., Mendham, J. and Denney, R.C. (1989). *Vogel's Textbook of Quantitative Chemical Analysis*. Longman Scientific and Technical, New York, US.

Jeske, M., Schultze, J.W., Thonissen, M. and Munder, H. (1995). Electrodeposition of metals into porous silicon. *Thin Solid Films*, **225**, 63-66.

Kamins, T.I. and MacKenna, E.L. (1971). Thermal oxidation of polycrystalline silicon films. *Metall. Mater. Trans. B.*, **2**: 2292-2294.

Kanungo, J., Maji, S., Mandal, A.K., Sen, S., Bontempi, E., Balamurugan, A.K., Tyagi, A.K., Uvdal, K, Sinha, S., Saha, H. and Basu, S. (2010). Surface treatment of nanoporous silicon with noble metal ions and characterizations. *Appl. Surf. Sci.*, **256**: 4231-4240.

Karmaker, A., Prasad, A. and Sarkar, N.K. (2007). Characterisation of adsorbed silane on fillers used in dental composite restoratives and its effect on composite properties. *J. Mater. Sci. Med.*, **18**: 1157-1162.

Khaikin, B.I. and Merzhanov, A.G. (1966). Theory of thermal propagation of a chemical reaction front. *Comb. Exp. Shock Waves,* 2: 36-46.

Kim, K., Lee, Y.H., An, M.H. Suh, M.S., Youn, C.J., Lee, K.B. and Lee, H.J. (1996). Growth law of silicon oxides by dry oxidation. *Semicond. Sci. Technol.*, **11**: 1059-1064.

Kirchsteiger, C., Vetere Arellano, A.L. and Funnemark, E. (2007). Towards establishing an international Hydrogen Incidents and Accidents Database (HIAD). *J. Loss Prevent. Proc*, **20**:98-107.

Klechka, E.W. (2001). Use of corrosion inhibitors on the Trans Alaska pipeline. COROTEC CORP. Supplement to Materials Performance. Accessed in October 2011 at: http://www.cortecvci.com/Publications/Papers/Petro_Chem/Pages07_09.pdf

Knag, M. (2006). Fundamental behaviour of model corrosion inhibitors. *J. Disper. Sci. Technol.*, **27**: 587-597.

Koch, E-C. and Clement, D. (2007). Special materials in pyrotechnics. VI. Silicon – An old fuel with new perspectives. *Prop. Explos. Pyrotech.*, **32**: 205-212.

Kosanke, K.L., Kosanke, B.J. and Jennings-White, C. (2004). Lecture Notes for Pyrotechnic Chemistry, *Journal of Pyrotechnics Inc*

Kuznetsov, Y.I. (1996). *Organic Inhibitors of Corrosion of Metals*. Plenum Publishers. New York, US.

Laye, P.G. and Charsley, E.L. (1987). Thermal analysis of pyrotechnics. *Thermochim. Acta.*, **120**: 325-349.

Leach, J.S.L. (1975). The role of surface films in corrosion and oxidation. *Surf. Sci.*, **53**: 257-271.

Lefrou, C, Nogueira, R.P., Huet, F. and Takenouti, H. (2010). Electrochemistry. In: Cottis, B., Graham, M., Lindsay, R., Lyon, S., Richardson, T., Scantleburg, D. and Stott, H. (Editors), *Shreir's Corrosion*, Volume 1, Elsevier, Amsterdam, Netherlands.

Lewis, E.A. and Irene, E.A. (1987). The effect of surface orientation on silicon oxidation kinetics. *J. Electrochem. Soc.*, **134**: 2332-2339.

Licciardello, A., Puglisi, O. and Pignataro, S. (1986). Effects of organic contaminants on the oxidation kinetics of silicon at room temperature. *Appl. Phys. Lett.*, **48**: 41-43.

Lindsay, R. and Lyon, S.B. (2010). Introduction to control of corrosion by environmental modification. In: Cottis, B., Graham, M., Lindsay, R., Lyon, S., Richardson, T.,

Scantleburg, D. and Stott, H. (Editors), *Shreir's Corrosion* Volume 1, Elsevier, Amsterdam, Netherlands.

Lovins, A.B. (2003). Twenty hydrogen myths. Rocky Mountain Institute, US. Accessed in September 2011 at: http://www.w2agz.com/Library/Hydrogen/E-20HydrogenMyths.pdf

Lui, F., Roper, C.S., Chu, J., Carraro, C. and Maboudian, R. (2010). Corrosion mechanism and surface passivation strategies of polycrystalline silicon electrodes. *Sensor. Actuat. A: Phys.* (in press).

Mack, S., Biro, D., Wolf, A., Thaidigsmann, B., Walczak, A., Speigelman, J.J. and Preu, P. (2010). Purified steam for industrial thermal oxidation processes. Paper presented at the 35th Photovoltaic Specialists Conference (PVSC), Honolulu, Hawaii, 20-25 June.

McLain, J.H. (1980). *Pyrotechnics from the Viewpoint of Solid State Chemistry*. The Franklin Institute Press, Philadelphia, Pennsylvania, US.

McLain, J.H. and Mayer, S. (1943). Delay trains for use in floating smoke pots. TDMR 732, Edgewood Arsenal, Maryland, US.

McLain, J.H. and Ruble, T.A. (1953). First fire charge composition. *US Patent 2 643 946.*

Meyers, P. (1999). Behaviour of silica in ion exchange and other systems. Paper presented at the International Water Conference, Pittsburgh, US, 18-20 October.

Mills, T.G. and Kroger, F.A. (1973). Electrical conduction at elevated temperatures in thermally grown silicon oxide films. *J. Electrochem. Soc.*, **120**: 1582-1586.

Modlin, D.N. and Tiller, W.A. (1985). Effects of corona-discharge-induced oxygen ion beams and electric fields on silicon oxidation kinetics. *J. Electrochem. Soc.*, **32**: 1659-1663.

Momentive. (2010). Silquest silanes products and potential applications. Accessed on 23 July 2009 at: http://www.momentive.com

Morgan, C.G. and Rimmington, C. (2010). Manufacture of pyrotechnic time delay compositions. *US Patent Application Publication, US2010/0037999Al.*

Na, W.K., Lim, H.M., Huh, S.H., Park, S.E., Lee, Y-S. and Lee, S.H. (2009). Effect of the average particle size and the surface oxidation layer of silicon on the colloidal silica particle through direct oxidation. *Mater. Sci. Eng. B - Solid*, **163**: 82-87.

Nakamura, K., Kurokuwa, A., and Ichimura., S. (1999). Hydrofluoric acid etching of ultra thin silicon oxide film fabricated by high purity ozone. *Thin Solid Films*, **343-344**: 361-364.

Nakayama, T. and Collins, F.C. (1966). Kinetics of thermal growth of silicon dioxide films in water vapour–oxygen–argon mixtures. *J. Electrochem. Soc.*, **113**: 706-713.

Ocal, C. Ferrer, S. and Gracia, N. (1985). Cabrera-Mott mechanism for oxidation of metals explains diffusion of metallic atoms through thin defective oxide layer. *Surf. Sci.*, **163**: 335-356.

Olander, B. and Albertsson, A-C. (2002). Evaluation of surface modification processes using a ternary XPS diagram. Rapid Communication. *Surf. Interface Anal.*, **33**: 541-544.

Pourbaix, M. (1966). *Atlas of Electrochemical Equilibria in Aqueous Solutions*. Pergamon Press, New York, US.

Pourbaix, M. (1973). *Lectures on Electrochemical Corrosion*. Plenum Press, New York, US.

Raja, P.B. and Sethuraman, M.G. (2008). Natural products as corrosion inhibitor for metals in corrosive media – A review. *Mater. Lett.,* **62**: 113-116.

Ricco, I.M.M. (2005). Alternative oxidants and processing procedures for pyrotechnic time delays. *MEng Dissertation*, University of Pretoria, South Africa.

Ricco, I.M.M., Conradie, C. and Focke, W.W. (2004). Alternative oxidants for silicon fuel in time delay detonators. *Combust. Sci. Technol.*, **176**: 1565-1575.

Rugunanan, R.A. (1991). Intersolid pyrotechnic reactions of silicon. *PhD Thesis*, Rhodes University, Grahamstown, South Africa.

Salonen, J., Lehto, V.P. and Laine, E. (1997). Thermal oxidation of free standing porous silicon films. *Appl. Phys. Lett.*, **70**: 637-639

Sastri, V.S. (1998). *Corrosion Inhibitors: Principles and Applications*. Wiley, Chichester, UK.

Sham, T.K., Coulthard, I., Lorimer, J.W., Hiraya, A. and Watanabe, M. (1994). Reductive deposition of Cu on porous silicon from aqueous solutions: An X-ray study at the Cu $L_{3,2}$ edge. *Chem. Mater.*, **6**: 2085-2091.

Shea, H., Gasparyan, A., Chan, H.B., Arney, S., Frahm, R.E., Lopez, D., Jin, S. and McConnell, R.P. (2004). Effects of electrical leakage currents on MEMS reliability and performance. *IEEE Trans. Dev. Mat. Rel.*, **4**: 198-207.

Sherif, E.M. (2006). Effects of 2-amino-5-(etylthio)-1,3,4-thiadiazole on copper corrosion as a corrosion inhibitor in 3% NaCl solutions. *Appl. Surf. Sci.*, **252**: 8615-8623.

Simoen, E., Gong, C., Posthuma, N.E., Van Kerschaver, E., Poortsmans, J. and Mertens, R. (2011). ADLTS study of $SiO_2$ and $SiO_2/SiN_x$ surface passivation of silicon. *J. Electrochem. Soc.*, **158**: H612-H617.

Stroscio, J.A., Bare, S.R. and Ho, W. (1985). Reaction of methanol on Si (111)-7 x 7. *Surf. Sci.*, **154**: 35-51.

Szklarska-Smialowska, Z. (1999). Pitting corrosion of aluminium. *Corros. Sci.,* **41**:1743-1767.

Tichapondwa, S.M., Focke, W.W., Del Fabbro, O., Mkhize, S. and Muller, E., (2011). Suppressing $H_2$ evolution by silicon powder dispersions. *J. Energ. Mater.*, **29**: 1-19.

Tomozawa, M. (2011). Water diffusion in silicon glass and wet oxidation of Si: An interpretation for high speed of wet oxidation. *J. Electrochem. Soc.,* **158:** G115–G118.

Twite, R.L. and Bierwagen, G.P. (1998). Review of alternatives to chromate for corrosion protection of aluminium aerospace alloys. *Prog. Org. Coat.*, **33**: 91-100.

Unger, K.K. (1979). *Porous Silica: Its Properties and Use as Support in Column Liquid Chromatography*. Elsevier Scientific, Amsterdam, the Netherlands.

Van Ooij, W.J., Zhu, D., Palnivel, V., Lamar, J.A. and Stacy, M. (2006). Overview: The potential of silanes for chromate replacement in metal finishing industries. *Silicon Chem.*, **3**: 11-30.

Van Ooij, W.J., Zhu, D., Stacy, M., Seth, A., Mugada, T., Gandhi, J. and Puomi, P. (2005). Corrosion protection properties of organofunctional silanes – An overview. *J. Tsinghua Univ. Sci. Technol.*, **10**: 639-665.

Wang, Z-H. and Jin, G. (2004). Silicon surface modification with a mixed silanes layer to immobilize proteins for biosensor with imaging ellipsometry. *Colloids Surf., B.*, **34:** 173-177.

West, J.M. (1980). *Basic Corrosion and Oxidation*. Ellis Horwood, Chichester, UK.

Williams, R. and Goodman, A.M. (1974). Wetting of thin layers of $SiO_2$ by water. *Appl. Phys. Lett.*, **25**: 531-32.

Williams, R.M. and Ezis, A. (1983). Slip casting of silicon shapes and their nitriding. *J. Am. Chem. Soc.*, **109**: 1387-1397.

Wolters, D.R. (1980). On the oxidation kinetics of silicon: The role of water. *J. Electrochem. Soc.*, **127**: 2072-2082.

Wolters, D.R. and Zegers-van Duynhoven, A.T.A. (1989a). Kinetics of dry oxidation of silicon. *Appl. Surf. Sci.*, **39**: 81-88.

Wolters, D.R. and Zegers-van Duynhoven, A.T.A. (1989b). Kinetics of dry oxidation of silicon. I. Space-charge limited growth. *J. Appl. Phys.*, **65**: 5126-5133.

Wolters, D.R. and Zegers-van Duynhoven, A.T.A. (1989c). Kinetics of dry oxidation of silicon. II. Conditions affecting the growth. *J. Appl. Phys.*, **65**: 5134-5141.

Xinhuanet (2011). 37 killed in factory explosion in Zambia. Accessed in August 2011 at: http://news.xinhuanet.com/english/2005-04/21/content_2857851.htm

Yuan, W. and Van Ooij, W.J. (1997). Characterization of organofunctional silane films on zinc substrates. *J. Colloid Interface Sci.,* **185**: 197-209.

Zhang, X.G. (2001). Electrochemistry of silicon and its oxide. Plenum Publishers, New York, US.

Zhu, D. and Van Ooij, W.J. (2003). Corrosion protection of AA 2024–T3 by bis–[3–(triethoxysilyl) propyl] tetrasulfide in sodium chloride solution. Part 2: Mechanism for corrosion protection. *Corros. Sci.,* **45**: 2177-2197.

# APPENDICES

## Appendix A: Deal and Grove model for the oxidation of silicon

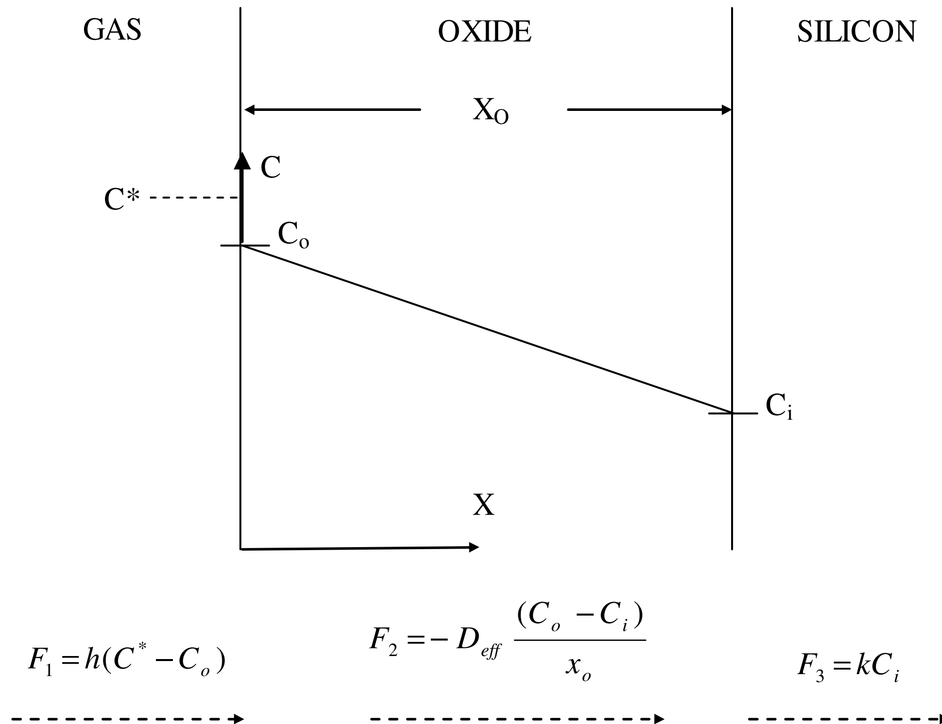


**Figure A–1** Model of the oxidation of silicon

Experimental evidence shows that oxidation of silicon proceeds by an inward transportation of the oxidant species rather than outward movement of silicon (Deal & Grove, 1965; Irene, 1988). The oxidant species has to go through the following stages:

i. Transportation from the bulk of the oxidising agent to the outer surface where it reacts or is absorbed

The flux of the oxidant from the bulk to the vicinity of the outer shell is given by:

$$F_1 = h(C^* - C_o) \qquad \text{(A-1)}$$

where

$h$ = oxidant transfer coefficient

$C_o$ = concentration of oxidant at the outer surface of the oxide

$C^*$ = equilibrium concentration of oxidant in the oxide

The equilibrium concentration of the oxidant is assumed to be related to the partial pressure of the oxidant in the gas by Henry's law:

$$C^* = Kp \tag{A-2}$$

Henry's law holds in the absence of dissociation or association of the oxidant at the outer surface. The oxidant is therefore assumed to be molecular $O_2$ and $H_2O$ in the case of dry and wet oxygen oxidation respectively (Deal & Grove, 1965).

ii. Transportation of the oxidant across the oxide film towards the silicon

The flux of the oxidant across the oxide layer is given by Fick's law where transport is in response to a concentration gradient:

$$F_x = -D_{eff}\left(\frac{dC}{dx}\right) \tag{A-3}$$

at any point x within the oxide layer, where $D_{eff}$ is the effective diffusion coefficient and $dC/dx$ is the concentration gradient of the oxidising species in the oxide.

$$F_2 = -D_{eff}\frac{(C_o - C_i)}{x_o} \tag{A-4}$$

If the transported species are ionic, they set up a space charge within the oxide film. The effective diffusion coefficient $D_{eff}$ incorporates the effect of such space charges in enhancing the rate of transport (Deal & Grove, 1965).

iii. The reactant then reacts at the silicon surface to form a new layer of silicon oxide.

The flux corresponding to the oxidation reaction is expressed by the first-order relation:

$$F_3 = kC_i \tag{A-5}$$

The steady-state analysis of the diffusive transport flux in series with the first-order interface reaction yields the linear-parabolic expression (Lewis & Irene, 1987).

# Appendix B: XRD spectra

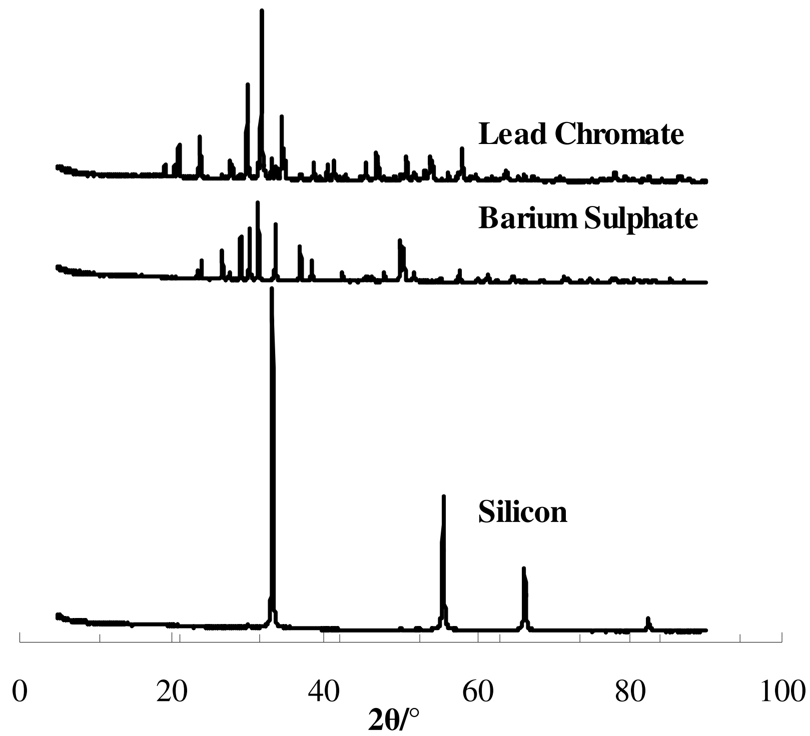


**Figure B-1** XRD spectra for material used in preparing pyrotechnic compositions

# Appendix C: FTIR spectra

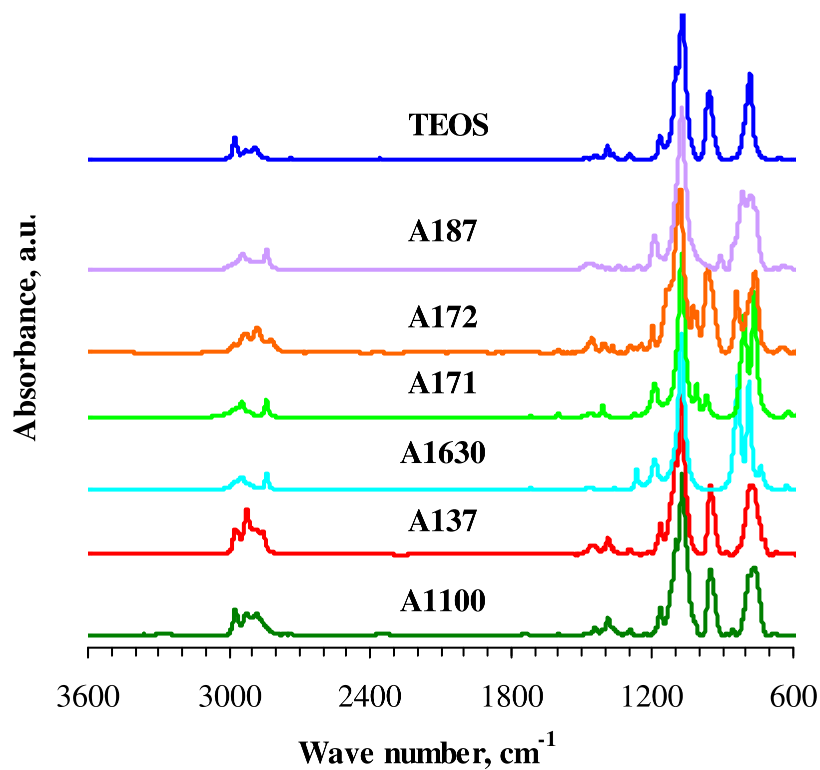


**Figure C-1** FTIR spectra of neat silanes

**Appendix D: Calibration curves**

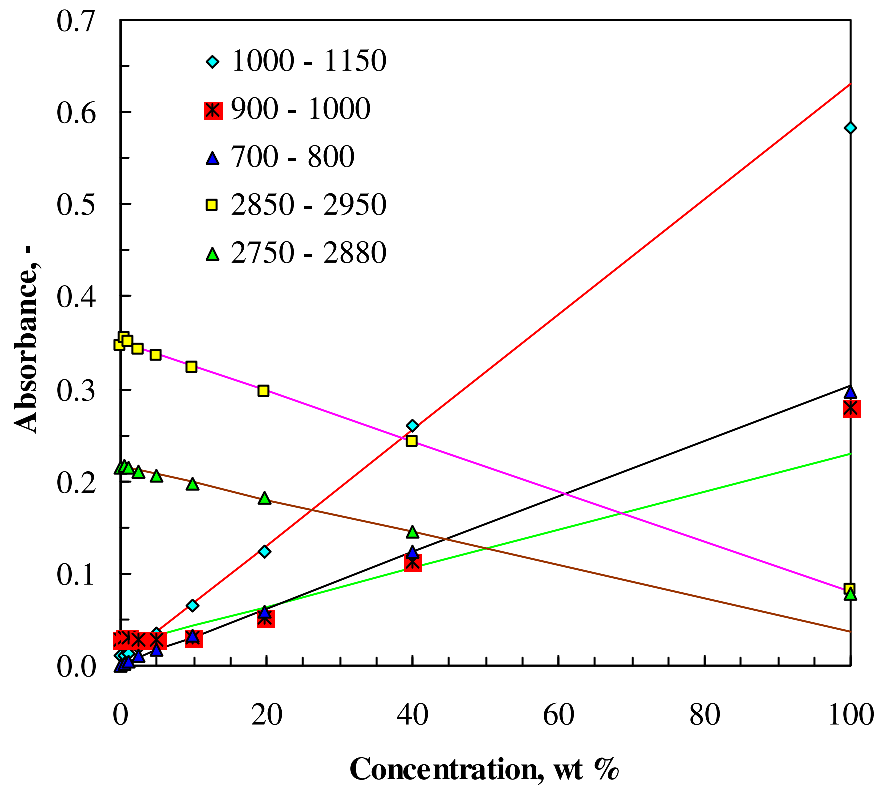


**Figure D-1** Calibration curves of silane A1100 in cyclohexane

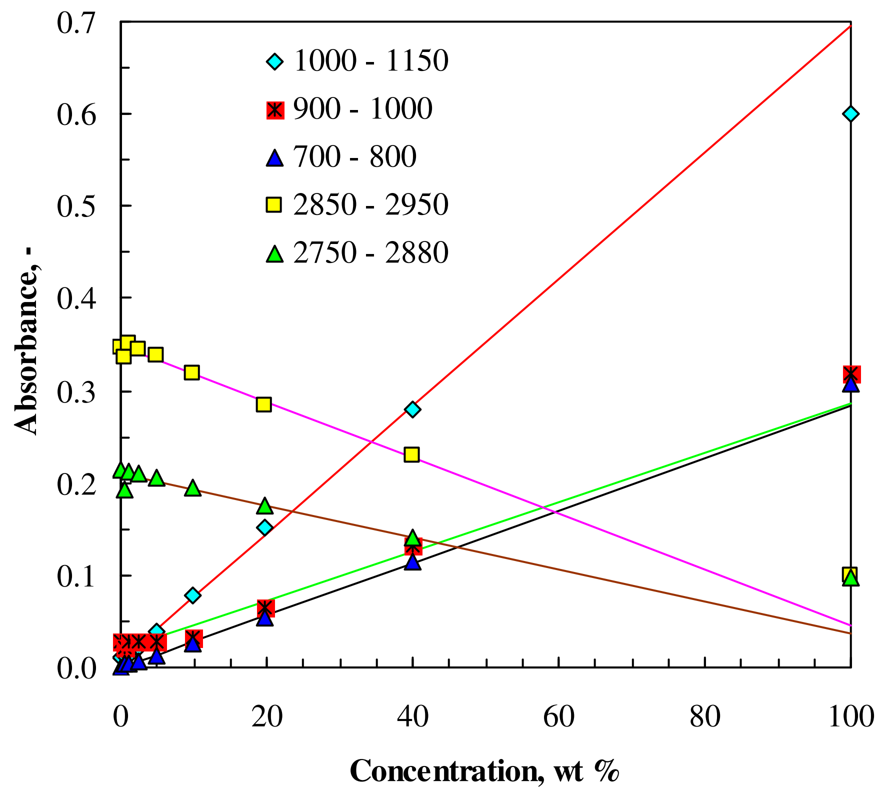


**Figure D-2** Calibration curves of silane A172 in cyclohexane

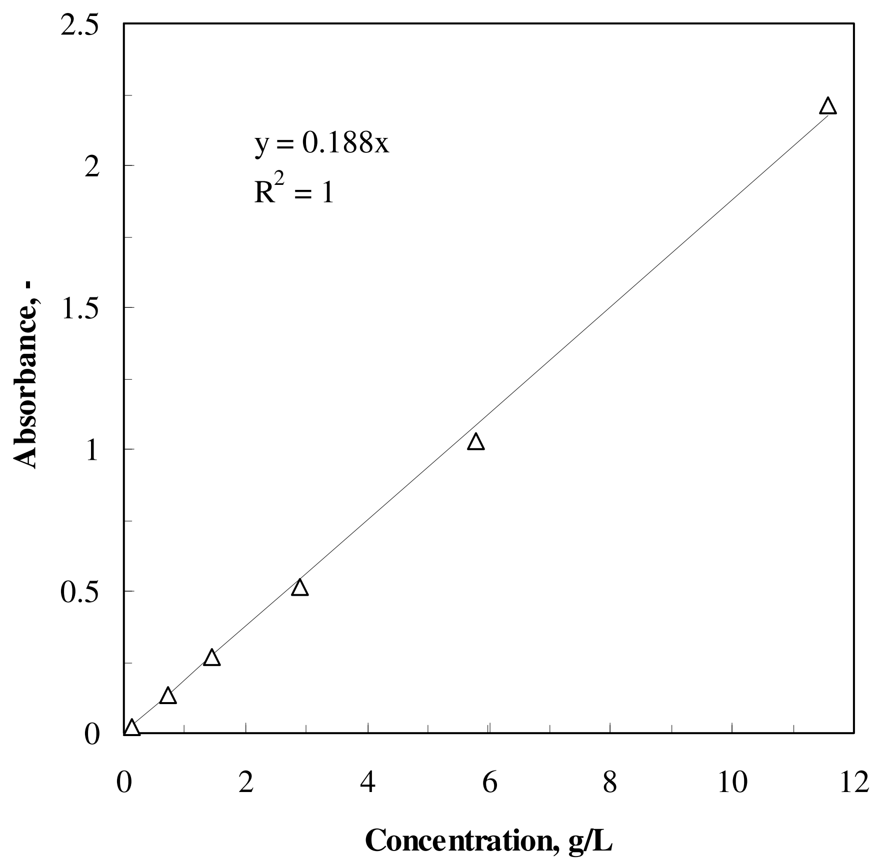


**Figure D-3** $[Cu(NH_3)_4]^{2+}$ calibration curve (UV-Vis)

## Appendix E: Copper ion concentration, solution pH and amount of hydrogen gas evolved as a function of time

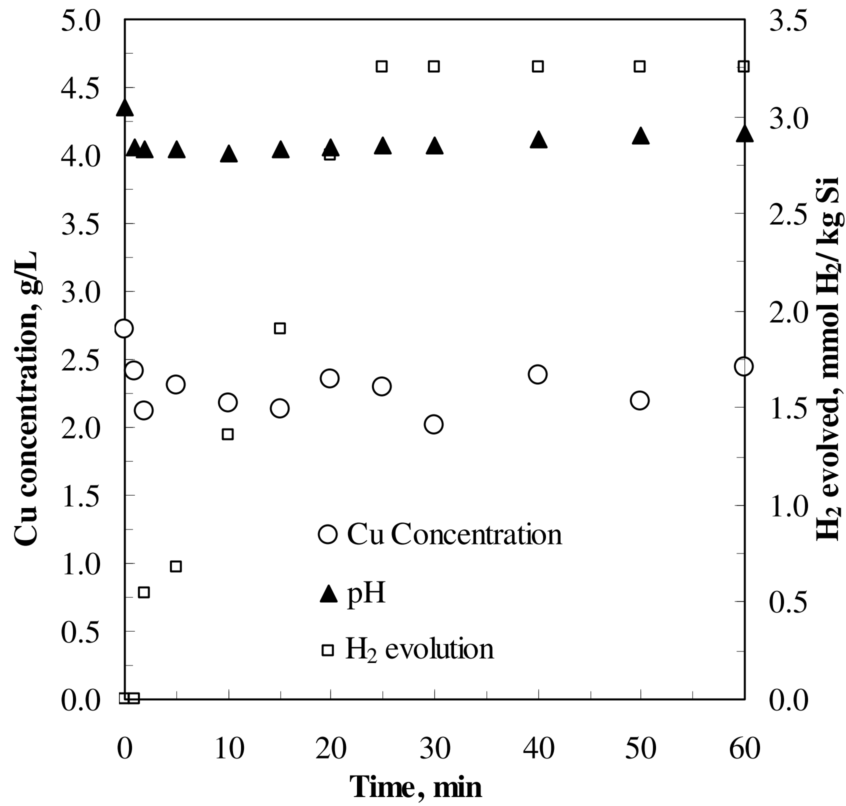


**Figure E-1** Copper ion concentration, solution pH and amount of hydrogen gas evolved as a function of time for Si powder dispersed in 0.04M $CuCl_2$ and ultrasonically agitated

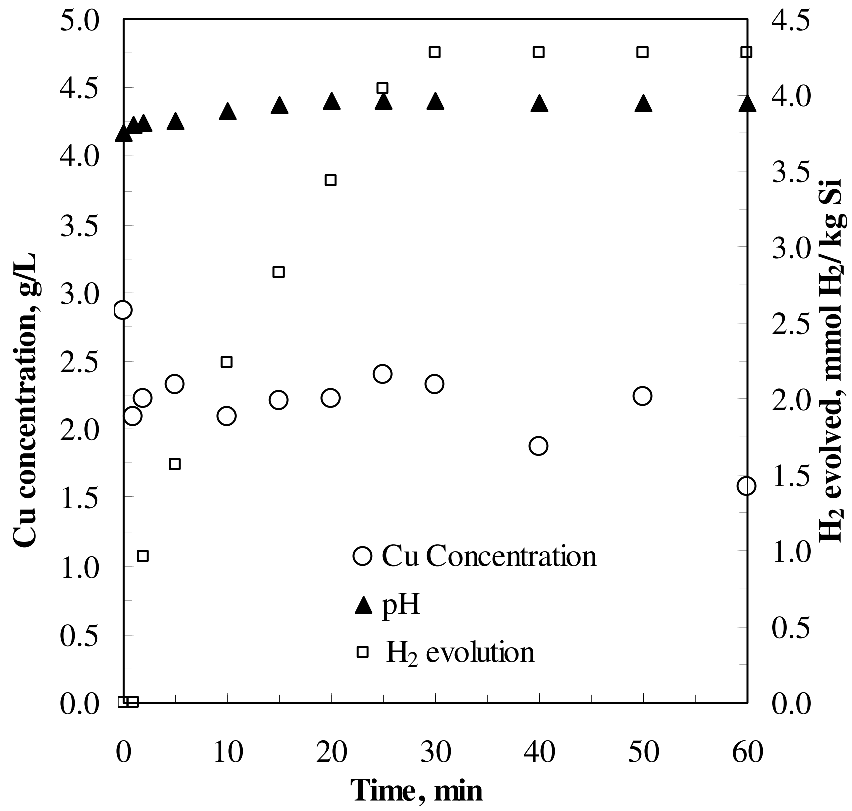


**Figure E-2** Copper ion concentration, solution pH and amount of hydrogen gas evolved as a function of time for Si powder dispersed in 0.04M $CuSO_4$ and ultrasonically agitated

**Appendix F: Calculation for the amount of hydrogen generated**

It is assumed that exactly one layer of Si reacts to form $SiO_2$ and assuming there is no oxide on the initial Si surface

Crystal structure of Si is diamond cubic–face-centered cubic

Atomic radius of Si = $110 \times 10^{-12}$ m

In a face-centred structure (FCC) unit cell the structure is cubic, having a cube edge length *a*, and the atomic radius is related through:

$a = 2R\sqrt{2}$

The cube edge length of Si is given by:

$a = 2R\sqrt{2}$

$= 2 * 110 \times 10^{-12} * \sqrt{2}$

= 0.311 nm

Area of Si unit cell = $a^2$ $= (0.311 \times 10^{-9})^2$

$\mathbf{= 9.68 \times 10^{-20}\ m^2}$

Area of Si measured using the BET = 9.68 $m^2$/g

Therefore,

$$\text{Number of unit cells per g Si} = \frac{9.68\, m^2 / g\ Si}{9.68\, x 10^{-20}\, m^2}$$

$\mathbf{= 1 \times 10^{20}}$ **unit cells/g Si**

Based on the atom arrangement of FCC unit cells, one surface has two atoms per unit cell surface.

Therefore there are $2 \times 10^{20}$ Si atoms/g Si

$$\text{The moles of Si at the surface of the Si} = \frac{2\, x 10^{20}\ atoms / g\ Si}{6.023\, x 10^{23}\ atoms / mole}$$

$\mathbf{= 3.32 \times 10^{-4}}$ **moles/g Si**

Assuming a 1 kg basis of Si = 0.332 moles/kg Si

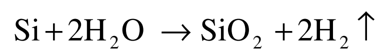

$$Si + 2H_2O \rightarrow SiO_2 + 2H_2 \uparrow$$

From the chemical reaction

1 mole Si: 2 moles $H_2$

0.332 moles/kg Si: 0.664 moles/kg Si

Therefore the amount of hydrogen produced assuming only monolayer reaction of Si surface is 0.664 moles $H_2$/kg Si or 664 mmoles $H_2$/kg Si

Average experimental $H_2$ evolution recorded = 8.3 mmoles $H_2$/kg Si

Therefore the approximate amount of surface Si available for reaction in the experiments is

$$= \frac{8.3\, mmoles H_2 / kg\ Si}{664\, mmoles H_2 / kg\ Si} x 100\%$$

**= 1.25%**

## Appendix G: Publications resulting from this research

Tichapondwa, S.M., Focke, W.W., Del Fabbro, O., Mkhize, S., and Muller, E., (2011). Suppressing $H_2$ evolution by silicon powder dispersions. *J. Energ. Mater.*, **29**: 1–19.

Tichapondwa, S.M., Focke, W.W. and Del Fabbro, O. Suppressing $H_2$ evolution by silicon powder dispersions by controlled silicon surface oxidation. *Prop. Explos. Pyrotech*. (submitted for publication).

Tichapondwa, S.M., Focke, W.W., Del Fabbro, O. and Sandenbergh, R.W. Suppressing $H_2$ evolution by silicon powder dispersions by introducing additional cathodic reactions. (to be submitted for publication).